Title

Investigating the Role of Mechanical Forces in the Catheter-Related Pathogenesis of Staphylococci, From Adhesion to Biofilm Formation

Author

Weaver, Westbrook McConnell

Publication Date

2013

Peer reviewed|Thesis/dissertation

UNIVERSITY OF CALIFORNIA

Los Angeles

Investigating the Role of Mechanical Forces in the Catheter-Related Pathogenesis of *Staphylococci*, From Adhesion to Biofilm Formation

A dissertation submitted in partial satisfaction of the requirements for the degree Doctor of Philosophy in Biomedical Engineering

by

Westbrook McConnell Weaver

2013

ABSTRACT OF THE DISSERTATION

Investigating the Role of Mechanical Forces in the Catheter-Related Pathogenesis of *Staphylococci*, From Adhesion to Biofilm Formation

by

Westbrook McConnell Weaver
Doctor of Philosophy in Biomedical Engineering
University of California, Los Angeles, 2013
Professor Dino Di Carlo, Chair

Intravenous catheter related blood stream infections (CRBSI) are the major cause of healthcare-associated infections to date, and result in both increased morbidity and mortality in patients with undeveloped and compromised immunity, as well as a significant cost burden on health systems. *Staphylococcus epidermidis* and *S. aureus* are both normal inhabitants of human skin and mucous membranes and also are the organisms most significantly cultured from these infections. CRBSIs from Staphylococci can be extremely harmful if left untreated even for a mater of a few days. These infections can result in serious conditions such as native valve endocarditis, and even bacteremia sepsis.

The pathogenesis is complex, involving multicellular choreography and host immune evasion, however it is well accepted that two key steps are (i) adhesion to the catheter lumen by planktonic cells and (ii) subsequent biofilm formation to establish a stable source of bacterial cells for infection. Adhesion is largely mediated by surface exposed adhesins, targeting a number of soluble host plasma proteins and extracellular matrix components. Biofilm formation has been shown to occur through a number of pathways, however a commonly occurring theme

is through secretion of polysaccharide intracellular adhesin (PIA) matrix, driven by expression of the chromosomal *icaADBC* operon.

We have developed a novel toolset using microfluidics to recapitulate the pathogenic environment incorporating clinically relevant fluid shear stress. Using this microfluidic assay, we show that shear stress from fluid flow modulated the pathogenic potential of *S. epidermidis*, both in terms of increased adhesive capability as well as the induction of biofilm formation is normally quiescent strains. Further, we have developed a high-throughput, multidimensional microfluidic assay incorporating functional adhesive protein microarrays and large scale microfluidic networks. This assay will be used to generate quantitative 'pathogenicity landscapes' in Staphylococci, towards the identification of novel therapeutic targets to mitigate and treat device related infections.

The Dissertation of Westbrook McConnell Weaver is approved

Gerard Wong

Jeffery F. Miller

Warren Grundfest

Dino Di Carlo, Committee Chair

University of California, Los Angeles

2013

Table of Contents

Biographical Sketch

Westbrook Weaver received his bachelor of science degrees in both Biomedical Engineering and Biological Chemistry from Tulane university in New Orleans, Louisiana in 2008. While attending Tulane, he worked as a research assistant in Dr. Larry D. Byers' lab in the biochemistry department, focusing on characterizing the inhibitory mechanisms of multivalent anions on the enzymatic activity of β-Galactosidases, towards a better understanding of their kinetics in synthetic biology driven rectors for biofuel production.

While conducting research at UCLA, Westbrook's focus has shifted toward the development of next generation technologies for biology and chemistry. Specifically, his focus has been on development of microfluidic tools and systems for high-throughput biology. His research has uncovered novel methods by which bacterial pathogenesis can be regulated by the host environment, and also that cancer cell physiology and chromosomal instability are driven by mechanical cell confinement. Currently, Westbrook is developing next-generation screening tools for high throughput determination of bacterial 'pathogenicity landscapes' to identify common mechanisms used by diverse pathogens in device-related infections, toward the identification of novel therapeutic targets to mitigate and fight infection.

I: Introduction

Intravenous catheters for long term patient support, both monitoring blood and delivering treatments, and nutrients are an indispensable tool for critical care. Since the adoption of silicon elastomer peripherally inserted central catheter (PICC) lines in the 1975s, the quality of critical care treatment has been incomparable to pre-catheter care[1]. However, with new technology always come unforeseen challenges. In the case of the PICC, the phenomenon of implanted device-related infection from bacterial pathogens has been a serious impediment to the effective use of the PICC line[2,3]. The high frequency of infections (upwards of 80%), combined with the recent emergence of multi- and pan-drug resistant strains of commonly isolated pathogens such as *Staphylococci, Escherichia coli,* and *Pseudomonas* has lead to both significant mortality and morbidity in patients as well as increased burden on hospital systems[4,5].

Interestingly, many of the organisms responsible for these healthcare-associated infections (HAIs) are commensal bacteria: part of the normal micro flora residing on a patient's skin[6,7]. In fact, this mode of entry (leading to the characterization of these bacteria as 'opportunistic' pathogens) is shared among a number of bacteria and fungi as well as a range of implantable devices. For example, urinary catheters are typically associated with Uropathogenic *E. coli* (UPEC) which infect the bladder and urinary tract epithelium, where as PICC lines can result in blood stream infections (BSIs) from both gram positives (such as *Enterococci* and *Staphylococci*), as well as gram negatives (mainly *Acinetobacter* and *Pseudomonas*). When the entirety of all types of device related infections, including PICC lines, urinary catheters, and ventilators are combined, both gram positives and gram negatives contribute a great deal to the overall numbers

of infections, where gram negatives comprise about 58% and gram positives contribute 33% (figure 1). The remainder is composed of fungi (namely *Candida* spp.) and anaerobes such as *Bacteroides*.

A

Type of Infection	Number of infections per year	Attributable cost per infection	Total Cost per year
Catheter-associated urinary tract infections	561,667	$749 - $1,007	~$512 M
Surgical-site infection	290,485	$11,087 - $34,670	~$6.5 B
Ventilator-associated pneumonia	250,205	$14,806 - $28,508	~$5.25 B
Central line-associated bloodstream infections	248,678	$6,461 - $29,156	~$4.35 B

B

	Susceptible	Multidrug Resistant	Total
Gram negative			**759 (57.6 %)**
Acinetobacter spp.	13 (8.1%)	147 (91.9%)	160 (12.2%)
Kelbsiella spp.	46 (29.5%)	110 (70.5%)	156 (11.9%)
Pseudomonas spp.	95 (63.3%)	55 (36.7%)	150 (11.4%)
Escherishia coli	57 (58.2%)	41 (41.8%)	98 (7.4%)
Enterobacter spp.	48 (54.6%)	40 (45.5%)	88 (6.7%)
Other gram-negatives	69 (64.5%)	38 (35.5%)	107 (8.1%)
Gram positive			**440 (33.4%)**
Enterococcus spp.	103 (71.5%)	41 (28.5%)	144 (10.9%)
Coagulase negative Staph	141 (100%)	0 (0%)	141 (10.7%)
Staphylococcus aureus	60 (50.4%)	59 (49.6%)	119 (9%)
Other gram-positives	36 (100%)	0 (0%)	36 (2.7%)
Anaerobes			**20 (1.5%)**
Bacteroides spp.	13 (100%)	0 (0%)	13 (1%)
Other anaerobes	7 (100%)	0 (0%)	7 (0.5%)
Fungi			**98 (7.4%)**
Candida albicans	0 (0%)	56 (100%)	56 (4.3%)
Other *Candida spp.*	0 (0%)	39 (100%)	39 (3%)
Other Fungi	0 (0%)	3 (100%)	3 (0.2%)

Figure 1: Hospital acquired infections are prevalent and present a large burden on hospital systems. A: Urinary tract infections are the most common HAI, however Catheter related infections are the most expensive. B: The bio-diversity of HAIs are large, representing both drug susceptible and resistant populations.

The frequency of these implantable device related infections has been a serious problem since their respective introductions to clinical practice and, although in recent years these numbers have been somewhat curbed by the adoption of better clinical practice for prevention of infection, the numbers are still astounding. It is estimated that more than 1.7 million HAIs occur in the US alone each year, indicating that ~5% of all patients admitted develop these infections [8]. This may seem like a small percentage, but the cost of infection (both human and hospital) is high. Typically patients receiving care involving a PICC line or urinary catheter are already ill, having either compromised immunity from HIV or other viral infection [9], from chemotherapy and radiation treatments in cancer patients[10], or underdeveloped immunity in the case of neonates and premature infants[11]. These patients may have increased morbidity and mortality when infected; however their prior conditions necessitate the use of the long-term implantable devices. Indeed, there were nearly 98,000 deaths in US hospitals alone in 2002 resulting from hospital-onset HAIs, placing HAI well within the top ten causes of death in the US [8].

The increasing rate of emergence of antibiotic resistant species poses a serious challenge in the effective treatment of these infections. Since the introduction of penicillin in 1932 as a clinical treatment, the timeframe of effectiveness for antibiotics has become shorter and shorter. For example, penicillin was an effective treatment for many common infections, including syphilis for decades [12], until penicillin emergent Staphylococci emerged, however with more modern ‘potent’ antibiotics, the time between first use in the clinic and the isolation of the first resistant strain has been increasingly shorter in recent years [13,14]. There are many convincing arguments that

over-prescription and use of antibiotics drives the selection of resistant strains[15,16], however regardless of the clinical practices that may be contributing to this phenomenon, antibiotic resistance poses a fundamental problem for treatment. Further, over the past decade multidrug and pan-drug resistant strains of both gram-positive and gram-negative bacteria have emerged [17]. In a recent European study of HAIs in 2012, five strains of gram negative bacteria (3 *Klebsiella*, 1 *Acinetobacter*, and 1 *Pseudomonas*) resistant to all usable antibiotic treatments were isolated in one year [18].

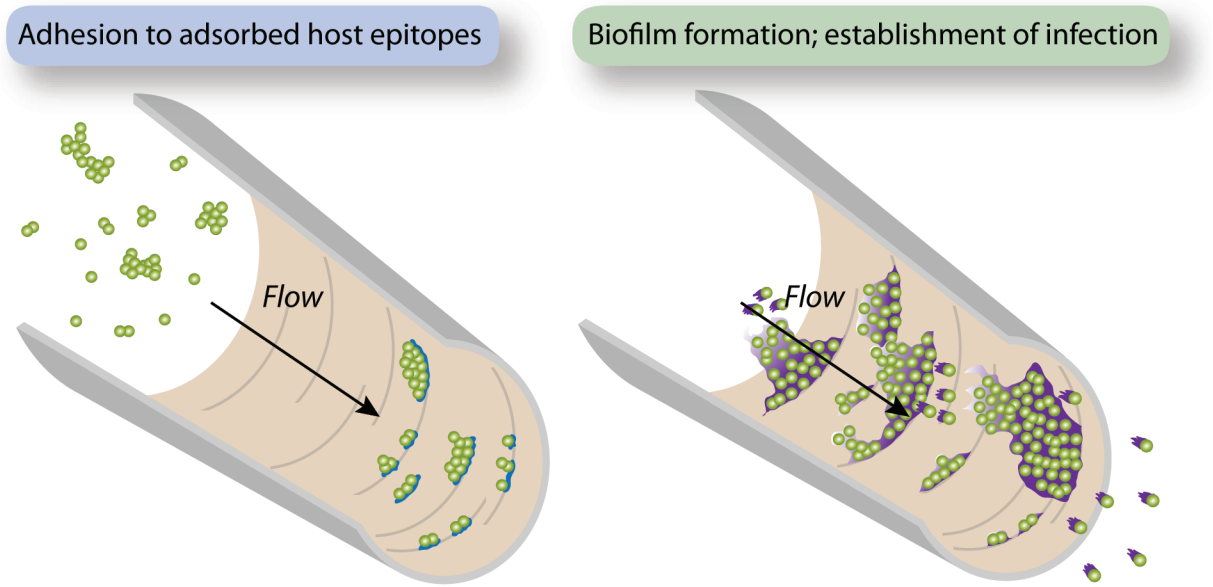

Figure 2: Two important steps in the catheter-associated pathogenesis of many commonly cultured HAI pathogens: adhesion to the device surface and subsequent biofilm formation on that surface.

In order to effectively combat HAIs to reduce patient morbidity and mortality as well as hospital costs will require a new era of treatments diverging from the common thread of antibiotics and antimycotics that target basic biological processed necessary for survival, such as cell wall synthesis and protein translation. This switch will require

the identification of new therapeutic targets, specific to the mechanisms of infections and pathogenesis. In the case of catheter related blood stream infections (CRBSIs), there are two potential key targets for the development of next generation treatments: (i) adhesion of bacteria to the device surface, and (ii) subsequent production of a biofilm matrix resulting in stable colony formation (figure 2).

Both adhesion and biofilm formation have been considered, for the past decade, promising targets for therapeutic development, however their mechanisms of action, as well as their regulation by environmental factors (both host and pathogen) remains largely unclear in regards to pathogenesis *in vivo*. There has been a large effort to understand the modes of adhesion and biofilm formation, with emphasis on Staphylococci and Pseudomonas spp., as these represent a majority of isolated organisms from blood stream infections for gram-positive and gram-negative bacteria, respectively [18]. In particular, Staphylococcal pathogenesis has proven to become more complex the more the scientific community learns. The suite of surface proteins involved in adhesion, termed Microbial Surface-exposed Recognizing Adhesive Matrix Molecules (MSCRAMMs), is dispersed through various species and strains highly irregularly, and appear to be expressed during pathogenesis, but there is no obvious correlation between each of these and infectivity [19,20]. A subset of these proteins has been studied *in vitro*, namely the clumping factors A and B (ClfA and ClfB) of *S. aureus* and the serine aspartate repeat protein G (SDrG) of *S. epidermidis*. Both of these proteins have been shown to bind human plasma fibrinogen, although at different locations, and are associated with increased infectivity [21,22]. ClfA and ClfB bind across the thrombin cleavage site in fibrinogen [23], where as SdrG binds 14 residues

near the N-terminus of the β-chain [24], resulting in different biological implications of these binding events. Even so, there are many other genes sharing sequence similarity to both clumping factor and SDr-type surface exposed proteins, however their binding targets have not been identified. Further, both *S. aureus* and *S. epidermidis* can adhere to surfaces coated with various extracellular matrix proteins, and both bacteria are spatially localized with both Collagen type I and IV in *ex-vivo* rat catheter models [25].

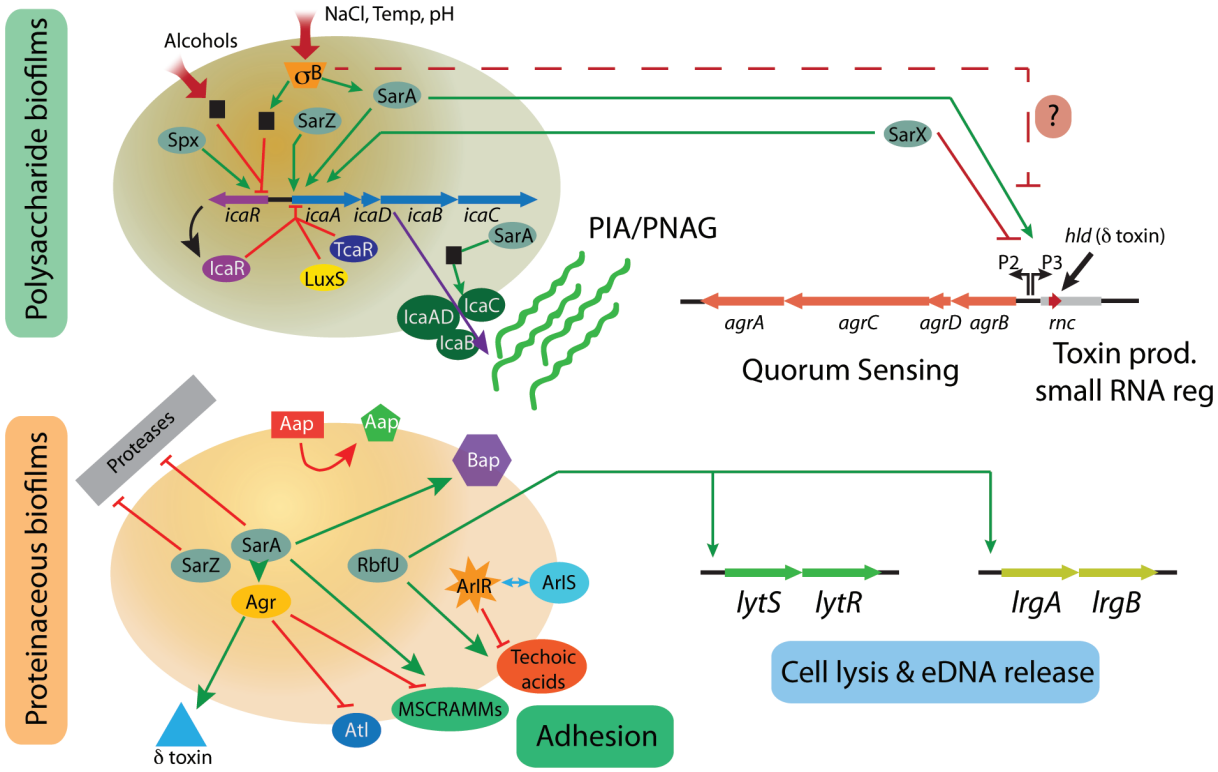

Figure 3: Biofilm and adhesive capability are both highly regulated in Staphylococci. Quorum sensing, oxidative state, osmotic pressure, as well as the presence of alcohols can modulate these pathogenic phenotypes.

Even with the emergence of some effective genetic manipulation techniques for *S. aureus*, there has been a lack of quantitative *in vitro* techniques to characterize these

mutants. *S. epidermidis* has proven to be notoriously difficult to perform genetic manipulation in, outside of a single strain developed using Tn917 transposon mutagenesis, allowing a genetic system to study gene knockouts [26–28]. Even with this strain, studies searching for disruption of adhesin genes are prohibitively difficult to perform, as the number and combination of targets (i.e. host matrix and plasma proteins) is very large and, as is the case with any other genetic technique, well plate assays cannot capture all the ranges of interaction strengths that may play a role in the environment of pathogenesis. This lack of dynamic range in the well plate assay can be explained by the step of this assay commonly overlooked in terms of importance: the wash step. This step involves the introduction of physical force to the binding assay, and ultimately determines, given a constant interaction affinity, how many cells will remain on the surface. When considering the reproducibility of these experiments, the wash step is the easiest point of introduction variability both between well and different experimental runs. Alleviation of this variability can be achieved by both the introduction of automation (i.e. liquid handlers) as well as washing the wells with a large force (i.e. full aspiration and re-suspension). Although this makes the experimental variability smaller, the dynamic range of interactions strengths that can be captured is dramatically reduced to only high-level interactions. There is no doubt to the argument that high level interactions are important and most likely play an important role in pathogenesis, however what cannot be answered by these assays is the importance of middle-range interactions. More importantly, the physical forces imparted on cells in a well plate is most likely much higher than those seen by bacteria in a catheter lumen, or in most parts of the cardiovascular system, save the aorta and upper arterioles [29].

In the same vein, the physical environment of a typically performed well plate assay for biofilm formation could not be farther from that of the pathogenic environment. From *in vivo* animal models of catheter infection, it is clear that bacteria can colonize both the inner lumen of that catheter, as well as the outer surface. In either case, the bacteria are exposed to a range of shear stresses from viscous fluid flow that may play an important role in infection, and even the regulation of virulence factors leading to changes in pathogenicity as compared to what is seen in a well plate assay. It has been demonstrated for both *S. aureus* and *S. epidermidis* that the local chemical environment plays a critical role in biofilm formation, with effectors ranging from alcohols and oxidative state to osmotic pressure and local cell density [30–32]. Cell density regulation occurs through a mechanism termed quorum sensing, which, as the name suggests, is the act of bacterial cells taking census of the number of cells within paracrine signaling range. Quorum sensing not only controls biofilm formation, but can also control the overall life cycle of a bacterial population by triggering switches from sessile lifestyles (i.e. biofilm embedded) to free-floating planktonic bacteria in the case of *Staphylococci* [30,33–35] (figure 3), also resulting in the modulation of a number of virulence determinants, including toxin production and coagulation [36]. Ultimately, quorum sensing may be a key regulator in the pathogenesis of many of the bacteria associated with HAIs, as inhibitors to *P. aeruginosa* quorum sensing block virulence factors *in vitro* [37].

It is clear that next challenge for both biological understanding of the key factors in implanted device-related pathogenesis to develop novel therapeutics, as well as the development of next generation diagnostic tools for identification and characterization of

bacteria isolated from blood cultures, is to create an *in vitro* platform to recapitulate the pathogenic microenvironment. Ideally, this device should have accurate and precise control over the physical forces imparted on cells during experimentation, as well as the ability to easily tune these forces. We are developing a novel microfluidic toolset to quantitatively investigate the pathogenic phenomena of bacterial adhesion to host proteins, as well as their subsequent biofilm formation under highly defined fluid shear.

II. Modulation of Staphylococcal adhesion to immobilized fibrinogen dictated by fluid shear stresses

Staphylococcus epidermidis is a frequent cause of hospital-acquired infections, especially in immunocompromised patients,[11] and patients with implanted intravascular devices.[2] In catheter-related infections, adhesion to the device surface is considered to be an initiating event in colonization and pathogenesis.

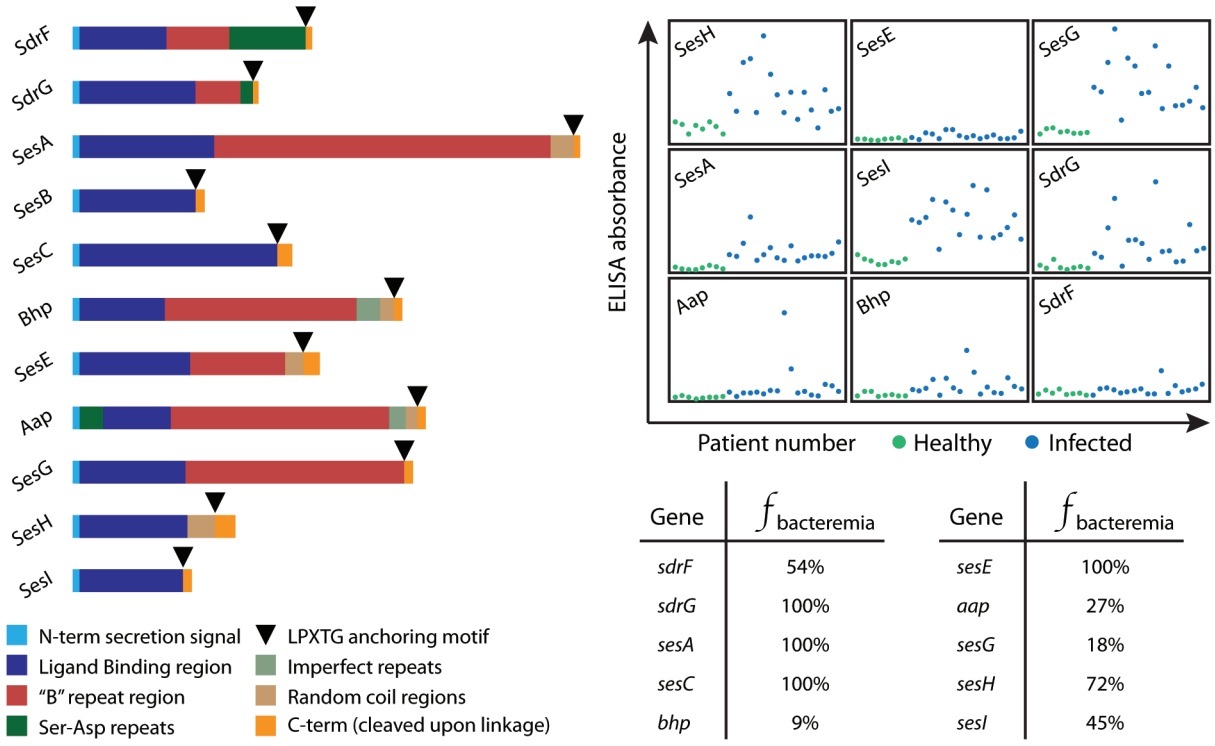

Gene	$f_{bacteremia}$	Gene	$f_{bacteremia}$
sdrF	54%	*sesE*	100%
sdrG	100%	*aap*	27%
sesA	100%	*sesG*	18%
sesC	100%	*sesH*	72%
bhp	9%	*sesI*	45%

Figure 4: Both known and putative (based on sequence homology) surface exposed adhesins in *S. epidermidis* are associated with infection.

When the polymer comes in contact with blood plasma, the surface quickly becomes coated with adsorbed plasma proteins, specifically plasma fibrinogen.[38] As *S. epidermidis* has been shown to express SDrG (serine aspartate repeat G), a surface adhesin that binds the β-chain of fibrinogen[24], this interaction is suspected to be

involved during colonization of catheters *in vivo*. The possible modes of adhesion are not limited to SDrG/fibrinogen, as many adhesins have been shown to be associated with infective strains (figure 4), however SDrG shows a strong correlation with infectivity and the binding target is known.

The initial colonization events occur in a complex, dynamic environment in the vasculature, involving both soluble factors in the blood, and mechanical forces exerted by flow. We hypothesize that shear forces from fluid flow may play an important role in these host-pathogen interactions. In fact, preliminary studies have implicated shear stress as playing a role in adhesin-ligand interactions, specifically for the *S. aureus* collagen adhesin CNA and collagen adsorbed on glass.[39], [40], [41]

Development of a model to characterize these dynamic interactions and evaluate the effects of environmental conditions in a more physiologically relevant context would open the door for development of potential interventions that could combat pathogenesis by targeting a specific event in colonization and pathogenesis.

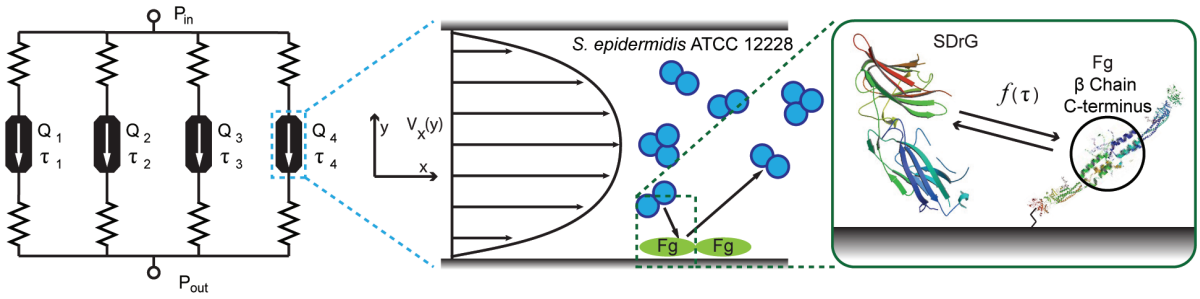

Figure 5: Schematic of microfluidic shear reactor. Four channels in parallel result in 4 separate shear stress chambers for the isolation of receptor ligand interactions between cells and coated surfaces.

Here we present a PDMS microfluidic platform that allows for probing these adhesin mediated host-pathogen interactions in a more physiologically relevant environment (figure 5). This platform directly incorporates protein patterning to areas within the channels corresponding to specific, highly defined wall shear stresses, as well as multiplexed channel geometry to assay multiple shear stress conditions simultaneously.

The advent of microfluidics and soft lithography has allowed for creation of micro-flow chambers with highly defined geometries to isolate small populations and even single cells for long term culture[42]. Platforms have also been developed to probe interactions between cells and shear stress from flow, implicating shear stress in many cellular processes involving morphology, [43] substrate attachment[44],[45] and gene expression.[46] For the study of bacteria, parallel plate flow chambers have been used to probe the ability of *S. aureus* to adhere to collagen and E. coli to erythrocytes under shear[47], however these simple chambers do not easily allow multiplexed experiments with multiple conditions or patterning of the substrates. Therefore, a parallelized microfluidic approach would provide a novel and useful tool to study shear-dependent interactions of bacteria with host proteins.

Numerous methods to create two dimensional cell adhesion patterns have been developed over the past decade, but few are compatible with functional protein immobilization within a microfluidic channel, such as 3D stamps [48], plasma etching [49], micromolding in capillaries (MIMIC) [50], and the Bio-Flip Chip (BFC) [51]. These methods have been widely used to create patterns, however they often result in denaturing of proteins on the surface disrupting molecular recognition, and are

performed prior to channel enclosure. Bonding requires harsh conditions [52], and can result in damage to the pattern's molecular fidelity and/or weak channels bonds incapable of withstanding the high pressures needed to investigate a large range of shear stresses. *In situ* methods to functionalize channel walls have expanded the possibilities of incorporating a patterned surface within a tightly bonded fluidic system,[53],[54] however, these techniques thus far use photolabile linkers, necessitating alignment of photomasks to the device as wells as expensive and bulky exposing equipment.

Our novel platform simple in that no excess equipment is needed, other than a syringe pump to drive flow, and only one level of microfabrication is required (i.e. no valves on or off chip). The patterning is performed *in situ* and utilizes flow boundaries to sequentially graft silanes to localized areas within the chamber. Flow confinement has previously been shown to spatially control the wetability inside PDMS devices[55], and we expand this concept here by incorporating a novel channel geometry to create coflow as well as the use of sequential silane grafting. The coflow allows spatial control over the first silane linkage step and subsequent treatment of the remaining surfaces with a second silane results in spatially resolved, orthogonally reactive channel walls within the platform.

The platform has two modes of operation (figure 6). The functionalization mode requires all inlets and outlets, and utilizes fluidic boundaries (figure 6 a,b) to create the molecular pattern within the channels. The perfusion mode of the device is used for shear attachment assays. In this mode, only one inlet and one outlet are used, resulting

in four parallel channels of varying wall shear stresses (over an order of magnitude) and insignificant cross-flow between chambers (figure 6 c,d).

We make use of this platform to investigate bacterial-host protein interactions, specifically the adhesion of *Staphylococcus epidermidis* ATCC strain 12228 to human fibrinogen (hFg) under varying shear stresses. This novel platform allows for investigation into bacterial host-pathogen interactions in a more physiologically relevant environment, shedding light on the events leading to colonization and pathogenesis *in vivo*.

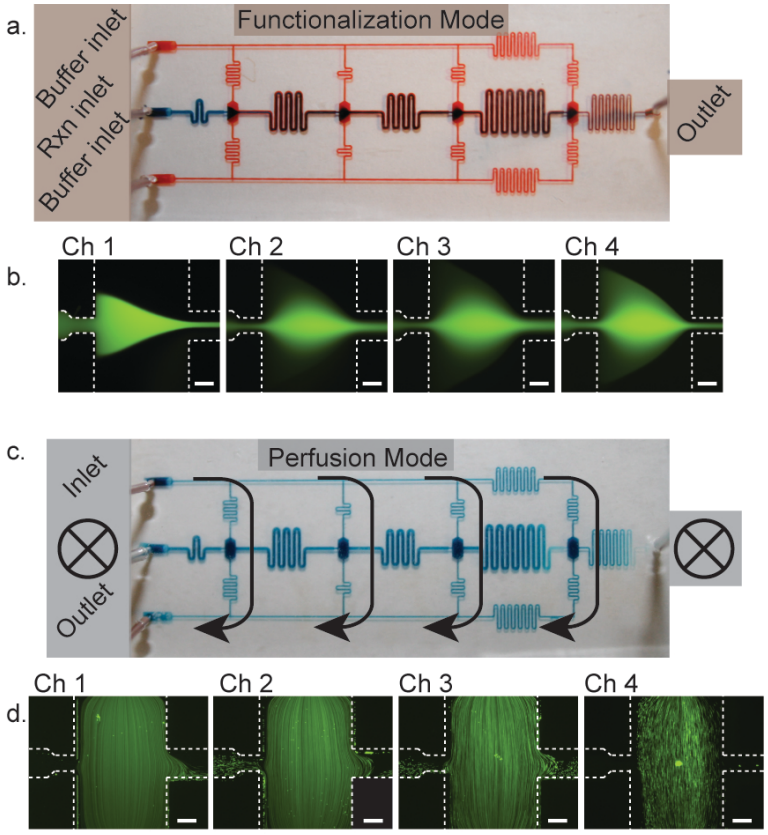

Figure 6: The microfluidic shear reactor has two modes of operation: surface functionalization mode (a,b) and perfusion/adhesion mode (c,d).

The *S. epidermidis* strain used in this study is non-biofilm forming strain ATCC 12228 strain that contains the gene encoding SDrG (SE0331). Cultures are streaked on Tryptic Soy Agar (Sigma) from -80^{0}C 20% (v/v) glycerol stocks. Tryptic Soy Broth (Sigma) is inoculated with an isolated colony and grown in a rotary shaker at 240 RPM and 37^{0}C until OD_{600} = 0.3 (~7hrs).

To characterize the specific adhesion to free hFg on the channel surface, the patterns were treated with anti-hFG in whole goat antisera (Sigma). The whole goat antisera was perfused through the device in perfusion mode at 1 μl min^{-1} for 120 min at 25^{0}C. The device was then washed with PBS at 2 μl min^{-1} for 30 min prior to bacterial perfusion.

The microfluidic platform is fabricated by standard soft lithography techniques utilizing PDMS and glass as the channel materials.[56] A master mold is fabricated by spin coating SU-8 2010 (Microchem) onto a clean Silicon 4" wafer to a height of 10 μm. The wafer is then pre-baked, exposed to UV through a photomask, post-baked, and developed according to manufacturer specifications. PDMS elastomer is mixed in a 10:1(m/m) ratio to crosslinker, degassed in a vacuum chamber, and poured over the master mold and cured.

To create the final device, inlet and outlet holes are punched in the cured PDMS, and the PDMS is bonded to a glass slide (Fisher) through oxidation via O_2 plasma in a Technics RIE parallel plate plasma etcher (Deposition pressure = 500 mTorr, Power = 40W, Δt = 5 sec). Connections are made between syringes and the device via 0.02" inner diameter PEEK Tubing (Upchurch Scientific).

The functionalization mode of the platform is used to create the protein pattern inside the device (Fig 2a,b). To establish a stable co-flow in the device, the two outside (buffer) inlets are infused at 2.5 μl min^{-1} for 5 min to allow flow to overcome the capacitance of the PEEK tubing and the channels (as well as the ramp up time of the syringe pump itself). Then the middle inlet is allowed to infuse interspersed with the side flows, all at a rate of 2.5 μl min^{-1} for 5 min. After stabilization, to conserve reagent volume, flow rates are lowered to 1 μl min^{-1} for buffer inlets and 250 nl min^{-1} for the middle reaction inlet (figure 6b). Both flow rates and flow times were optimized to create stable co-flow in each chamber, measured visually using 1 mM fluorescein dye in DI water (data not shown). To stop co-flow and wash with buffer, the middle inlet is stopped, while the side inlets are allowed to continue at 5 μl min^{-1} for 10 min. This method was used to both stabilize co-flow and wash out reaction solutions for each step in functionalization unless otherwise specified.

The chemistry utilized to create the pattern relies on the sequential grafting of silanes to oxidized silicon based surfaces. First, a 1 % (v/v) 3-aminopropyl-triethoxysilane (APTS) solution in a 5% (v/v) H_2O in ethanol (EtOH) solvent, with 10% (v/v) acetic acid as an acid catalyst, is perfused with the solvent in the reaction inlet. The reaction is allowed to go for 45 min, and then the device is washed with the reaction buffer. Next, all inlets are replaced with pure EtOH and perfused at 5 μl min^{-1} for 10 min. The devices are then cured in a 95^0C oven for 30 min to ensure condensation of silanol bonds and elimination of H_2O. During this bake step the PDMS surfaces are expected to return to a hydrophobic state.

In the second silanization step, a 0.2 % (v/v) Octadecyltrichlorosilane (OTS) solution in dry EtOH is infused in all inlets at 2 μl min^{-1} for 15 min, then washed with dry EtOH and evaporated in a 95^0C oven for 30 min. This results in a pattern of primary amines in the region in the center of the chamber (figure 7b), while all other glass surfaces are functionalized with an 18 chain hydrocarbon, rendering the surfaces hydrophobic (figure 7a).

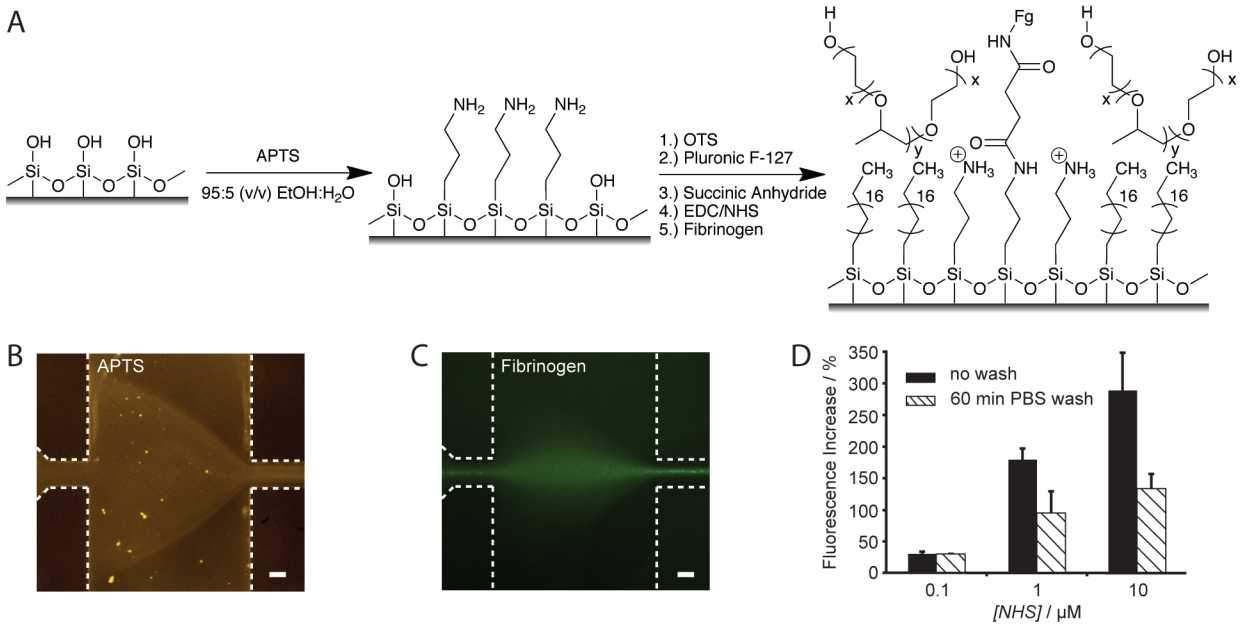

Figure 7: Surface functionalization of microfluidic channels *in situ*. A: process flow for functionalization relies on fluidic patterning of sequential silane reactions to pattern orthogonal surface functionalities. B,C: Surface chemistry is measured by surface fluorescence of labeled reactants. D: By titrating the surface in the limiting reactant (NHS), the total amount of final surface concentration of fibrinogen can be tuned.

To selectively passivate the now hydrophobic glass surfaces, as well as the hydrophobic PDMS surfaces, a 4% (v/v) pluronic F-127 (PEG –PPO-PEG) block copolymer (Sigma), in 10 mM HEPES buffer pH 7.4, is infused through all inlets. The

PPO block adsorbs strongly to the 18 chain hydrocarbon pattern through hydrophobic interactions, however is repelled from the charged primary amine surface.

Further covalent modification of the primary amine pattern is accomplished first through conversion to a free carboxylate group by addition of excess (200 mM) succinic anhydride in 100 mM bicarbonate buffer pH 9.0. The free carboxylates are converted to activated esters via EDC/sulfo-NHS (200 mM and 10μM, respectively) in a 100 mM MES buffer pH 6.3. Finally, 100 $\mu g\ ml^{-1}$ human fibrinogen (hFg) in 35 mM PBS is infused, resulting in a chemically stable amide bond linkage between the protein and the surface (figure 7c). Protein linkage is followed by a 60 min PBS wash to remove any unlinked protein from the surface (figure 7d).

All experiments are performed when bacteria reach early log phase (OD_{600} = 0.3) to control for possible differential adhesin expression as a function of growth phase.[57] The bacterial suspension is washed twice with PBS, then diluted tenfold in PBS and stained with both DAPI (5 $\mu g\ ml^{-1}$) (live stain) (Invitrogen) and Sytox green (2 $\mu g\ ml^{-1}$) (dead stain) (Invitrogen). After incubation, the cultures are perfused through the device in perfusion mode at varying flow rates and fluorescent images are taken on a Nikon Ti Eclipse inverted microscope with a CoolSnap HQ2 cooled CCD camera.

For clustering data, images are analyzed in Nikon Elements Advanced Research software package. The images are first cropped in Adobe Photoshop to isolate the functionalized region of the microchannel, then run through an intensity thresholding algorithm in Nikon Elements, calculating the area (in μm^2) of the region corresponding to greater than an intensity of 10,000 (AU). This area is divided by the whole cropped image area and reported (figure 8a).

Single colony adhesion data was processed via manual colony counting in Adobe Photoshop. The adhesion fraction (ppm) is calculated as the adhered number of single colonies divided by the total number of bacteria that passed over the surface (figure 8b).

All statistical analysis was performed using a welch's t-test for two populations with unequal variances. The statistical tests were performed using the R statistical analysis program (The R foundation for Statistical Computing).

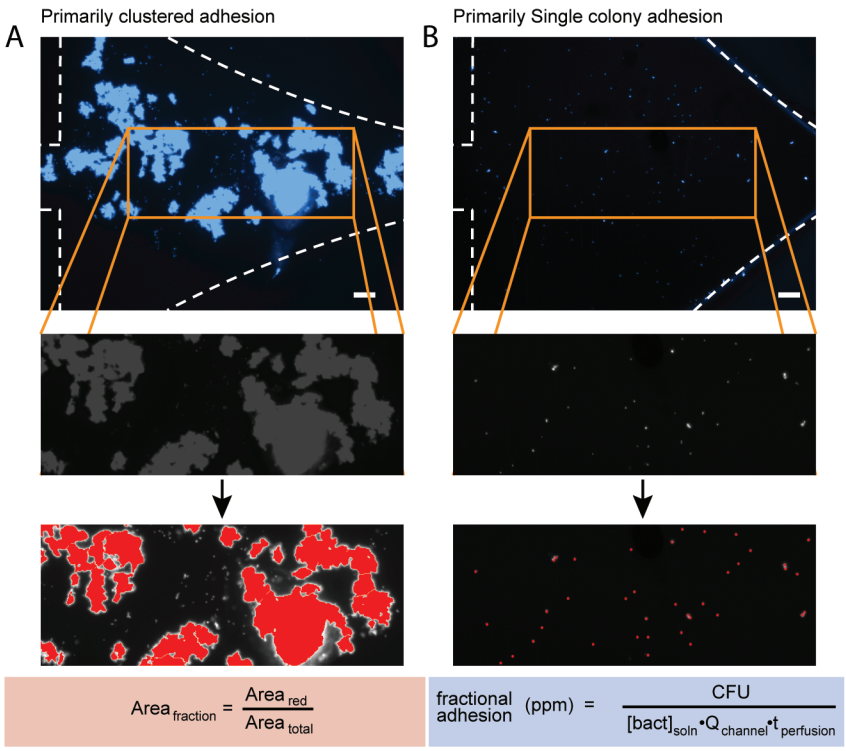

Figure 8: Methods of image analysis to quantitate large clusters of adhered bacteria and single colonies. A: Large cluster area fraction was calculated using an intensity thresholding algorithm, dividing the thresholded area by the total field of view area. B: Single colonies were identified by intensity thresholding, however they were counted in number per area, and reported as the fraction of total bacteria that passed over the surface, given concentration, flow rate, and time.

In order to create a high fidelity molecular surface pattern in the platform, it is necessary to actively reject both protein adsorption and non-specific cellular attachment off of the patterned area. Initially, it seems unnecessary to pattern the channel walls. However, as the shear stress in every part of the device is not the same, during attachment assays, or longer term detachment assays, bacteria may initially adhere upstream of the interrogation area and then detach and reattach in the field of view, thus obfuscating measurements. It is clear from figure 9a and 9c that *S. epidermidis* non-specifically interacts with surfaces that are not patterned with protein, necessitating active blocking of these surfaces.

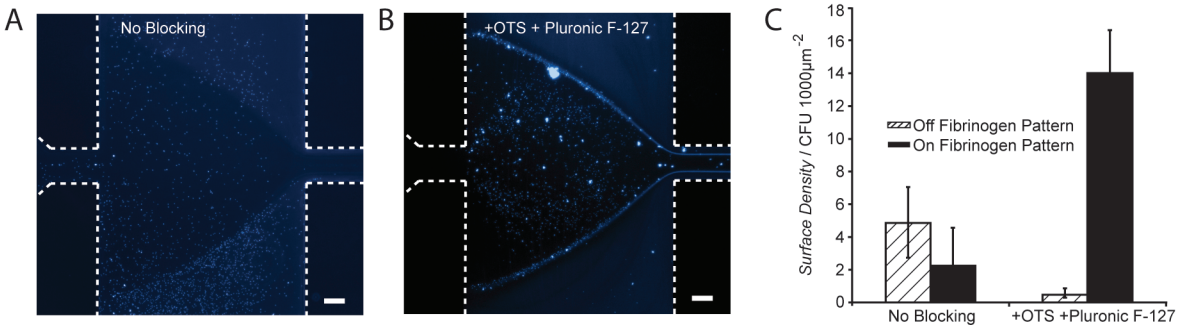

Figure 9: Specific surface chemistry for PEG based blocking is necessary for directing cells to the ligand pattern within the channel. A pluronic-based blocking method combined with hydrophobic silanization of the glass channel surface sufficiently blocks the adhesion of *S. epidermidis* 12228.

PDMS surfaces can be modified utilizing silane chemistry after oxidation (just as glass surfaces), however the stability of these surfaces is limited over multiple reactions, and quickly returns to a hydrophobic state during processing to minimize surface energy.[58] In our platform, the PDMS walls return to a hydrophobic state after the first APTS linkage step and subsequent heating (figure 10). An mPEG-silane (MW 5000)

based passivation method is possible with PDMS and glass surfaces which have been oxidized immediately before the passivation reaction (figure 10 g,h), however when performed in our device this process does not successfully block adhesion (figure 10 c,f). This is most likely due to the additional bake step after the APTS linkage (as described in materials and methods) rendering the PDMS inert to silanization by increasing hydrophobic recovery, eliminating the effects of oxidation with oxygen plasma. However, when a hydrophobic based PEG grafting method is used, a successful pattern is achieved (figure 10 d,e,f). These unexpected differences between glass and PDMS reactivity after oxygen plasma are important to note when planning future functionalization approaches.

Here we create a simple and inexpensive two-step method to passivate both hydrophilic glass and native hydrophobic PDMS surfaces (figure 7a). Following initial reaction witih APTS, treatment of the channels with highly reactive OTS in dry EtOH renders any unreacted hydrophilic silanol-presenting surfaces hydrophobic. Secondly, the entire channel is treated with a triblock copolymer (PEG-PPO-PEG) Pluronic F-127 (Sigma). The poly(propylene oxide) blocks adsorb strongly to the octadecane groups on the surface via hydrophobic interactions, but are rejected from the positively charged primary amines. With this treatment, non-specific adsorption of bacteria is nearly completely rejected from any surface not patterned with APTS (figure 6b,c), thus further isolating bacteria-protein interactions.

In a separate experiment we investigated the ability to sequentially silanize surfaces, without detrimentally affecting initial immobilized chemistry. Pre-treatment of oxidized surfaces of glass and PDMS with APTS prior to an mPEG-Silane preserves the

ability to covalently conjugate fluorescently tagged protein onto the surfaces (figure 10 h), indicating that sequential deposition of silanes can be used to create a surface pattern.

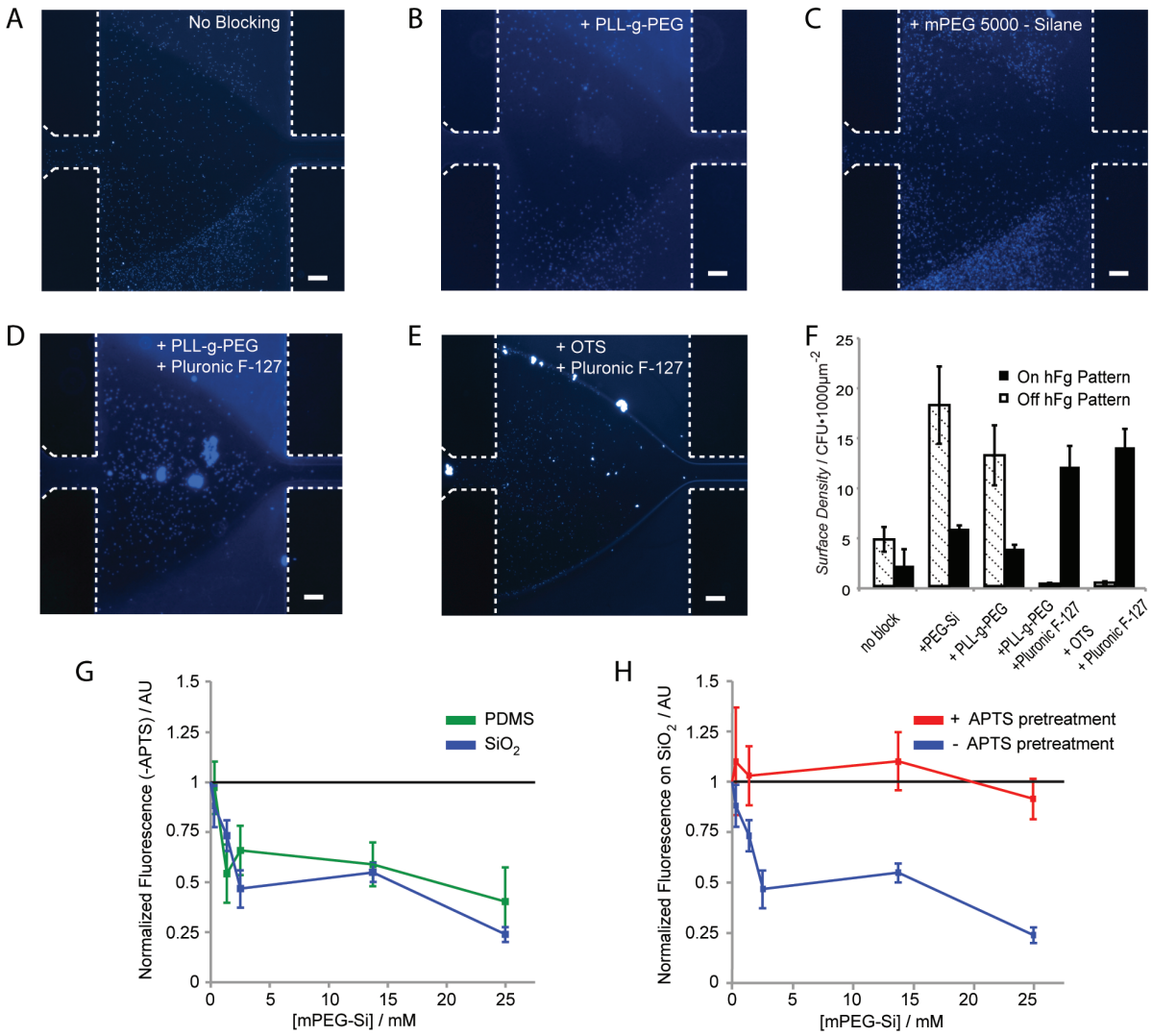

Figure 10: Summary of the various surface chemistries for blocking glass and PDMS channel walls from *S. epidermidis* 12228 adhesion.

The molecular interaction between *S. epidermidis* 12228 and hFg has been initially characterized as a function of shear stress in this novel platform. Interestingly, the adhesion of bacteria to hFg coated surfaces has two modes. Single colonies

adhere in high fractions at lower shear stresses and decrease with increasing shear stress, however, large clusters of bacteria adhere to the coated surfaces with a biphasic dependence on shear stress (figure 11 a). At low shear stresses, only small area fractions of clusters are observed, and the cluster area fraction increases with increasing wall shear stress toward the intermediate shear stress regime (~1 Pa). Above this wall shear stress, the cluster area fraction rapidly decreases to nearly no adhesion at 10 Pa wall shear stress.

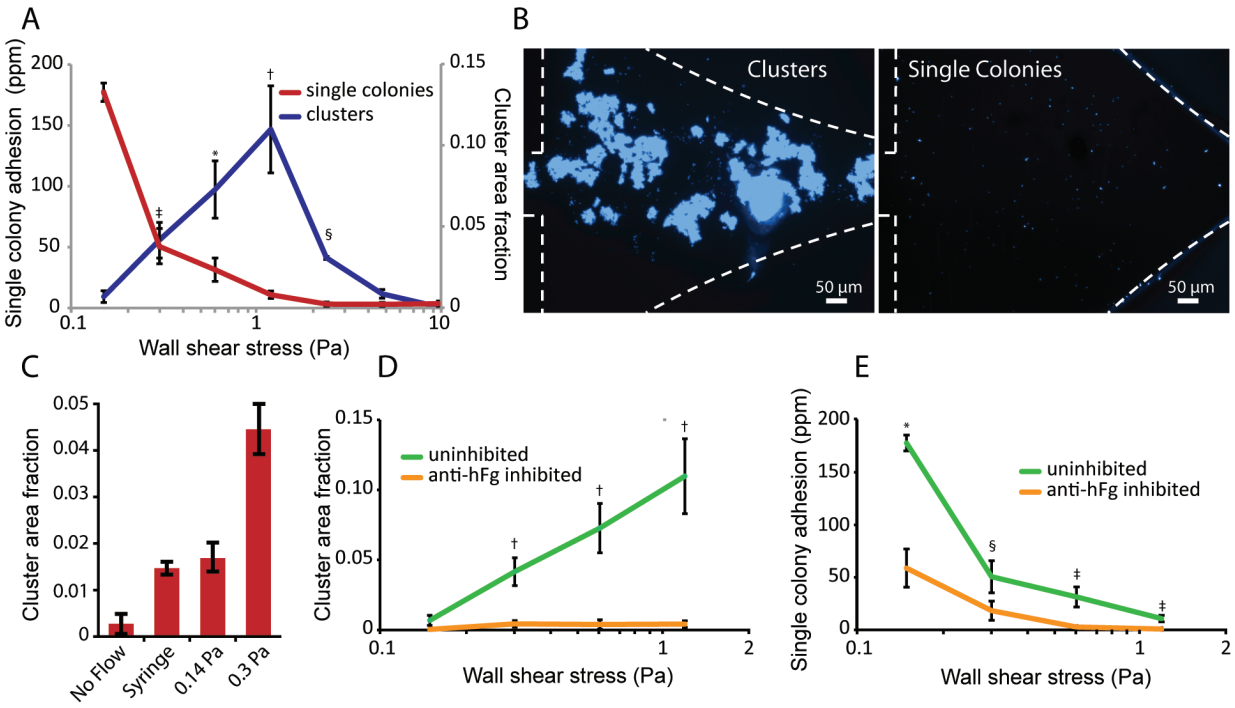

Figure 11: Adhesion of *S. epidermidis* to immobilized fibrinogen under flow occurs via two modes. At low shear, single colonies dominate adhesion, however at moderate shear stresses (~1 Pa) large cluster adhesion dominates. Both modes are specific for exposed fibrinogen epitopes on the surface (d, e).

To determine that cluster formation is not an artifact of particulate segregation at channel bifurcations in the device, multiple experiments were conducted with varying

inlet flow rates to offset the wall shear stresses in the device. The inlet flow rates were specifically chosen to be 2.25, 9, and 18 $\mu l\ min^{-1}$ so that there would be overlap between shear stresses between separate devices. A second control was performed to ensure that clustering was neither an artifact from vortexing bacterial suspensions after staining incubations or from flowing through the syringe and PEEK tubing (figure 11 c). There is statistical significance ($P<0.0025$) between no flow controls and syringe controls, indicating a role of shear flow in cluster formation. This shear induced cluster formation is further corroborated both by the functional dependence of cluster area on calculated shear in the device chambers, as well as the statistical significance between these cluster area fractions and the syringe control.

Adhesion of *S. epidermidis* 12228 to the patterned surfaces is dependant upon the presence of free hFg. Incubation of the patterned protein surfaces with anti-hFg in whole goat antisera prior to bacterial perfusion results in significant inhibition of adhesion, both for single colonies and clusters (figure 11 d,e). This supports the hypothesis of adhesin-dependant attachment of *S. epidermidis* 12228 to hFg coated surfaces via specific host-microbe interactions.

We have successfully developed a simple an inexpensive method for creating molecular patterns in a microfluidic shear device. The platform is advantageous in that it only requires syringe pumps to drive flow, with both functionalization and testing requiring a simple single layer device without valves. The basis of the pattern creation is the use of fluid flow boundaries and robust silane chemistry, such that initially homogenously reactive surfaces are converted to spatially resolved, orthogonally reactive surfaces, the reactivity of which are determined by the silanes themselves.

The method of *in situ* channel wall modification allows this platform to be expanded to many other assay types. As the molecules are covalently linked to the surface, preserving their overall structure, antibody and enzymatic assays, such as ELISA assays and cDNA immobilization for probe hybridization can be adapted well to this platform. The device design itself allows for easily increasing throughput both in terms of the number of parallel channels as well as the number of functionalization channels. By increasing the number of functionalization channels, more than two types of silanes could be linked to the surface in a spatially mutually exclusive pattern, creating a stripe type pattern similar to the bar code chips used to analyze protein concentrations in whole blood.[59]

Using this molecularly patterned shear attachment assay platform, we have begun investigations into the complex mechanisms of the attachment of *S. epidermidis* ATCC 12228 to covalently immobilized human fibrinogen. Molecular recognition is likely due to SDrG, as this is the fibrinogen adhesin present on this strain, and the treatment of the coated surfaces with an antibody against hFg significantly inhibits both cluster and single colony adhesion.

A previously unreported mode of attachment though cluster formation has been initially characterized on this platform. One hypothesis for the unique dependence of cluster attachment on shear stress considers two regimes. In the low shear stress regime, clusters may not form at all, and as shear stress increases, cluster formation is induced through a mechanism that is not yet understood. It is reasonable to postulate a shear activated cell-cell adhesion mechanism, as previous studies have implicated shear stress activation of the adhesion of uropathogenic *E. coli* to mannose containing

oligosaccharides via FimH.[60],[61] In the high shear stress regime, cluster attachment exhibits similar decay as single colonies in the low shear stress regime (figure 11 a), suggesting a similar mechanism of shear stress overcoming the total strength of binding, most likely involving multiple receptor-ligand interactions (avidity) per cell.

A more in depth and rigorous characterization of these adhesion mechanisms is necessary for a more complete understanding of *S. epidermidis* attachment to human plasma fibrinogen. This platform has the ability for dynamic characterization of bacterial adhesion-ligand interaction in physiologically relevant conditions. We are undertaking further evaluation of this complex interactions by creating mutant strains defective in various segments of the adhesin proteins. This can offer new perspectives on the design of anti-adhesin therapeutics to inhibit the initial stages of *Staphylococcal* colonization and pathogenesis.

The clinical relevance of this platform is in its potential use for investigation of novel anti-adhesive drugs that can prevent colonization and infection, as well as for further evaluation of the clinical isolates of pathogenic microbes. Integration of this platform into a clinical setting will enable correlation of adhesion profiles with clinical outcomes, allowing a more complete perspective on the roles that adhesins play during pathogenesis.

III. The induction of biofilm formation phenotypes by clinically relevant fluid flows in clinical isolates of *S. epidermidis*

S. epidermidis is a normal inhabitant of human skin and mucous membranes and is currently a leading cause of healthcare-associated infections (HAIs) [62]. This organism is a prominent colonizer of implanted polymer devices, including intravascular catheters [7]. Catheter-related bloodstream infections (CRBSIs) are a significant cause of morbidity and mortality in hospitalized patients, especially those with underdeveloped or weakened immunity [3].

Biofilm formation appears to be a key component in the pathogenesis of infections caused by *S. epidermidis,* among many other organisms responsible for device related infections including *S. aureus,* UPEC, and *Pseudomonas*. Previous reports suggest that there is a preferential ability of certain strains of *S. epidermidis* to cause infection, and that biofilm formation is a promising therapeutic target for CRBSI [63–65]. Many *S. epidermidis* biofilms are largely composed of the polysaccharide intercellular adhesin (PIA), a poly β 1-6 N-acetylglucosamine [66], production of which is associated with the upregulation of the chromosomal *icaADBC* gene cluster [67]. *S. epidermidis* isolates display strain to strain variation in PIA-dependent biofilm production. The two main groups are those lacking the *ica* locus (*ica*-), which are unable to form PIA-based biofilms, and those containing *ica* genes (*ica*+). Within the *ica*+ group are strains that constitutively secrete PIA (biofilm^{c}), strains that do not produce PIA under any *in vitro* conditions that have been tested (biofilm^{-}), and strains that can be induced (biofilm^{i}) to secrete PIA by alcohols, thought to simulate a heat shock-like response by unfolding native proteins, and osmotic stressors such as NaCl [68–70]. It is important to

note that some clinically isolated strains have been shown not to fit in these categories. Specifically, there are those that lack the *ica* locus and are still able to form biofilms after significantly longer culture periods than *ica*+ strains [71,72], as well as *ica*+ strains that have the insertion sequence IS257 in *icaA* [73,74]. These biofilms contain primarily proteinacious, rather than PIA-based, matrices. In our clinical isolates, however, biofilm formation is PIA-mediated.

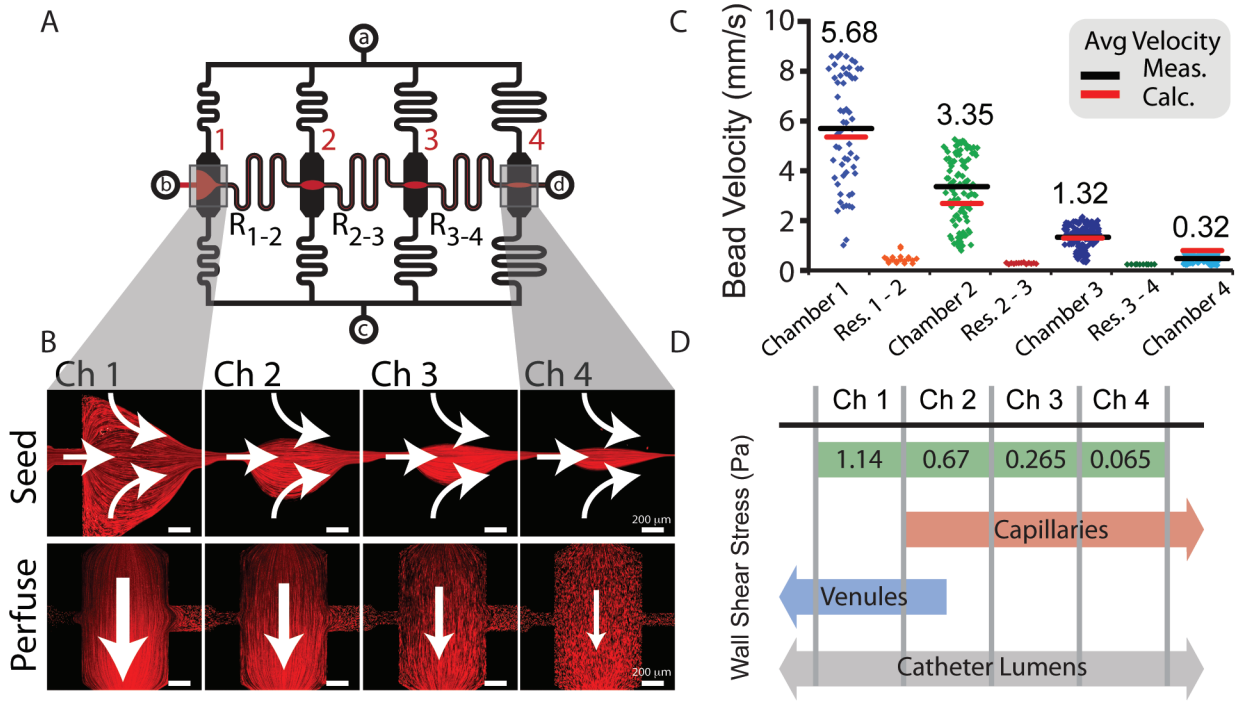

Figure 12: Device schematic. A: Four chambers are connected in parallel, with a side channel connecting them for cell seeding. B: device operation (1 μm red fluorescent beads in flow). C: Shear stresses calculated via bead velocity measurement. There is n osignificant crosstalk between channels during operation. D: Shear ranges in the cardiovascular system, as well as various catheters.

The catheter microenvironment, where biofilm formation is key for establishing infection, is an inherently mechanical environment characterized by fluid flow and shear

stress. To better understand the role of these fluid-induced stresses on biofilm formation, we used a parallel microfluidic device [75] that directs planktonic cell adhesion to isolated chambers within micro-channels (red in figure 12a, b), and subsequently exposes multiple sessile populations of bacteria to well-defined fluid flows and shear stresses in a single experiment, with no crosstalk between shear stress chambers connected in parallel (figure 12c). The shear stresses applied in the microfluidic biofilm assay ranged from 0.065 to 1.14 Pa in a single experiment (figure 12 d), representing wall shear stresses present in capillaries and venules (between 0.05 Pa and 4 Pa) [29,76], and catheter lumens (0.02 to 3 Pa in a typical 1.9 Fr catheter). The spectrum of shear forces acting in catheters under normal operating conditions of flow rates from 1 – 10 mL/hr was determined using fluid flow models of both single and double lumen catheter sections we created using COMSOL Multiphysics (figure 13). We investigated a variety of clinical isolates of *S. epidermidis* to determine the potential variation in PIA-based biofilm formation in response to clinically-relevant fluid forces experienced by *S. epidermidis* during pathogenesis.

Two ATCC strains representing *ica*- (12228) and *ica*+ (35984 or RP62A) *S. epidermidis* were used as a negative and positive control, respectively, for PIA-based biofilm formation. Five clinical isolate strains previously isolated and described by Milisavljevic et al. were also used, all containing the *ica* locus, and representing distinct PIA-forming biofilm phenotypes [31]. The PIA negative group is represented by strain A-10, the constitutive PIA-based biofilm formers are represented by A-26, and the inducible strains are represented by A-5, W-166, and Z-173.

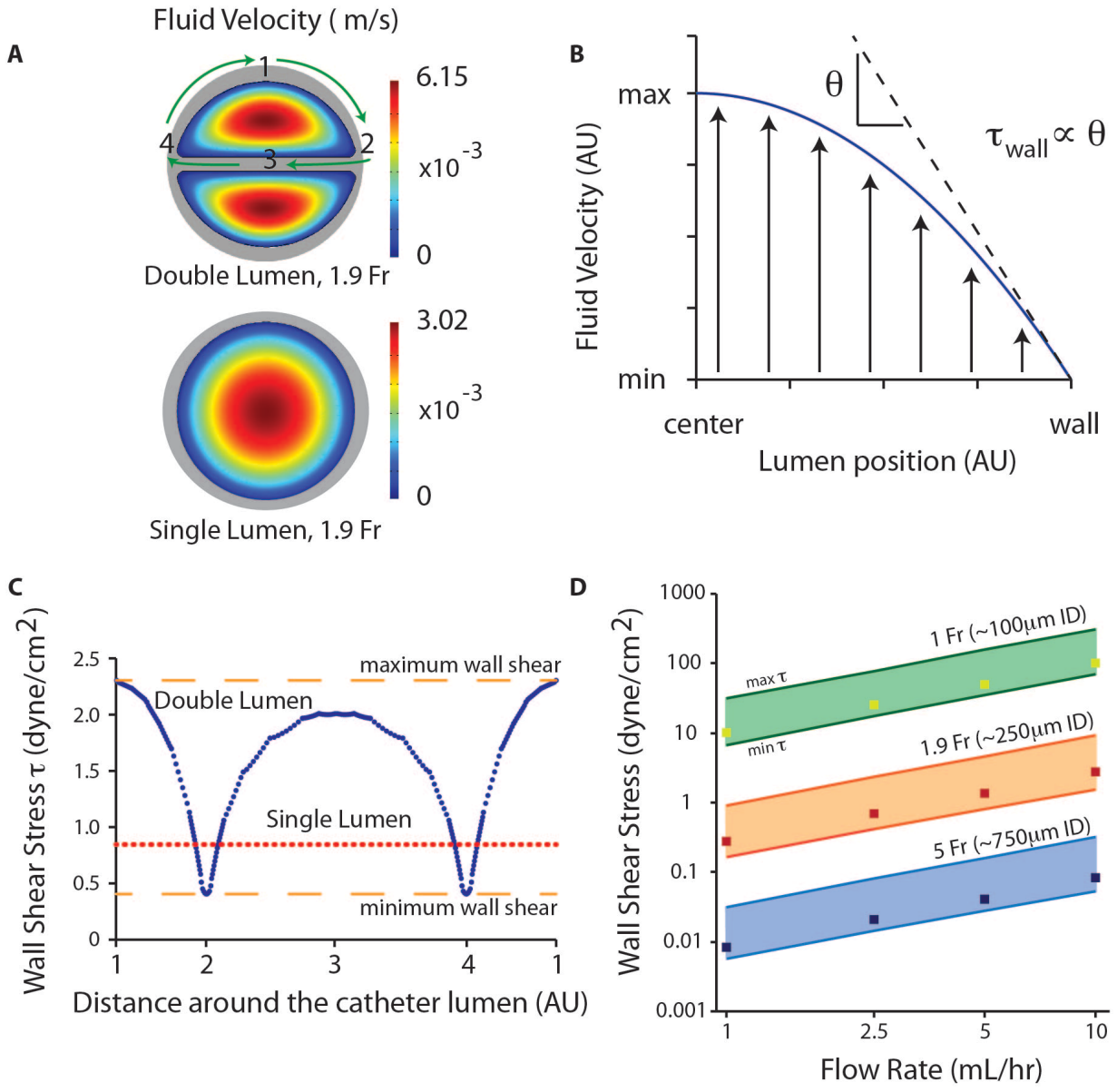

Figure 13: Finite element modeling of complex catheter lumen shapes to extract shear stresses present during normal operating procedure in the clinic.

Bacteria were grown for overnight culture in Tryptic Soy broth with 2.5% Glucose (Sigma) in a shaking incubator at 240 RPM and 37°C. Frozen stocks were kept at -80°C in 25% glycerol, and streaked onto 1.5 % Tryptic Soy Agar (Sigma). Isolated colonies were subsequently picked for overnight broth culture prior to biofilm

experiments, and grown to OD_{600nm} = 0.6 before washing with PBS and resuspending 1:10 in PBS prior to inoculation in the microfluidic biofilm assay.

Semi-quantitative microtiter plate assays for biofilm formation were performed as previously reported [31]. Overnight cultures grown in Tryptic Soy Broth (TSB, Becton Dickenson) were diluted 1:100 in culture medium, and 200μl was plated in a flat bottom polystyrene 96 well plate (Greiner Bio). For experiments using EtOH induction, overnight cultures were diluted 1:100 in culture medium containing 1 – 4 % v/v EtoH, and grown for 12 hours. Subsequently, these subcultures were diluted 1:100 in the respective induction medium and plated in triplicate in well plates as described above. Biofilms were grown for 24 hours, then washed with sterile water, fixed with methanol (Sigma), and stained with 2% crystal violet (Sigma). Well absorbance was measured at 570 nm using a plate reader system (Tecan Infiniti F200). Fold increase in biofilm in these experiments were presented as a ratio of the well absorbance relative to negative control wells where no bacteria were seeded.

The device utilized for this study operates in two modes: (i) seeding of bacteria in a pattern to areas of known shear, and (ii) subsequent exposure of isolated populations of sessile bacteria to shear. All flow is achieved using a syringe pump (Harvard apparatus) and plastic syringes (Becton Dickenson), connected to devices using PEEK tubing (Upchurch Scientific) and luer lock stubs (Fisher).

Prior to seeding, channels were converted to a hydrophobic state utilizing a slight modification of our previously published method of *in situ* silane chemistry [75], using an octyl(tri-ethoxy)silane (OTES).

Bacteria were seeded in a specific pattern within the device by using a modification of the functionalization setup previously described [75]. Briefly, devices were pre-equilibrated with phosphate buffered saline (PBS) pH 7.4 prior to seeding bacteria in the chambers. To seed, bacteria were injected into inlet (b), while PBS was injected into inlets (a) and (c). Seeding was performed for 1 hour then the device was converted to perfusion mode by blocking inlet (b) and outlet (d). Perfusion was carried out in a 37°C incubator, flowing TSB with 2.5% glucose at 18 μl/min for high flow rate devices, and 4.5 μl/min for low flow rates.

After perfusion for 6, 12, or 24 hours, biofilms in the microfluidic assay were first washed at 4°C with PBS at 18 μl/min or 4.5 μl/min for 20 min and fixed by flowing through 400 μl of 4% paraformaldehyde at the respective flow rate used for culture. The devices were incubated at 4°C for 12 hours, and then washed with 400 μl of PBS at 10 μl/min.

PDMS/Glass milli-scale wells were created to allow culture of biofilms without flow while maintaining the same substrate materials and surface modifications present in the microfluidic devices. These wells were constructed by pouring thin (~ 5 mm) strips of PDMS. Wells were punched in these strips using a 1 mm diameter biopsy punch, and the wells were bonded to 18 mm diameter glass coverslips (Fisher) using O_2 plasma, resulting in wells with ~ 5 μl volume. These wells were then placed in the bottom of a 12 well flat bottom plate (Greiner Bio). Bacteria were seeded in these wells by washing overnight cultures (OD_{600} = 0.6) 3 times in PBS and resuspending 1:10 in PBS. Wells were seeded for 1 hour, and then the well plates were aspirated, washed with PBS, and filled with either TSB, or TSB supplemented with 4% v/v EtOH.

To collect cells after culture within the microfluidic device, cells were physically excised. To accomplish this, devices were disconnected from media flow after 24 hours of culture, and the outside surfaces of the devices were washed with 70% EtOH and dried using a Kimwipe. A razor scalpel was flame sterilized, and used to cut out a hole in the PDMS above each chamber in the device. A sterile 10μl pipet tip was used to scrape cells from the exposed chamber inner surfaces, and these cells were streaked onto Tryptic Soy Agar plates and grown at 37^0C for 18 hours. Single colonies were picked from these plates and used for further screening using microtiter plate assays.

All staining was performed in 4°C, using a flow rate of 10 μl/min for total volumes of 400 μl for microfluidic staining, and by adding 5 μl of solution to the milli-wells. PIA was stained for 3 hours using a 100 μg/ml solution of FITC labeled Wheat Germ Agglutinin (WGA) (Sigma) in PBS pH 7.4 with 0.5% BSA. Bacterial cells were stained using DAPI (Sigma) and Ethidium Homodimer I (EtHDI) (Invitrogen) diluted to 1 μg/ml in PBS containing 1% ascorbic acid. Biofilms were stained for 30 min with DAPI and EtHDI, then visualized using a Nikon Ti inverted widefield fluorescence microscope with a quantitative gray scale cooled CCD camera (Coolpix) or a Nikon A1 Confocal Laser Scanning Microscope (CLSM).

Crystal violet staining in microtiter plates detected biofilm irrespective of matrix composition whereas in the microfluidic assay we stained specifically for PIA. As those strains able to form biofilms in microtiter assays directly correspond to those stained specifically for PIA, this indicated biofilms including a significant PIA fraction, and PIA staining was used as a surrogate for biofilm formation.

Fold increase in area stained by FITC-WGA was used to quantify biofilm accumulation in microfluidic assays and milli-well plate assays. To obtain these values, images were taken at the same exposure time (1 sec) under a 20X magnification using an extra long working distance dry Nikon objective. Each chamber in the microfluidic biofilm assay was captured by taking 20 images and stitching them together (5 wide X 4 high).

Using a postprocessing intensity thresholding algorithm in the Nikon Advanced Research software package (version 3.2), pixel area with intensity values above a threshold (corresponding to biofilm matrix) within the chamber are quantified, and presented as a ratio to the area stained by the FITC-WGA immediately after seeding prior to perfusion (example images are shown in the panels in figure 14a). There is a background level of staining for non-biofilm forming strains likely due to the polysaccharides on the cell surface, however, biofilm and cells not forming biofilm are still well resolved. Fold increases < 1 indicate a reduction in the number of cells on the surface, increases between 1 and 5 indicate cell growth, whereas increases > 5 indicate biofilm production.

All statistical tests were performed using variations on the Student's t-test. To compare different conditions and/or strains, the t-test comparing two populations of unequal variances was used. To determine if any condition led to significant biofilm induction (compared to 1), t-tests comparing a population to a specified value were used. All data are presented as averages of at least three experiments, with all error bars showing standard deviation about the mean.

Using conventional microtiter plate assays, we verified that the strains used in this study represent the three main biofilm phenotypes. Clinical strain A-26 (*ica*+, biofilm^{c}) formed strong biofilms under standard conditions, similar to ATCC 35984, whereas strains A-10 (*ica*+, biofilm^{-}) and ATCC 12228 were unable to form biofilms, irrespective of culture conditions (figure 14a). Strains A-5, W-166, and Z-173 (*ica*+, biofilm^{i}) were all induced to form biofilms upon supplementation of media with ethanol (figure 14b).

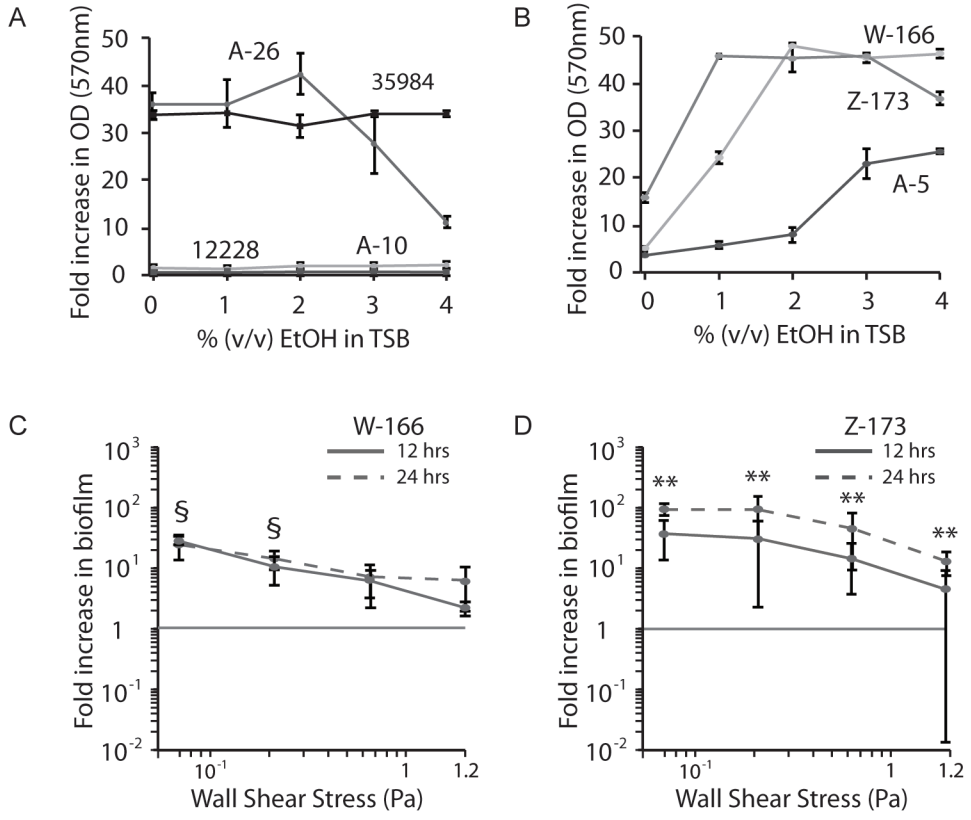

Figure 14: A,B Microtiter plate assays for biofilm formation suing crystal violet as readout. Ethanol is used to elicit a biofilm induction in these experiments. C,D Clinical strains representing strains isolated from the NICU less frequently than A strains.

After culturing bacteria under fluid flow for 6 hours, the constitutive ATCC strain 35984 produced PIA-positive biofilms across all shear levels, while the *ica*- strain ATCC 12228 produced no biofilms at any shear (figure 15a). Biofilm was quantified as the ratio of the chamber area stained by WGA compared the baseline just after seeding and prior to exposure to shear, presented as fold increase in figure 15d. This measurement reflects biofilm accumulation in each chamber respective to that chamber's initial condition, and accounts for the differences in seeding pattern shapes between chambers, resulting from fluid flow during seeding (figure 15a). To characterize initial conditions in our microfluidic channels, we demonstrated that although the patterns were different sizes (figure 15b), the surface density of bacteria remained the same, averaging 1 CFU for every 2 μm^2 (figure 15c).

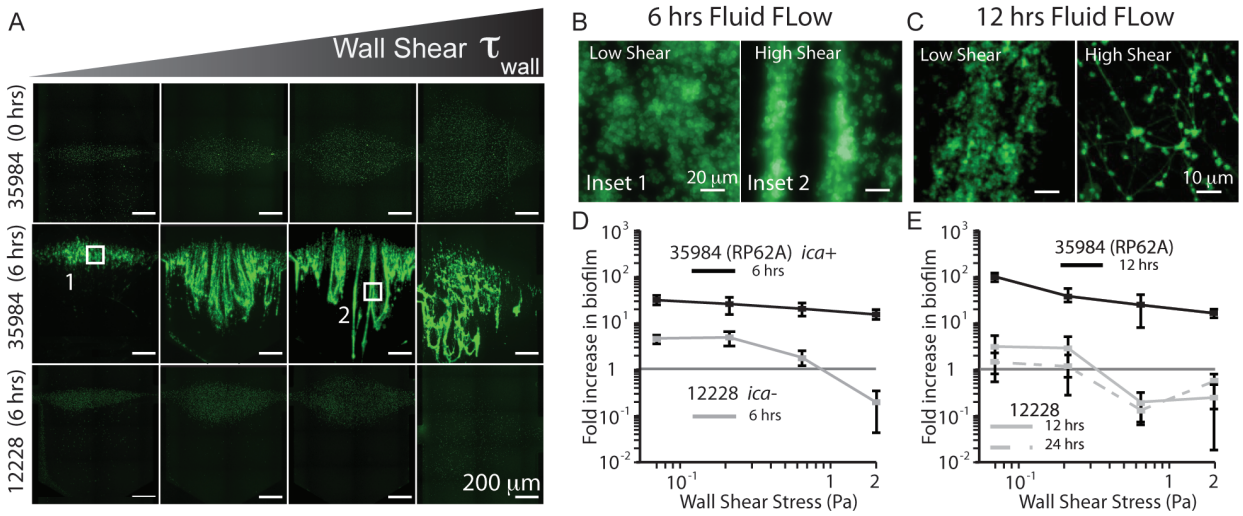

Figure 15: A,D,E: Laboratory strains grown under flow in the microfluidic assay. Strain 35984 is a positive control for biofilm formation, whereas strain 12228 is a unable to form biofilm. B,C: for 35984, shear stress level effects biofilm structure.

Due to non-zero staining of 12228, our metric of fold increase in the area stained by WGA allowed measurement of the amount of cells present on channel surfaces after

shear. Figure 2D indicates that 12228 cells were able to multiply on the surface at low shear, but numbers actually decreased over time at higher shear (fold increases < 1), indicating that cells were detached from surfaces under these conditions.

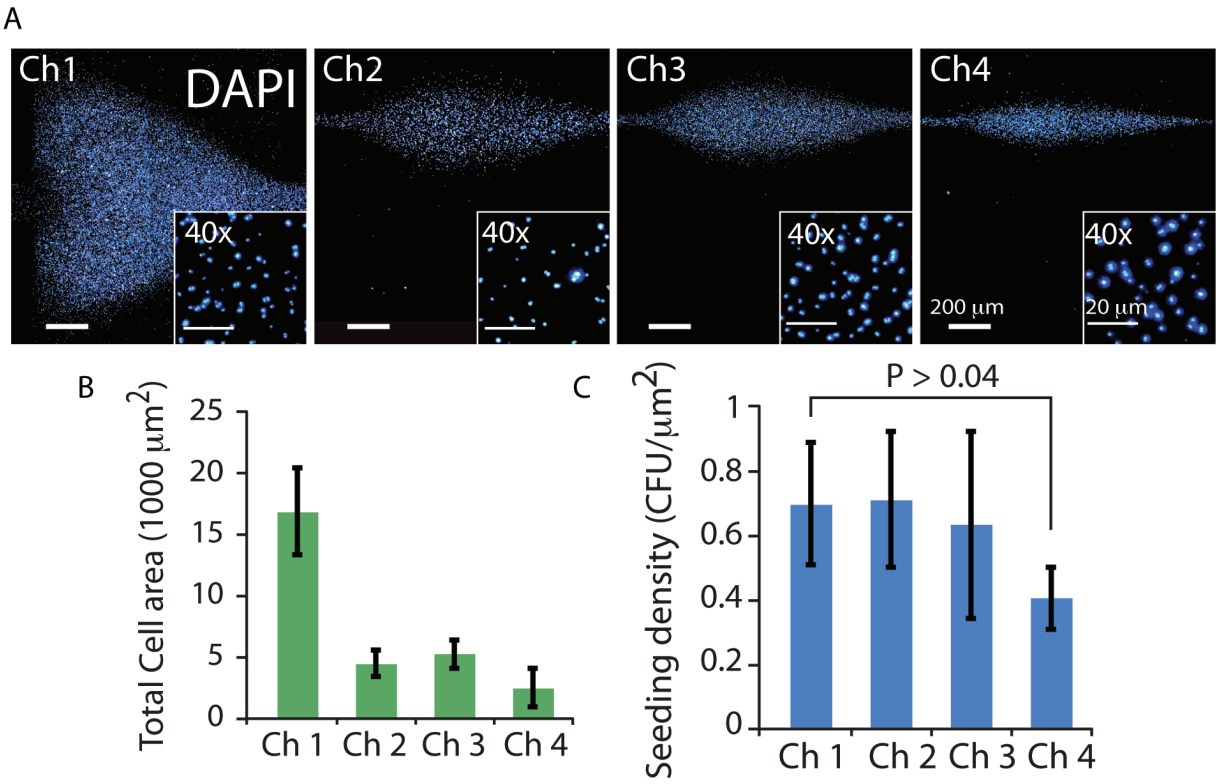

Figure 16: A: Fixed, adhered *S. epidermidis* 12228 cells on the microfluidic channel surface. B: Total cell area (number of cells) decreases with increasing chamber number, but (C) cell surface density is preserved.

PIA biofilms produced by the constitutive strain 35984 at low fluid flow displayed an isotropic structure (figure 15b, inset 1). In contrast, higher shear resulted in biofilms with aligned PIA streamers of ~20 μm in width extending in the direction of flow (figure 15b, inset 2) and loop structures under the highest shear (figure 15a). These architectural differences in shear-dependent biofilm formation became more evident with increasing time. After 12 hours of culture, large (~40μm) streamers formed at low

shear, and a web-like PIA matrix architecture connecting small, dense colonies was observed at high shear (figure 15c).

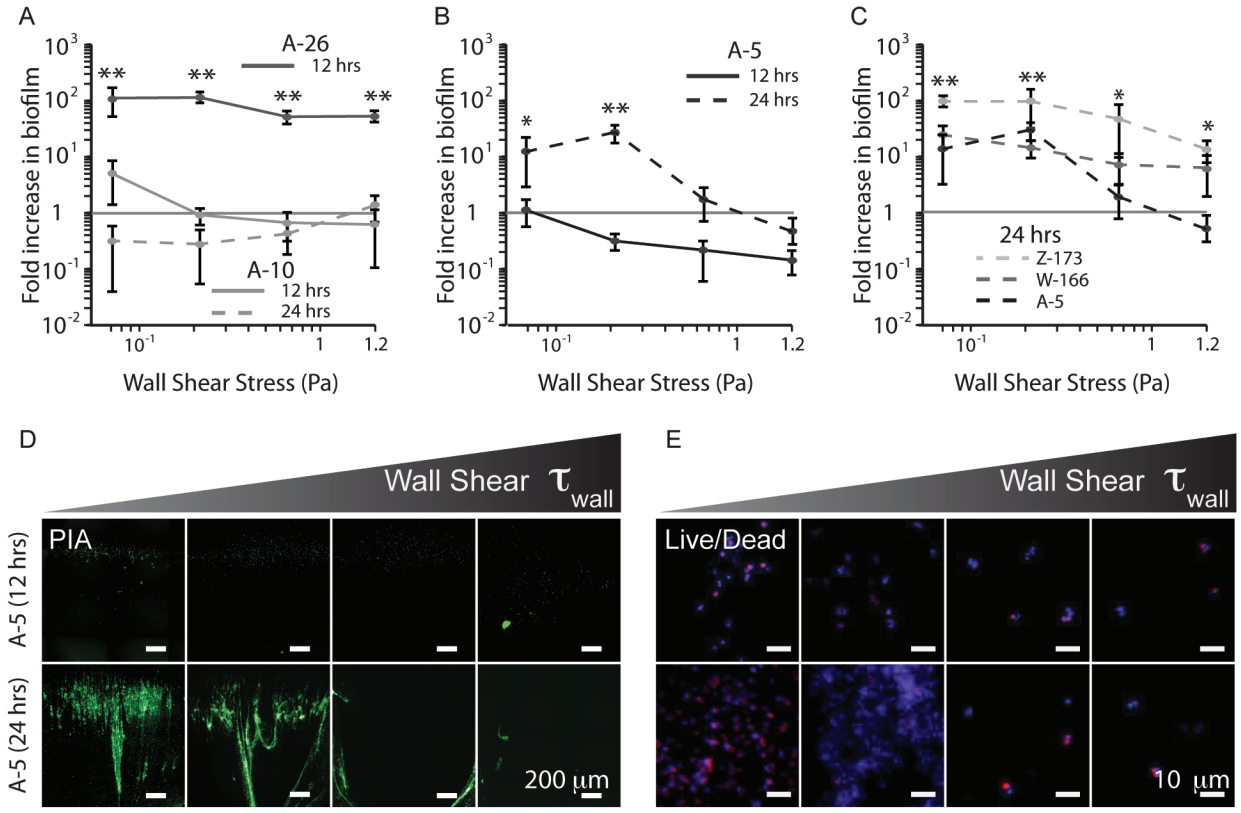

Figure 17: Clinical isolates of *S. epidermidis* display a range of biofilm phenotypes under flow. B,D,E: Strain A-5, normally not forming biofilm in a well plate, forms significant biofilm under moderate shear in the microfluidic assay. C: Other strains of *S. epidermidis* displaying a shear induced response.

Over longer culture periods of 12 and 24 hours, 35984 continued to produce substantial biofilms across the spectrum of fluid flow, while, as expected, 12228 did not form biofilms (figure 15e). Using our microfluidic device, we were able to quantitatively measure the phenotype of biofilm formation under flow for these well characterized ATCC strains with high confidence ($P<0.01$ for all shear stresses when comparing

35984 and 12228). These results laid the groundwork for assays using clinical isolates with a broader range of biofilm phenotypes.

The clinical isolates A-26 (*ica* +, biofilm^{c}) and A-10 (*ica* +, biofilm^{-}) displayed similar PIA-based biofilm formation phenotypes under flow as 35984 and 12228, respectively. A-26 displayed ~100 fold increase in PIA matrix over all shear stresses after only 12 hours of shear, whereas A-10 was unable to form biofilms after 24 hours (figure 17a). Both of these strains contain an intact *ica* locus, however, they display drastically different PIA-based biofilm formation phenotypes in both static and flow culture.

Unexpectedly, upon exposure to fluid flow and shear (instead of ethanol, the usual inducer), strain A-5 (*ica*+, biofilm^{i}) formed significant PIA biofilms (figure 17b,d,e). After 12 hours of exposure to fluid flow, A-5 had viable cells on the channel surface (figure 17e) but displayed no significant change in PIA secretion (figure 17b). However, after this initial lag phase, there was significant production at 24 hours of culture and 0.265 Pa (figure 17b) compared to A-10 (biofilm^{-}) ($P < 0.005$).

Other ethanol-inducible strains (W-166 and Z-173) also formed PIA biofilms when exposed to fluid shear alone. These strains formed biofilms across a broader spectrum of shear stresses than A-5 (figure 17c, figure 14c,d) resulting in larger biofilms at higher shear ($P < 0.03$). Interestingly, in comparison with A-5, successful biofilm formation at higher shears in these strains corresponded to a stronger induction by ethanol in microtiter plates (figure 14b).

Further investigation of fluid flow-mediated biofilm formation in A-5 revealed a bi-phasic dependence on shear stress (figure 18). Quantification of the fold increase in

secreted PIA matrix showed that at low enough shear (0.016 Pa), A-5 cultures no longer yielded WGA signals that were significantly different from the PIA negative control (A-10) at 0.167 Pa ($P > 0.25$). This result is also consistent with the fact that A-5 does not form biofilm in static culture. Notably, as observed for A-10 (figure 18c) the inability to secrete PIA does not prevent cells from adhering to the channel surface, as there were still viable cells in the channel following 24 hours of culture.

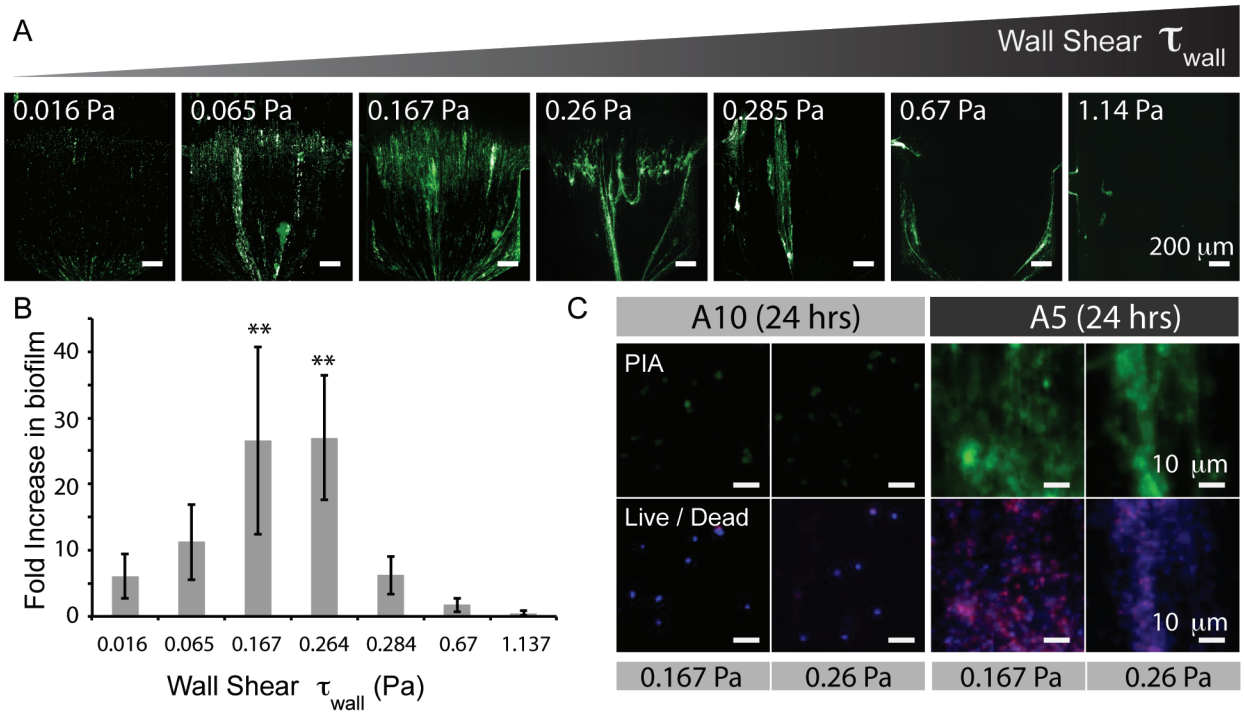

Figure 18: Strain A-5 displays a biphasic dependence of biofilm formation on fluid shear stress. A: Representative images of complete range of shear stresses assayed. B: Quantitation of biofilm formation over two orders of magnitude in shear. C: Strain A-10 is unable to form biofilm under flow, however cells remain on the channel surface after 24 hours.

Our results suggested PIA secretion in A-5 was a result of fluid shear, however, it was unclear if this was induction of a phenotype, or selection of a low frequency pre-

existing mutant genotype. To address this question, we harvested biofilms from the device to characterize their induction by EtOH without flow.

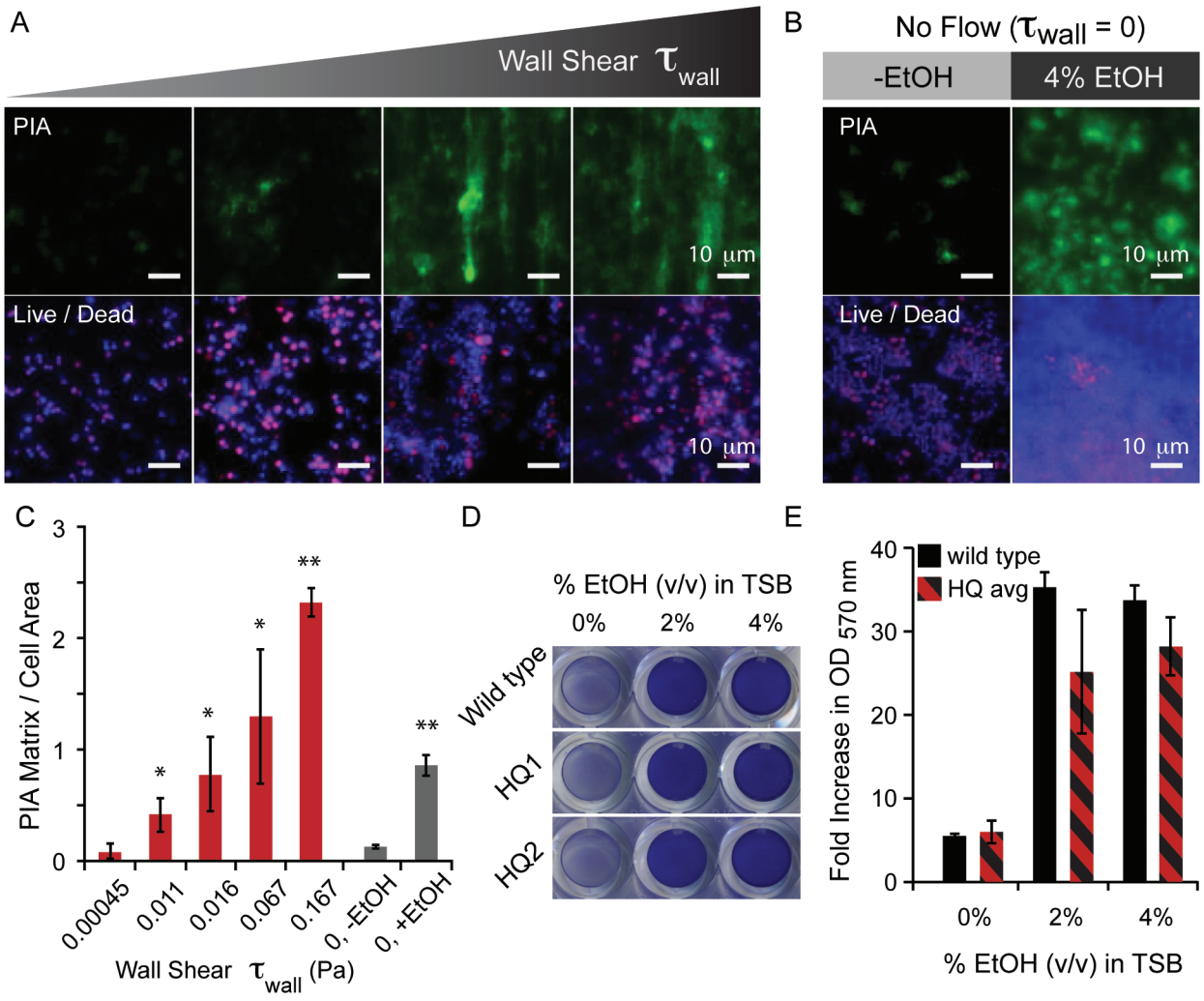

Figure 19: A-C: Extremely low levels of fluid shear results in no significant biofilm formation by A-5, yet cells remain on the channel surface. D,E: Removal of cells forming biofilms results in a reversion to wild type biofilm phenotypes without flow.

Cells from shear-induced biofilms that were excised from the device maintained the wild type A-5 phenotype in microtiter plate assays. Six clones from 2 separate devices were harvested from the channels after exposure to conditions resulting in induction (0.167 Pa) and assayed in microtiter plate format. Each clone, secreting

significant PIA under shear, was unable to form biofilms when grown in media without flow and all were induced to form biofilms with the addition of 2% and 4% EtOH, showing no significant difference from wild-type (figure 19c and e and figure 20). Further, assaying A-5 in device at very low shear stresses (0.0045 Pa) resulted in no statistical difference ($P>0.25$) from A-5 grown without flow (figure 19 a-c) in terms of PIA matrix per cell area, and this readout increased with increasing shear stress in our device ($P<0.01$).

The fluid flow microenvironment plays a significant role in the production and architecture of *S. epidermidis* PIA-positive biofilms. Table 1 summarizes the biofilm formation phenotypes of the *S. epidermidis* strains tested in this study under normal culture conditions, as well as under ethanol stress and fluid shear. In strains constitutively producing PIA, the presence of fluid shear results in the formation of biofilms streamers, with higher shear leading to faster streamer formation. These structures were likely a result of the local fluid flow environment, as 'streamers' in *P. aeruginosa* have been observed by Rusconi et al. to be influenced by local fluid streamlines in curving flows [77,78].

After 12 hours of culture, markedly different PIA matrix structures formed, with more homogenous and dense matrices at lower shear, and complex web-like structures at higher shear. This may have important implications concerning the potential of these strains to cause infection and their susceptibility to antimicrobial treatments, the effectiveness of which can be reduced by altered metabolic profiles in the biofilm [79,80].

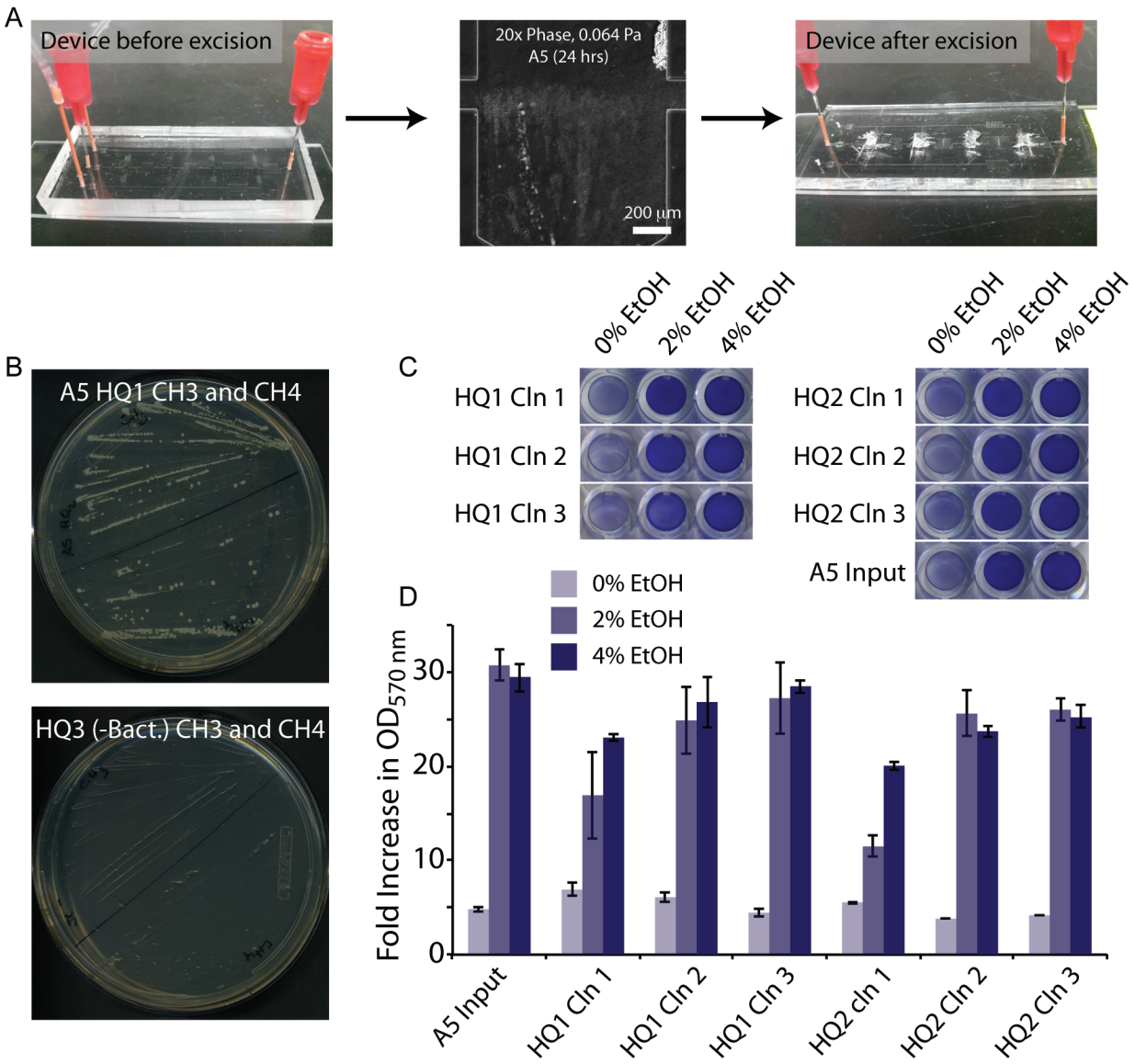

Figure 20: Collection of cells forming biofilms under flow. After removal of A-5 cells from flow and growing in normal *in vitro* culture conditions, the cells revert to a wild type biofilm formation phenotype.

Correlation between microtiter plates and microfluidic devices showed that PIA is the main matrix component for the strains used in this study. Microtiter plates detected biofilms irrespective of matrix composition. In contrast, staining in the microfluidic device was specific for PIA matrix. If strains were observed to be biofilm^{+} in microtiter

plates and biofilm$^-$ in the microfluidic device, this would indicate PIA was not the main component. This was not the case in our experimental conditions, showing that PIA is the main matrix molecule.

Most importantly, we have demonstrated that clinical strains of *S. epidermidis* shown to produce biofilms when exposed to alcohols (A-5, W-166, and Z-173) are also induced to secrete PIA when exposed to fluid shear alone. Specifically, for strain A-5, we have shown no significant PIA to be present at very low to no fluid shear, whereas PIA matrix production increases significantly with increasing shear stress. This trend was observed when considering either total PIA or PIA matrix normalized by the number of cells present in each measurement. Secondly, we show that the same cells that produce significant PIA under flow revert to a wild-type phenotype when excised from the device and grown in microtiter plates. This strongly supports the hypothesis that PIA production is induced by the environment rather than selection of a stochastically arising subpopulation of cells that were expressing high levels of PIA and potentially would stick better to the substrate.

Previously, Yarwood et al. have shown that *agrD* mutants in *S. aureus* form stronger biofilms than wild type when grown under static culture, however, no differences were observed when grown under flow [33]. We hypothesize that this may result from fluid flow washing away soluble quorum sensing molecules, mimicking the environment created by a Δ*agrD* background. From our results and these previous data, we speculate that fluid flow induction may occur through two mechanisms: (i) mechanical sensing of fluidic forces at the cellular level and/or (ii) quorum sensing dysregulation by convective transport of soluble molecules away from cells.

Regardless of the mechanism, the induction of PIA-positive biofilms in *S. epidermidis* by fluid shear is strain dependent, enabling bacteria that do not produce biofilms under static conditions to increase their pathogenicity by secreting PIA, solely due to experiencing fluid shear. This is particularly relevant as the fluid shear stresses we have shown to induce PIA secretion are present in catheters under normal operating conditions. Our results warrant further investigation into the molecular mechanisms involved in the regulation of biofilm formation, as well as a reconsideration of catheter luminal designs and operation, with mechanical forces in mind.

IV. Developing a next Generation Functional High Throughput screen for 'Pathogenicity Landscapes' of adhesion and biofilm formation

It is clear, both from the data presented in chapters I and II as well as data obtained in the past few years by others, using biochemical, genetic, and well plate assays, that the paradigm of implanted device related pathogenesis is increasingly complex and convoluted. Adhesion of both *S. aureus* and *S. epidermidis* to immobilized host proteins including fibrinogen and fibronectin are specific interactions and contribute to the colonization of abiotic surfaces *in vitro*. Our previous experiments using microfluidic devices have demonstrated that clinically relevant shear forces from fluid flow can modulate both the magnitude of cells that can adhere to a surface, as well as the mode by which they adhere. Further, the presence of these shear forces appear to induce the formation of more biofilm in clinical isolates of *S. epidermidis* that do not form biofilm under normal conditions in a well plate.

After compiling pathogenic modulation by alcohols, osmotic stress, oxidative state, quorum sensing, and now fluid flows, what is left is the question: 'What now?' The scientific community has a wealth of information, however when we attempt to put it all together the holes become evident. For example, the Sar family of transcription factors in Staphylococci has been implicated in biofilm formation, adhesin expression, quorum sensing autoinducer production, and toxin production however the overall effect of sarA on biofilm phenotypes remains under debate[81,82]. Upstream of these in the environmental sensing cascade is thought to be σ_B, a global regulator for environmental signaling, which has also been implicated in infection[83]. This all fits accordingly to the data acquired from a few model strains, however clinical strains of both *S. aureus* and *S.*

epidermidis display a vast assortment of phenotypic responses to environmental stresses. Specifically, the strain set of *S. epidermidis* acquired by V. Milisavljevic over a period of 1 year from the Neonatal Intensive care units (NICUs) from both Columbia and Cornell in New York City were grouped by their puled field gel electrophoresis (PFGE) patterns into groupings containing a letter (indicating similar patterns) and a number (indicating highly similar patterns) (e.g. A-10, A-26, and W-166, where A-10 and A-26 are more similar to one another than W-166). However, the phenotypes of the A strains are vastly different when characterizing biofilm formation (as seen in chapter II). It is intriguing that the genomic patterns of these strains align; however their pathogenic phenotypes are vastly different. Further, these differences in phenotype *in vitro* do no necessarily correlate to their isolation frequency in the NICU, where three A strains (some forming biofilm *in vitro* and some unable) were all isolated with high frequency in the hospital.

In order to take what we have learned about adhesion and biofilm formation and assess their importance in a clinically relevant context, a higher order system both in terms of throughput and the number of tunable parameters will be necessary. To this end, we are developing a next generation functional screening platform based on the integration of microfluidics and functional protein microarrays. This approach employs a 'top down' approach to the question of environmental regulation of device-related pathogenesis. By having some basic understanding of the connectivity of a system (i.e. colonization affects biofilm formation through cell surface density, etc.), we can infer the functionality of that system by systematically tuning inputs to that system, and measuring a quantitative outcome (figure 21). This will allow us to both develop a

library of expected outcomes form this system and simultaneously infer higher order connectivity within the system (i.e. bottlenecks or weak points that could be utilized as therapeutic targets). Here we do not aim to identify the mechanism of those key steps, nor develop the therapeutics; only to better inform a more directed approach using molecular techniques to do just that.

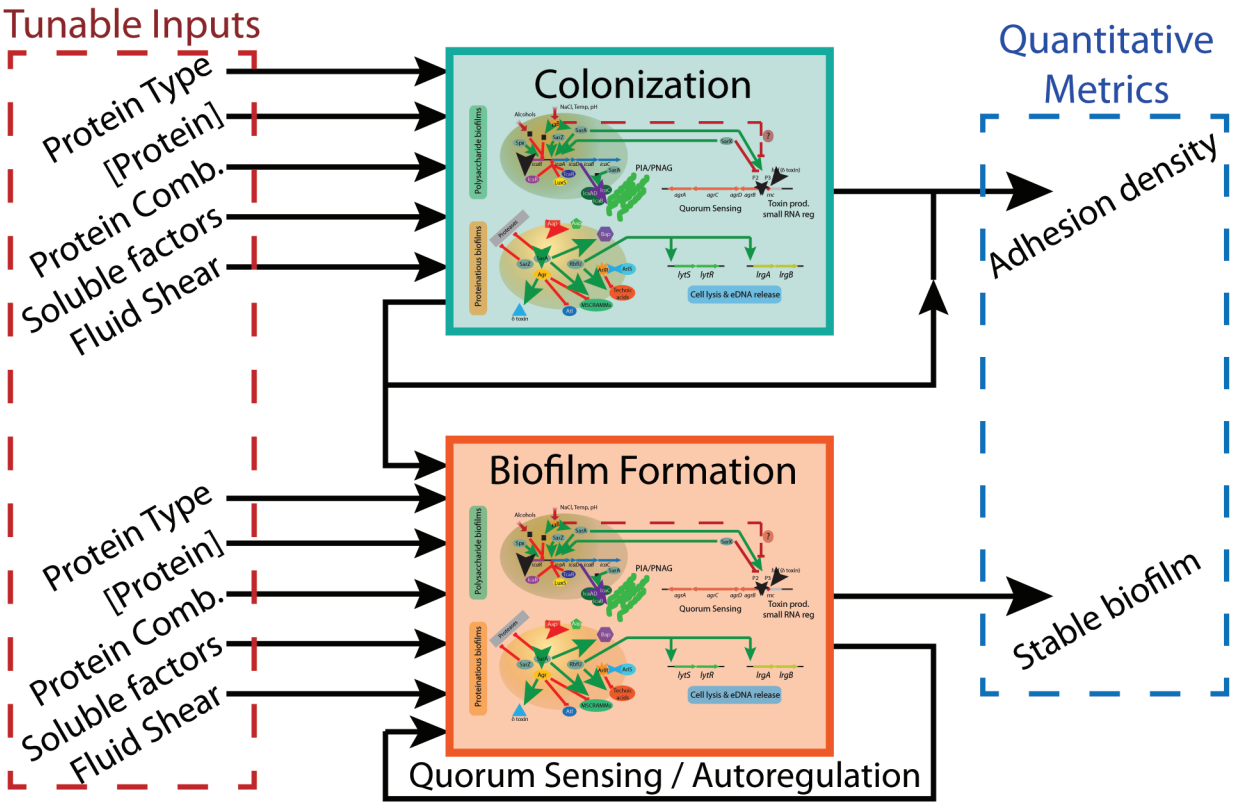

Figure 21: A 'top down' engineering approach to address the 'system' of environmental regulation of implanted device-related pathogenesis.

In this platform, the use of microfluidics, as in our previous experiments, will allow precise control over the mechanical microenvironment imposed on cells. Simultaneously, printed protein microarrays will enable multiplexed investigation of the contribution of multiple host proteins to both adhesion and biofilm formation. Specifically, this screen incorporates 4 extracellular matrix (Fibronectin, Collagen-I,

Collagen-IV, and Laminin) and 1 plasma protein (Fibrinogen). These proteins represent a diverse range or targets for adhesion, as some (such as fibronectin and fibrinogen) are known adhesive targets of both *S. aureus* and *S. epidermidis* [24,84–86], and the remaining proteins have shown indirect contributions (such as Collagen-I) to colonization [87,88], or their adhesiveness are yet unknown (Collagen-IV and Laminin).

The physical structure of the chip is a hierarchical arrangement of repeating subunits composed of eight channels connected in parallel, where each channel contains a subarray of protein spots (figure 22). These chambers are repeated in triplicate for on chip repeatability. These subunits are further connected in parallel to one another to create shear arrays of 24 chambers (3 subunits). Connection of the subunits in this manner results in the shear stress distribution seen in figure 22. In each subunit, the shear changes by a factor of 2 between each chamber, however each subunit is linearly offset from the next. This results in three windows of shear stress linearly offset, however within these windows the shear changes by $\log_2$ (figure 22). Ultimately, the range of shear addressed in a single experiment is 384 fold (this window can also be offset by changing the inlet flow rate). In these experiments we use an inlet flow rate of 1.5 mL/min, giving a range of shear between 4.4 Pa and 0.011 Pa, encompassing all the ranges we have previously shown to induce phenotypic responses from *S. epidermidis*.

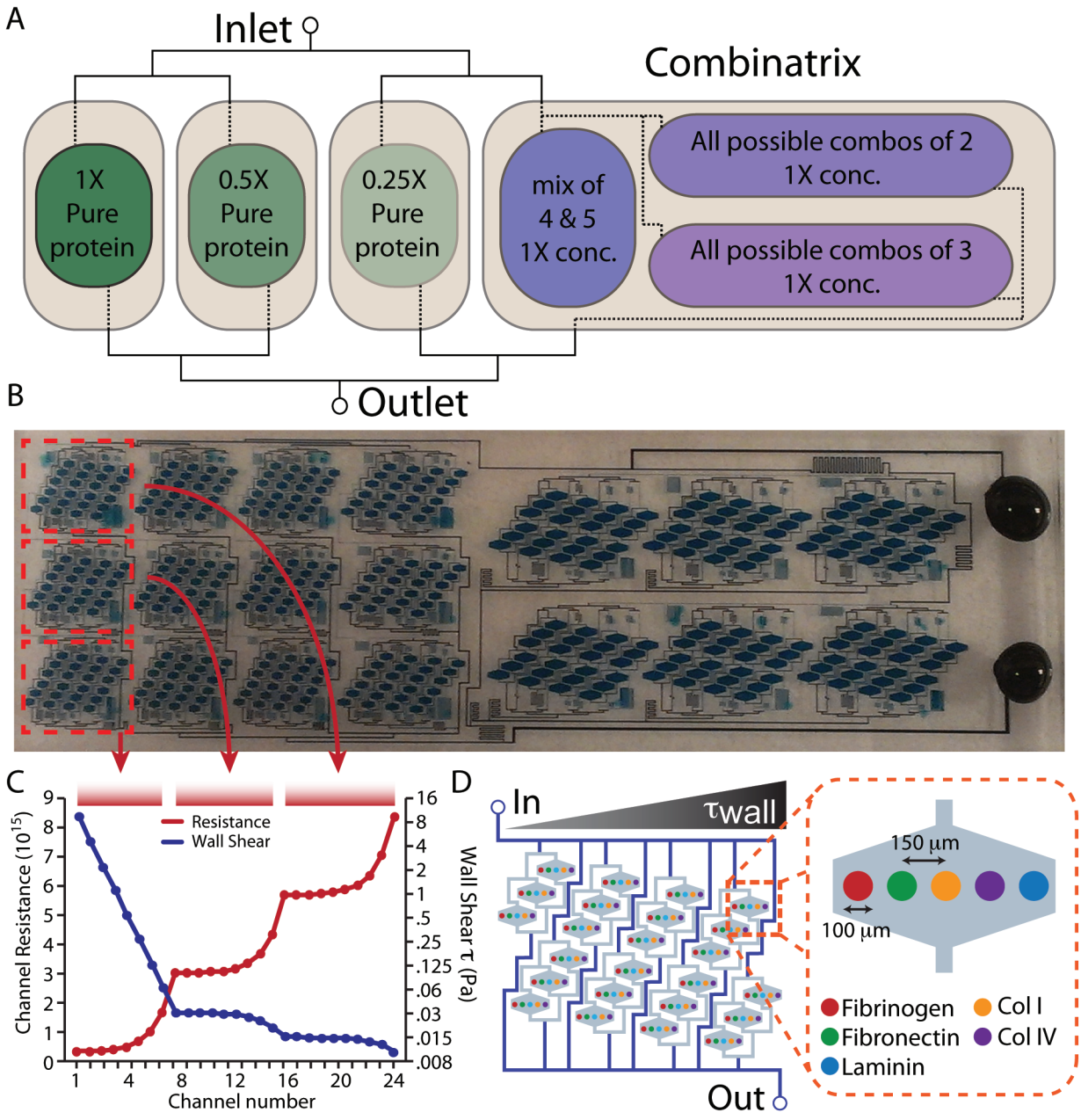

Figure 22: Overall design concept of the assay. In a single experiment, a range of 384x shear stress and 5 protein types and combination are tested in triplicate.

When the microfluidic devices are scaled up to meet the needs of a multiparameter high throughput assay such as this one, the channel design becomes increasingly complicated due in most part to the complex arrangement of channels (as seen in figure 22), constrained to the practical limitations of a 1" x 3" glass slide.

Calculation of the shear stresses in parallel microfluidic channels illustrates why these channel lengths are needed. The channel resistance is what determines the overall flow rate in a channel at a given applied pressure across the channel. Similar to Ohm's law for electric circuits $V = IR$ (where voltage *V* is applied across an element with resistance *R*, leading to the driven current *I* through that element), fluid flow can be described using the equation $\Delta P = QR$ (where a pressure *P* is applied across a channel with resistance *R*, driving flow *Q* through that element). Solving the Navier Stokes equation for a simplified channel structure of two parallel plates (figure 23) assuming that the height dimension, h, is much less than width, w, i.e. w ~∞ and there is no change in velocity along that direction, the description of a parabolic velocity profile in the y direction (from 0 to h) is obtained: $u(y) = \frac{\Delta P}{2\mu l}\left[y^2 - \left(\frac{h}{2}\right)^2\right]$. Further, the use of the simple relation for flow rate, pressure drop, and resistance gives: $u(y) = \frac{QR}{2\mu l}\left[y^2 - \left(\frac{h}{2}\right)^2\right]$. The channel resistance can also be solved in terms of measureable parameters and is described by: $R = \frac{12\mu l}{wh^3}$ where *w* >> *h.* Further, the wall shear stress τ_{wall} can be determined in this parabolic velocity profile by taking the derivative of velocity as it approaches the wall: $\tau_{wall} = -\frac{\partial u}{\partial y}|_{y=h/2}$, and solving this with the previous equation in mind yields: $\tau_{wall} = -\frac{6\mu Q}{wh^2}$ to describe the wall shear stress in a given channel as a function of controllable parameters, namely channel geometry (*w*, and *h*) as well as fluidic parameters like μ, and flow rate *Q*.

What is gained from these equations is a quantitative way to design channel systems to impart specific shear stresses on cells cultured on the walls within those chambers. Further, parallelization of channels in a fluidic circuit mimics the properties

of that in an electrical one. If a single channel splits into two (or more generally, *n*) channels, then the splitting of current (or fluid) can be described using the product of flow rates and resistances: $R_1Q_1 = R_2Q_2 \ldots = R_nQ_n$ simply because the pressure drop across all the channels must be equal because they originate form the same point and recombine downstream at the same point (figure 23). Secondly, the sum of all the individual flow rates in each branch must be equal to the total input flow rate in the upstream channel (i.e. $Q_{tot} = Q_1 + Q_2 + \cdots Q_n$). All of this allows rational design of large-scale fluidic networks, such as the one illustrated and shown in figure 23.

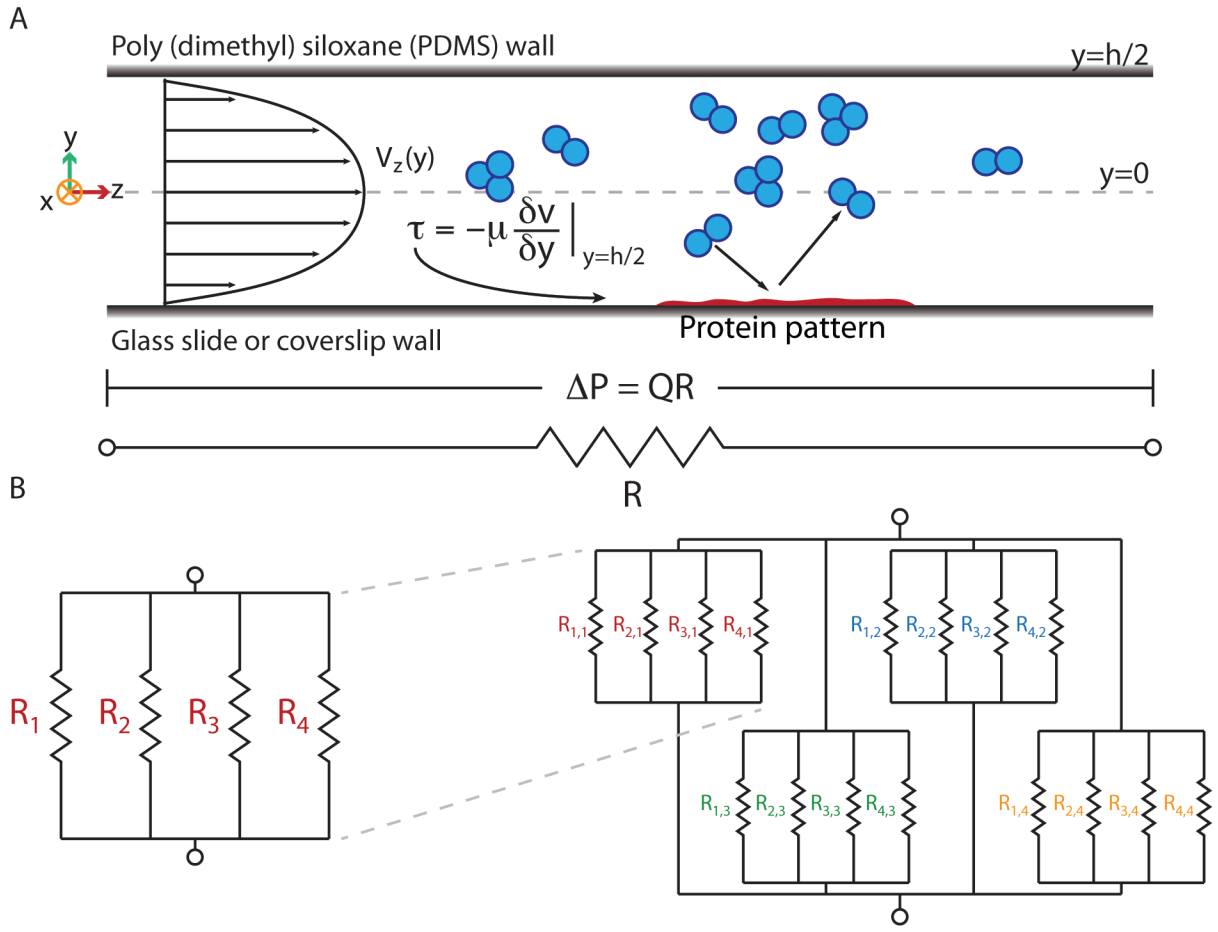

Figure 23: In specific cross sectional channel geometries (i.e. w >> h), the shear stress can be calculated using measurable channel and fluid properties. Further, multiplexing

channels into fluidic networks allows parallelization of shear stresses, however requires increasing channel footprints.

Although both microfluidic shear chambers and functional protein microarrays are not novel concepts, their successful integration has not been achieved, and there are many challenges associated with their functional combination. The first, and most obvious challenge is physically creating a sealed channel with one surface having a printed pattern. Typically with PDMS-glass microfluidic chips, an oxygen plasma step is required for irreversible bonding, however this would completely destroy any surface modifications previously made to the surfaces, and would most certainly destroy a protein pattern. Alternatively, there are some chemical methods to bonding, namely by using an epoxy coated glass slide and vinyl terminated PDMS microchannels, which have only been partially cured. By placing the channels on the epoxy surface and heating, chemical linkage between the two can be achieved [89]. This solves the problem of preserving the molecular structure within print spots, however the print will not be stably linked to the surface, leading to desorption after resolubilization in the channel. This was intended in the system developed by Fordyce et al to create transcription factor binding landscapes to synthetic DNA oligos [89,90], however not desirable for the case of adhesive patterns.

The use of PDMS as the microchannel material leads to the second challenge. PDMS is excellent for prototyping microfluidic channels because of its low cost, moldability, and it can be easily linked to glass surfaces. However, PDMS is an elastic material, and under moderate operating pressures in microfluidic channels (greater than 10 Psi) has been shown to deform up to 200% of the original channel height [91]. If our

assay is to have precise and accurate control over shear stress in the channels, then any significant changes in channel cross-section from hydrostatic pressure must be avoided. If the channel height in a 500 μm width by 50 μm height channel changes to 75 μm, then the shear stress (at the same fluid flow rate) will decrease by a factor of $75^2/_{50^2}$, meaning that a 50% change in height leads to a 225% change in shear stress. Further, as our microfluidic channel design is highly parallelized, the relative flow in each chamber relies on the channel resistances, and the same 50% height change in a straight channel results in a 338% change in resistance, assuming all other dimensions remain the same. In summary, not only does a new bonding method need to be engineered, but also entirely new materials for the microfluidic channels should be chosen to maintain channel dimension fidelity under high pressure.

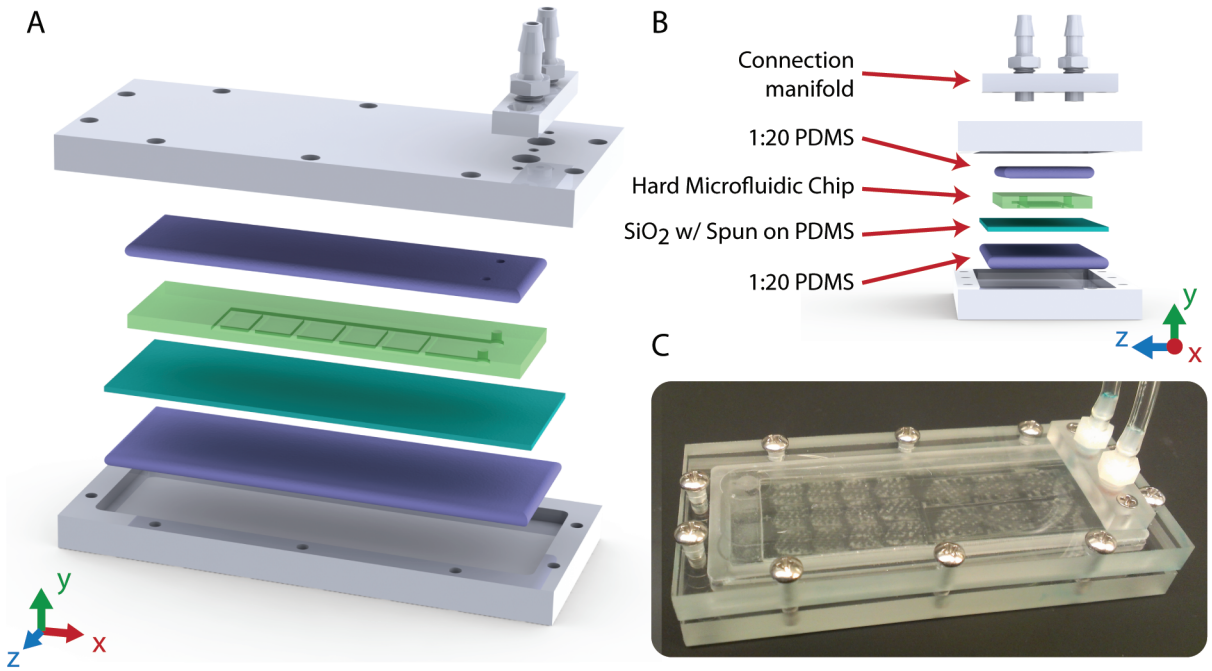

Figure 24: Schematic and implementation of a novel chip clamp design, utilizing a thin (~5μm) layer of PDMS spun onto a glass slide interfacing with a hard epoxy chip. B:

Soft (1:20) PDMS pieces are used as cushions in the clamp (hard acrylic) so that the glass slide does not break during compression. The top and bottom acrylic pieces are held together using 4-40 machine screws.

To overcome these challenges, we have developed a novel microfluidic chip allowing both for easy bonding of printed surfaces with microfluidic channels, channel dimension fidelity under flow, as well as the ability to remove the channels from printed or cultured surfaces for easy cell collection and downstream analysis. The mechanism of bonding relies on a thin (~5μm) layer of PDMS spun onto a glass slide, combined with a hard chip made of a two-part epoxy resin (figure 24). This solves both the channel dimension, as well as bonding. The two surfaces are mechanically bonded together using an external clamp system, where the PDMS layer acts as a gasket to create a liquid-tight reversible bond. The chip clamp system is custom designed and fabricated in polycarbonate. Fundamentally it is two plates with recessed areas that are clamped using 4-40 machine screws (figure 24). In addition to the two-plate system, a connection manifold for inlet and outlet tubing is integrated on the top face. This allows for easy connection of source fluid to the chip without the introduction of bubbles.

The microfluidic chip itself is composed of a two-part epoxy resin that, when cured, has an elastic modulus in the 10's of GPa range; much grater than that of PDMS (~1 MPa). The fabrication of these chips relies on multiple replica molding steps, involving a silicon master mold and PDMS negatives. Specifically, silicon masters are generated using standard photolithography using KMPR 1025 and 1050 negative photoresist. Molds are treated with Rain-X to avoid PDMS sticking by bathing the silicon wafers in pure Rain-X for 2 hours at room temperature, followed by washing with pure

ethanol, and sonication for 1 min in the ethanol solution. Silicon wafers are then dried under a continuous stream of filtered nitrogen air. Next, a PDMS negative mold is made by pouring PDMS and crosslinker over the mold at a 1:10 m/m ratio of crosslinker to base, prior to pouring on the mold, the PDMS/crosslinker mixture should be degassed under vacuum for 1 hour to remove bubbles. Subsequently, 15 grams of the mixture is poured over the wafer (4" diameter) to yield a PDMS piece that is ~2 mm tall. Curing is performed at room temperature for at least 24 hours on a flat, level surface. The PDMS devices are peeled from the mold, cut to fit on a 1" x 3" glass slide, treated with oxygen plasma at 50 mTorr for 30 seconds, and silanized with a 0l2% v/v octadecyl(trichloro)silane solution in pure Ethanol for 15 mins. The devices are washed in pure ethanol and sonicated for 1 min, then dried under nitrogen. Subsequently, to create a positive mold of the channels in PDMS, the treated negative PDMS mold is placed, device side up, on a clean silicon wafer pretreated with Rain-x. Freshly mixed (1:10) and degassed PDMS is poured over the device on the clean wafer (45 grams), and allowed to cure at room temperature for at least 24 hours. After full curing, the negative mold can by cut out of the most recently poured PDMS slab, leaving a positive PDMS mold o the channels. The OTS treatment is what prevents the PDMS chains from interacting at the PDMS/PDMS interface and allowing the device to be cut away. Subsequently, the mixed two-part epoxy can be poured into the positive mold to make hard channels.

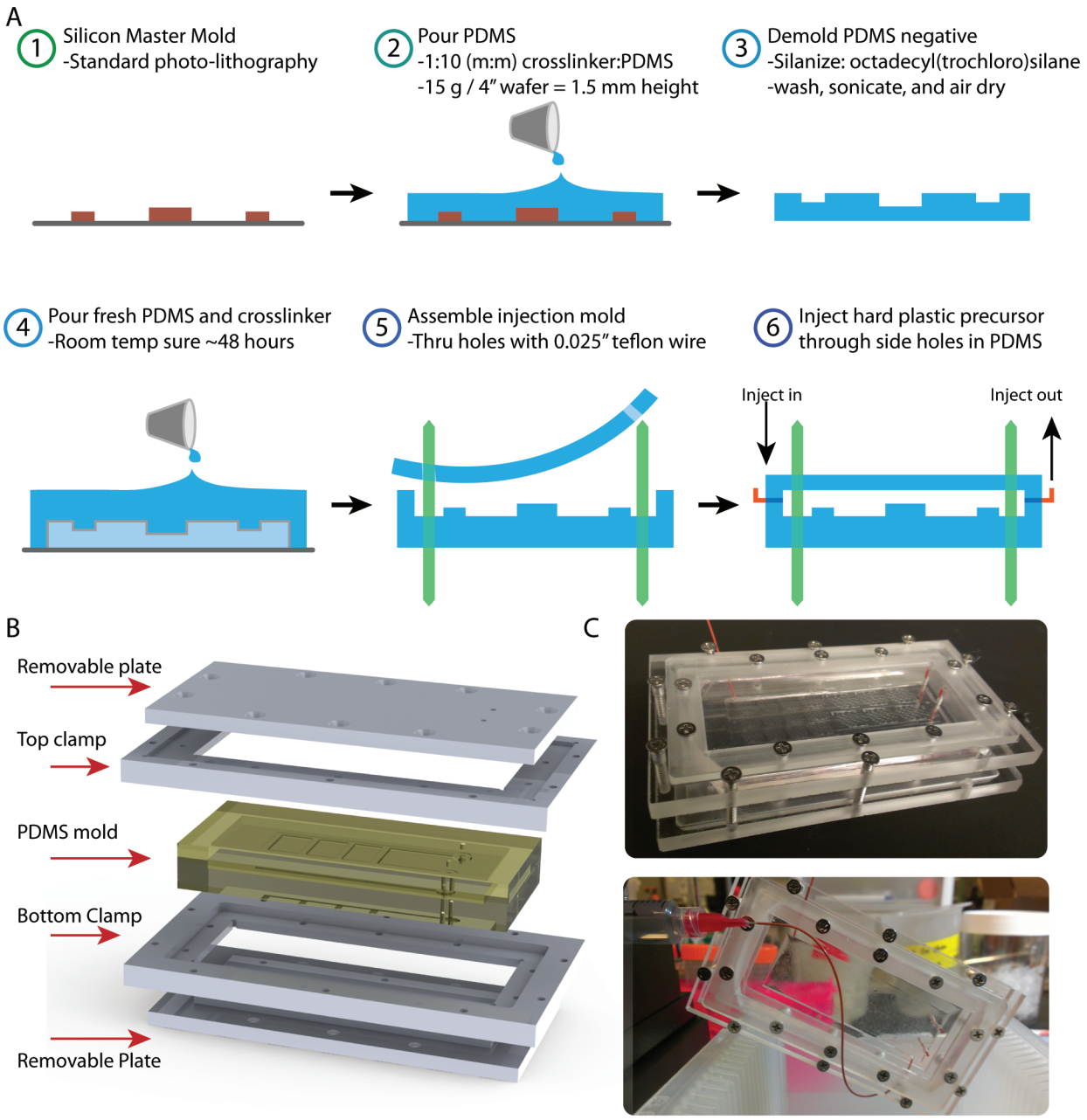

Figure 25: A: Process flow for hard chip fabrication using PDMS replica molding and injection of a two-part epoxy resin. B: Schematic of the injection mold clamp and C: Images of the clamp during injection.

The hard epoxy chip is subsequently put into the chip clamp to interface with a 5μm PDMS gasket on glass, requiring the epoxy chip to be very uniform in height, and

relatively thin (~2 mm) in overall height. To ensure the proper fabrication controls are in place for each chip, an injection mold for epoxy chips was created (figure 25). The exploded view of the clamp can be seen in figure 25, indicating the necessary components. The mold itself is created in PDMS, with the PDMS positive mold described above, and a 5mm thick slab of PDMS as the top. Inlet and outlet holes in the epoxy chip are created by using 1/32" diameter Teflon coated steel wires that span the space where epoxy will be filled. An acrylic clamp for the PDMS mold holds the mold together, so that the positive pressure from injection does not open the mold. Inlet and outlet hold for the epoxy are punched using a 0.024" diameter biopsy punch (this same punch size is used for Teflon coated steel wire holes). Epoxy resin is injected using a 10 mL BD plastic syringe on a Harvard Apparatus high force syringe pump. The total volume needed to inject one device is ~2 mL.

In order to have quantitative control over the adhesion environment during our screens, it is important to ensure that printed proteins are stably linked to the surface and remain linked under flow. Secondly, the linkage chemistry needs to be specific, strong, and fast. The volumes spotted during microarray printing are very small (~1nL per spot), and the spots dry out within minutes even in a humidified environment. To this end, we have used biotin-streptavidin chemistry to link the printed proteins to the PDMS surface (figure 26). The proteins to be printed are biotinylated, prior to printing, by reacting an NHS-long chain biotin (NHS-LC-biotin) with free lysine residues on the protein of interest in a 1:10 molar ratio of protein: biotin. The PDMS surface, also prior to printing, is coated with a stable, functional, layer of streptavidin. This is achieved using a modification of our previous silane chemistry on glass sufaces *in situ*. First, the

PDMS surface is aminated using a 1% v/v APTS solution in a 95% EtOH 5% H_2O solution (with the addition of AcO as an acid catalyst: 10%v/v). Subsequently, the surface is biotinylated using NHS-LC-biotin at a concentration of 100 μM in a 1X PBS solution pH 7.4. Finally, streptavidin is added at a concentration of 50 μg/ml and allowed to react for 1 hour at room temperature in 1X PBS pH 7.4.

A comparison of multiple methods of linkage between the PDMS surface and streptavidin, including covalent methods and biotinylation can be seen in figure 26. Although covalent methods are, by definition, stronger than any receptor ligand interaction, it is clear in this case that biotinylation of the surface leads to significantly more streptavidin on the surface. It is likely that the low efficiency of the covalent reaction comes from performing sensitive reaction under non-optimal conditions. Specifically, the conversion of the aminated PDMS surface to a free carboxylic acid involved the use of highly reactive anhydrides (either succinic or glutaric). These reactions should be carried out in dry DMF under argon, however DMF has been previously shown to swell PDMS significantly, which drives hydrophobic recovery and competes with the surface reaction. A second option for this reaction would be to use an aqueous bicarbonate buffer, however this leads to even less efficiency as seen in figure 26. Thus, biotinylation in an aqueous environment is best suited for this system. Initially, the surface was titrated with NHS-LC-biotin to determine the optimal concentration for biotin linkage. The efficiency of reaction was measured by using a fluorescent conjugate of streptavidin, and measuring surface fluorescence after excessive washing (figure 26). Further, the interaction between streptavidin and biotin

is very strong ($K_D = 10^{-14}$M) [REF], and there is no change in the amount of streptavidin on the surface after significant washing and subsequent drying using a nitrogen stream.

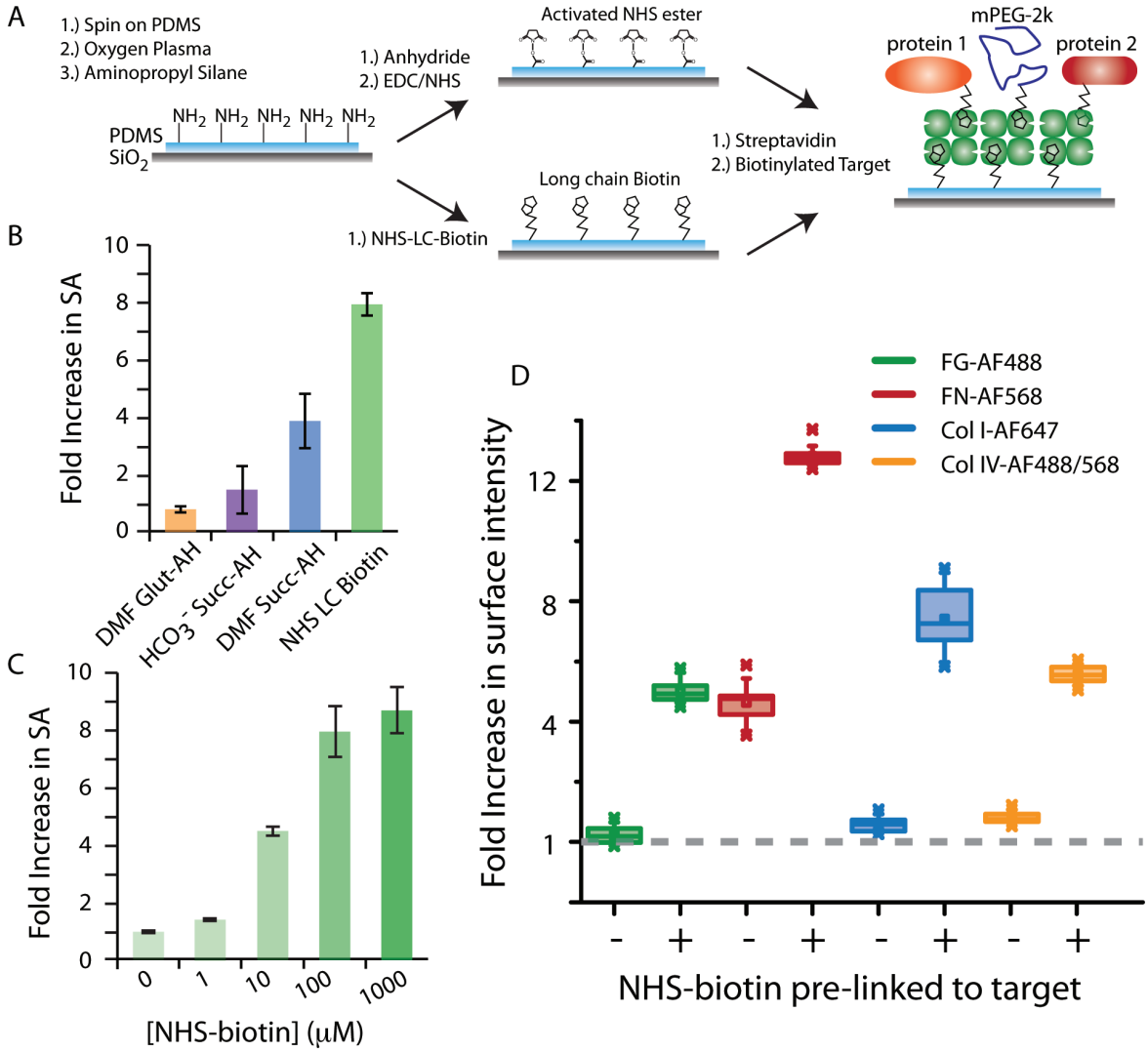

Figure 26: Developing a strong and specific linkage between printed proteins and the PDMS gasket is key for the successful integration of microfluidics and protein microarrays. A: Reaction schemes investigated as mechanisms of linkage. B,C: Using a biotin binding method to link streptavidin of the PDMS surface is the most efficient strategy, given solvent limitations imparted by PDMS. D: Linkage of biotinylated target proteins to the streptavidin coated PDMS gasket is specific for biotinylation.

These large-scale fluidic networks impose a very specific organization of adhesion chambers stemming from lack of real estate. This in turn generates a second significant challenge associated with building this platform: the generation of non-canonical microarray patterns on demand to interface with fluidic channels. Typically, microarray patterns are printed in equally spaced 'm x n' patterns (i.e. equally spaced rectangular patterns) or arranged in a hexagonally closes packed (HCP) arrangement. This has been developed as the standard method because it is the best way to maximize the amount of individual spots on a glass slide (a typical microarray substrate). Even the first successful integration of microarray plotting of DNA libraries and microfluidics utilized rectangular arrays, and built the microfluidic device around that geometric constraint [89].

We have developed a novel approach to generating on demand, user defined patterns of microarray spots. The mechanics of printing are simple, utilizing a printhead holding floating stainless steel quill-type pins. This printhead is moved in both the z- and y-directions using orthogonal servo motors and parker linear motion systems. The x-direction is orthogonal to both y and x, and controls a platter holding the glass slides, rather than the printhead itself (figure 27). The servos are controlled using a 3-axis motion control PCI card from Galil motion control systems (card: DMC1832). This design is a revision of the designs put forth by Derisi et al. The novel aspect of our software lies in the reconfigurability of microarray print patterns without requiring any lines of code to be altered. This capability is key for the functional integration of fluidic circuits to printed arrays.

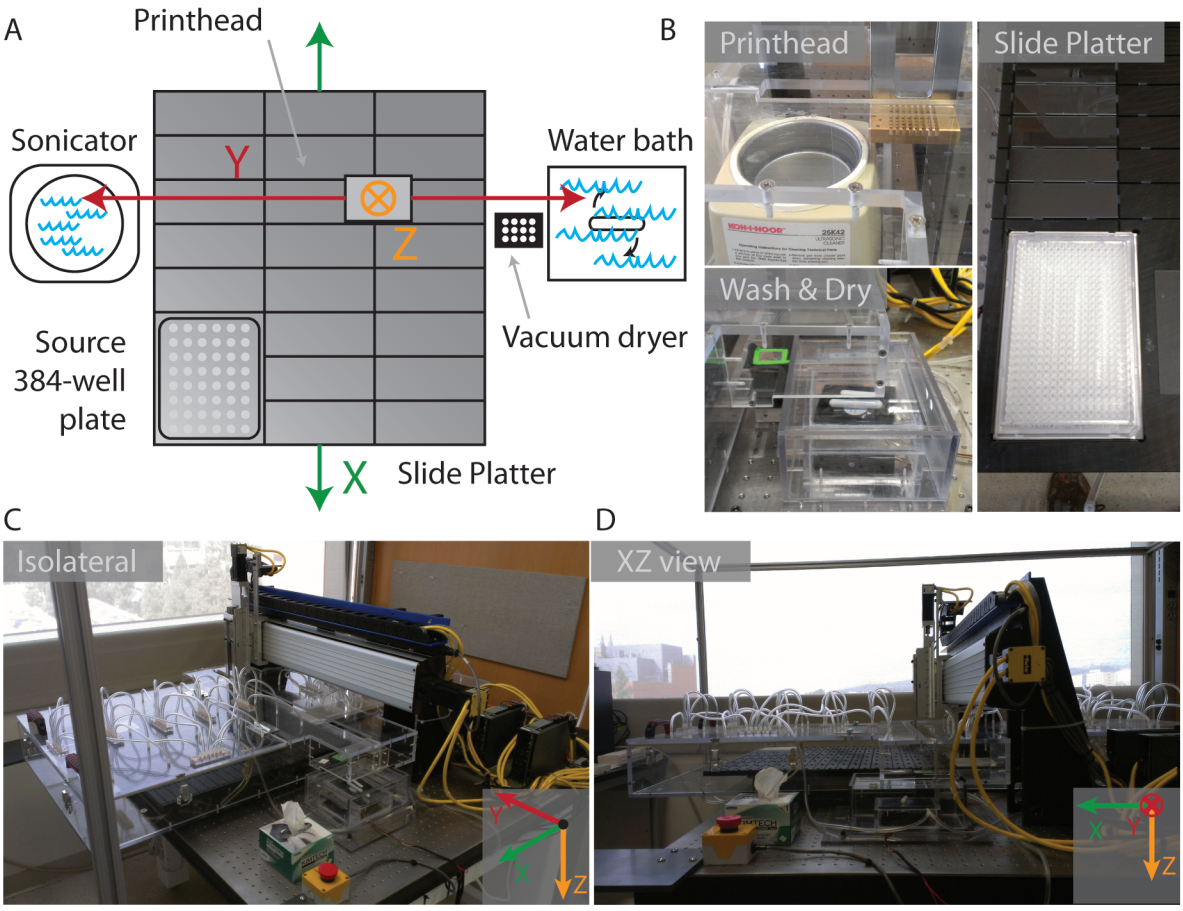

Figure 27: Three-axis servo robot that controls the motion of a printhead containing floating pins. Both pin washing, as well as substrate loading is automated and performed inside a humidified chamber (acrylic box).

The printing software allows a user to print any pattern that can be generated in an AutoCAD *.dxf file. Specifically, the user will draw, using the circle command, the x and y locations of each spot, where the layer number corresponds to the well number from which the spots will be printed (figure 27). This allows spots to be easily organized and aligned to channel structures, which can be in the AutoCad file as long as they reside on the layers designated for microfluidic channels (in this case they are named KMPR 25, KMPR 50, and KMPR 75). There are also two layers built in for alignment purposes, named ‘slide edge’ and ‘center’. These allow the downstream software to

map spots to the slide edge and isotropically shrink or stretch the patterns to be printed, relative to the exact center of each slide (figure 28).

The software package currently is split between two platforms: Matlab and LabView. A custom script written in Matlab imports and reads the *.dxf file from AutoCad, an converts these points into arrays containing the x and y coordinates of each point, as well as an index indicating which well the points should be printed from. Subsequently, this dataset is imported into a LabView program, which also controls the physical motion of the servos and printhead. The LabView program contains an intuitive User Interface (UI) through which the operator of the printer must initially connect the PCI controller to the motor amplifiers and home the motors (all through the click of one button on the UI). The UI also allows for control over the x-y-z locations of each station addressed during printing. The print loop contains an initial wash cycle, followed by dipping the pin in the correct well of a 384 well source plate, blotting excess liquid from the tip on a sacrificial slide, and printing on the target slide (up to 100 spots per load) (figure 28). The wash cycle itself contains a loop, where the pin is initially sonicated in a surfactant solution, washed in a large-volume DI water bath, then dried using a vacuum manifold. The UI allows the user to manually align each station prior to printing, and check the subroutines to ensure correct operation prior to running a full print. Once the stations are set, they do not have to be reset as long as the printhead is not removed and stations are not moved.

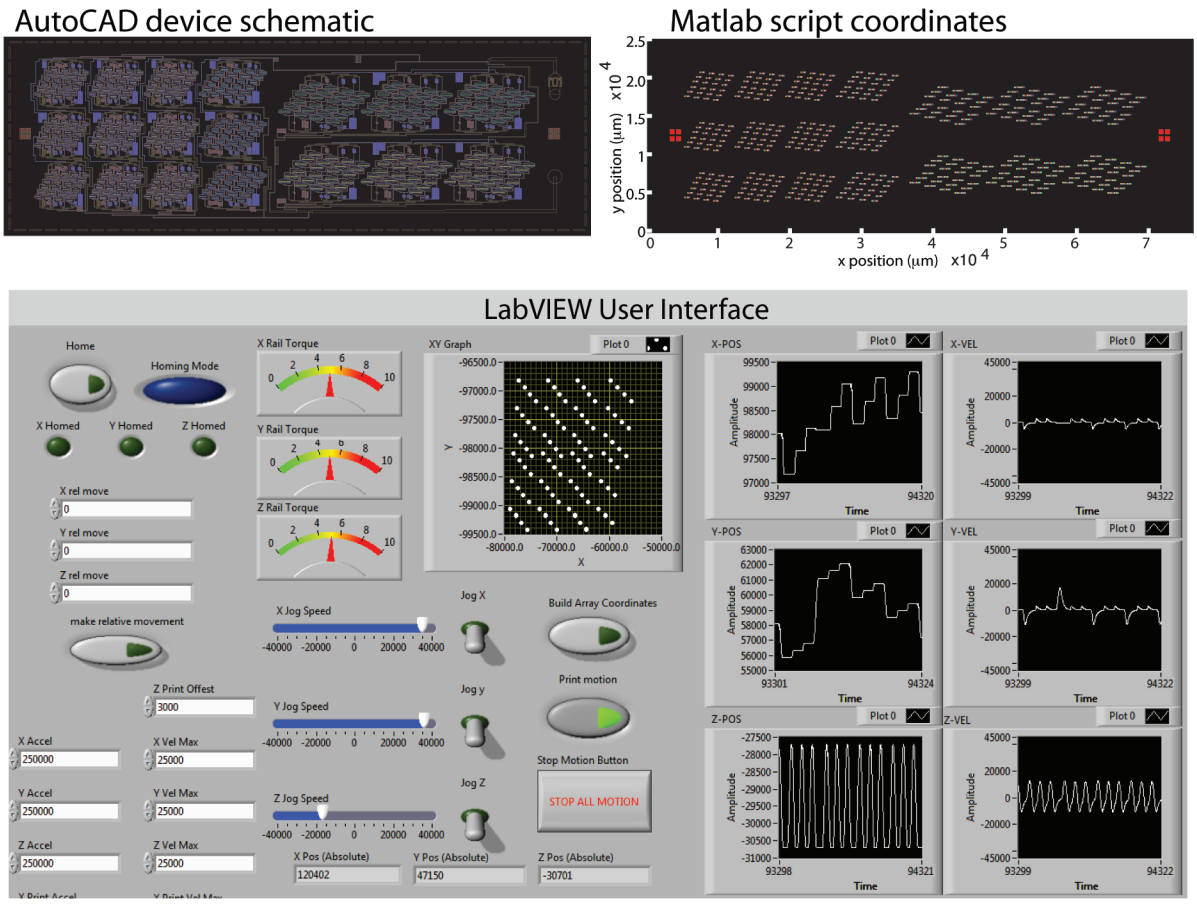

Figure 28: Matlab script allows instantaneous conversion of an AutoCAD *.dxf file to a coordinate matrix that is used for printing by the motion control UI in LabView.

After stations and slides have been mapped, and the AutoCad file has been converted using the Matlab script, the user presses the ‘Build Program’ button on the LabView UI. This performs a full download of all the points in the array, as well as station locations and auxiliary code to the EEPROM memory of the PCI card. It is beneficial to download all information to the card prior to running the program because there is no data sent along the PCI bus during printing, making a smoother transition between subroutines and less stress on the EEPROM memory itself. Subsequently, the user presses the ‘Begin Print’ button and can leave the robot to print slides, coming back later to pick up the finished arrays. During the print, the LabView program simply

monitors the digital outputs of the PCI card and, based on the digital output signature, calls various subroutines previously downloaded to the card (e.g. washing, loading, or printing subroutines). The UI tracks print progress by monitoring outputs from the PCI card, and displaying a progress bar in real time (figure 28).

Characterization of the specificity and homogeneity of printed proteins was accomplished using fluorescence microscopy and quantitative image analysis of fluorescently labeled proteins. Each spotted protein was pre-labeled with NHS-LC-biotin and a mutually exclusive set of fluorophores. This allows for determination of protein location, homogeneity and type from the fluorescent signature of the spot (figure 29). Spot homogeneity is a function of the type of protein spotted, where typically more filamentous proteins such as collagen I result in a slightly lower CV than other proteins. The CV for collagen I, the lower limit of homogeneity, was measured as 0.119, indicating a satisfactory homogeneity (i.e. ~12% or less variation on protein density within the spots. Further, spot size is determined heavily by how well the surface has been prepared. These surfaces are PDMS layers on glass, however they are hydrophilic immediately after coating with streptavidin. The streptavidin coating is necessary to ensure stable linkage, however the more hydrophobic the surface is, the closer the spot size is to the lower limit (the size of the tip, which is a 100 μm square, on edge). After streptavidin coating, the slides are washed in decreasing concentrations of PBS, and finally with ddH_2O. After washing, the slides are dried under an air knife pressurized with filtered nitrogen gas and stored in an air-tight container with silica gel. Typically, the amount of time required to desiccate the substrates before spot size is less than 125 μm is 7 days. The spot size must be a highly controlled parameter as the

sub arrays printed are to fit within a channel of approximately the same size, and also because there should be no mixing of neighboring spots during printing.

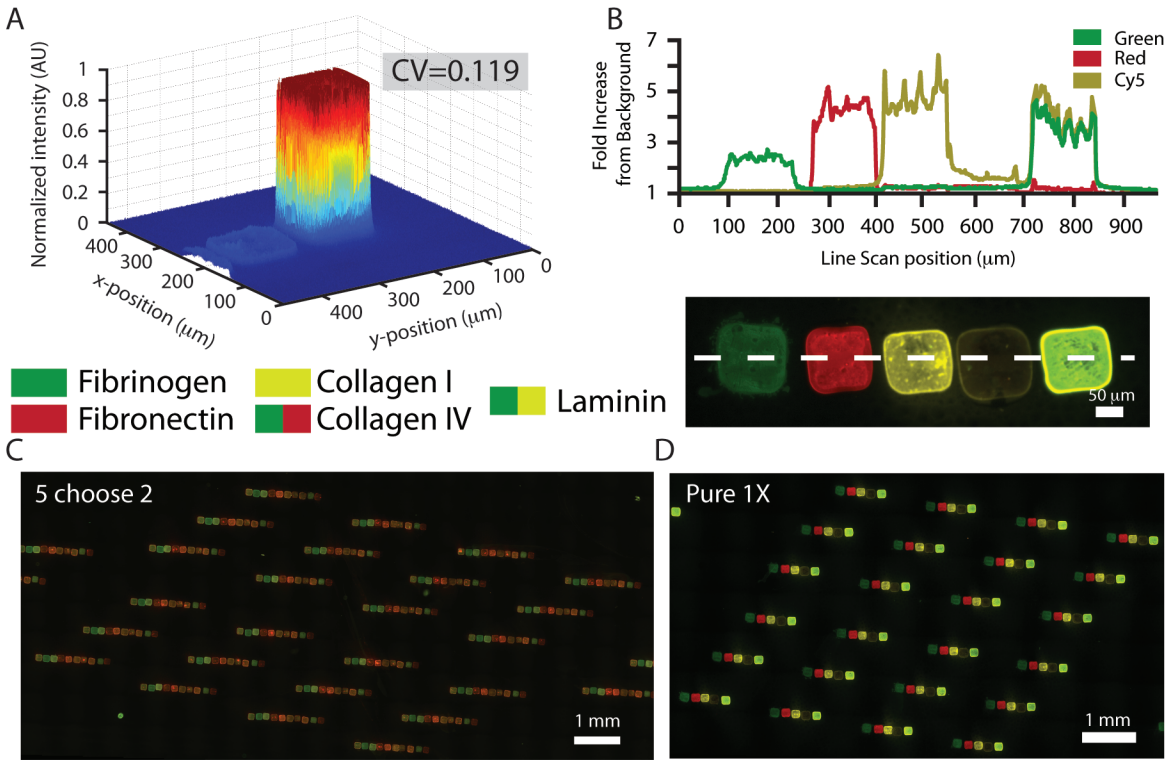

Figure 29: Protein printing is specific and homogeneous. A: Quantitative image analysis indicated that printed protein spots have, at most, 11.9% variation in their surface density. B: Each protein is labeled with a mutually exclusive set of fluorophores so that spots can be easily mapped during image analysis. C,D: Large stitched images of sub arrays for the high throughput assay. C shows the 5 choose 2 array, where all possible combination of two proteins are present. D illustrates the pure protein array.

Alignment of the molded microchannels to the printed pattern is a crucial part of the fabrication process and, as the channels are packed closely together on the chip, the tolerable error in alignment is +/- 100 μm. This is not practically achievable using a hand alignment, especially as the device clamp can misalign the substrate during

tightening. We have designed an x-y and rotational alignment system, controlled using fine adjustment screws, for accurate alignment of the device to the printed substrate.

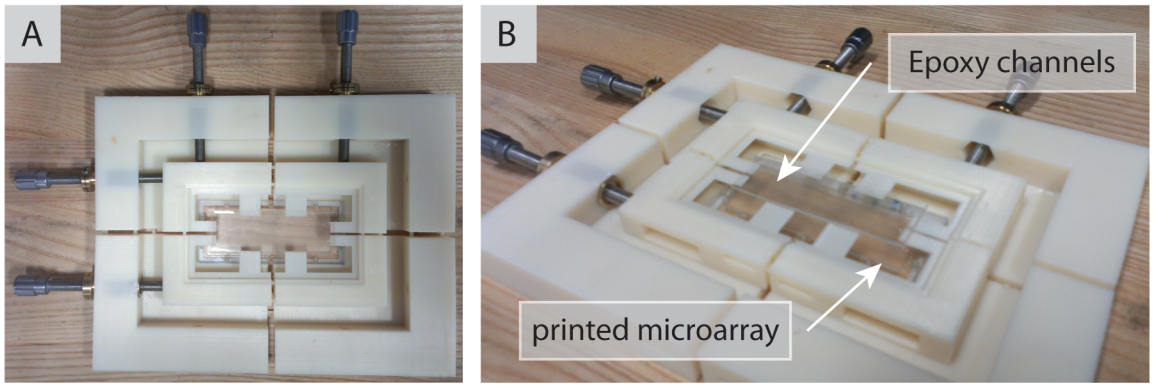

Figure 30: 3D printed alignment system for printed microarrays and microfluidic channels. Two frames of references are controlled with fine thread screws to perform alignment by hand under a dissection microscope.

The alignment system uses two frames of reference; one being that of the printed array (fixed) and the other moveable frame of reference is the device (figure 30). The alignment system was designed in Solidworks, and fabricated in a 3D printer using ABS plastic as the print material. Four pieces make up the clamp that is in the frame of reference of the chip, and these clamp the chip from the side only, purposefully leaving space to screw the chip clamp together after alignment. The outer frame of reference of the printed array is clamped using the 4 large pieces, and hold both the bottom half of the chip clamp and the array substrate. During the print, alignment marks are printed on the PDMS gasket layer along with the microarray itself. These marks are composed of coomassie stained protein ladder that has been reacted with NHS-LC-biotin. These printed spots (visual to the eye under a dissection microscope) are then aligned to crosses molded into the epoxy chip from the original master mold (figure 30).

Together, these new devices and automated robotics allow for the functional integration of functional printed protein microarrays with large-scale microfluidic networks. A number of significant challenges were over come to achieve this integration, ranging from surface chemistry to novel channel bonding using a PDMS gasket. Further, the process from device design to physical integration is either automated or tightly controlled at each step, leading to both increased throughput and reproducibility. Ultimately, the goal of this platform is to be used as an adhesive and biofilm formation screen for bacteria under physiologically relevant fluid shear and surface composition. With that in mind, the challenge of validating the functionality of the 'pathogenicity landscape' assay itself arises.

V. Assessment of the bulk adhesive capabilities of genetically diverse Staphylococci as a precursor to 'pathogenic adhesive landscapes'

It is well accepted that variation between species of bacteria, as well as strains within a single species is quite significant. This phenomenon is at least a partial contributor to the uncertainty regarding what adhesive interactions are important in pathogenesis and what biofilm pathways, if any, can lead to increased pathogenicity. Here we are currently focusing on Staphylococci as a model organism for two reasons: (i) they are the leading cause of HAIs to date and (ii) there is a vast landscape of pathogenic genotypes and phenotypes among them.

There is also overlap between *S. aureus* and *S. epidermidis* in both adhesin type (from sequence homology) and biofilm formation mechanisms [63,84,85]. It is also known that there is overlap between the quorum sensing systems in the two species, specifically the agr and luxS systems [33,92], indicating that they can sense each other's presence when in close quarters. Three clear and significant differences between the two are, first, their ability to coagulate blood. *S. epidermidis* is referred to a coagulase negative *Staphyloccoci* for the very reason that is cannot coagulate blood[93]. This is pertinent to the comparison of adhesins because Clumping factor A and B in *S. aureus* are both surface exposed proteins that bind the thrombin cleavage site of fibrinogen (leading to coagulation). At least one of these two isoforms are found in most *S. aureus*, and this is expressed during pathogenesis [21,22]. The second main difference between *S. aureus* and *S. epidermidis* is in toxin production. *S. aureus* contains a suite of cytolytic toxins produced *in vivo* including leukotoxin, γ-hemolysin and α-toxin, to name a few [94–96]. Production of these toxins *in vivo* is what

stimulates an immune response from the host, resulting in inflammation and, if left untreated, sepsis. The third, and possibly the least well understood, is the promiscuity with which antibiotic resistance genes are passed in *S. aureus* [13,96,97]. The underpinnings of the mechanisms controlling the rise and fall of MRSA strains (many of which are also toxin hyperproducers) are poorly understood, but regardless of the selection pressures involved, increased antibiotic resistance poses a serious threat to the effective treatment of these infections.

It may seem for these points that *S. aureus* is the dangerous pathogen, and *S. epidermidis* is the friendly cousin. *S. epidermidis* contains only one toxin (δ toxin) [38] and this is not extremely common in clinical strains; there are few multidrug resistant strains (at least in a well plate format), and the is no blood coagulation. Despite all of this, *S. epidermidis* is even more commonly isolated from catheter related blood stream infections than *S. aureus*. It is true that *S.* epidermidis can wreak less havoc in a short time span once in the bloodstream (lack of toxins and coagulases), however severe cases of bacteremia an sepsis are caused by *S. epidermidis* and it is not understood what aspects of the pathogen or the host (or both) are contributing to this infectivity.

As mentioned previously, two steps of pathogenesis considered to be important for infection are (i) adhesion to the implanted device surface, followed by (ii) the secretion of an extracellular matrix, allowing cells to form stable colonies, inside the catheter lumen. Both *S. aureus* and *S. epidermidis* share the potential to utilize these two steps in their pathogenic cycles. They both contain the necessary components; being either the adhesin genes themselves, the biofilm operons and regulators, as well as the common staphylococcal accessory gene regulator *agr* and the *luxS* quorum

sensing circuit in *S. epidermidis.* The *agr* locus encodes four gene products necessary for quorum sensing based communication in a population. The activity of this locus can has been shown to control biofilm phenotypes *in vitro*, and has also been linked to the expression levels of various adhesin genes in *S. aureus* [98]. Further, it is becoming increasingly evident that the activity of the *agr* locus, as well as biofilm and adhesin genes is intimately linked to the extracellular environment. Previous reports have implicated osmotic stress, alcohols, pH and oxidative state to the regulation of these pathogenic factors, indicating their importance *in vivo* during pathogenesis [30,31,70]. We have shown here, in chapters I and II, that the mechanical microenvironment from fluid flow also has the ability to modulate pathogenic phenotypes in *S. epidermidis*, both in terms of adhesion and biofilm formation.

The mode of adhesion appears to be determined by the shear stress regime under which the planktonic cell are adhering, where single colonies dominate at low (~0.1 Pa) shear, where large cluster formation (on the order of 100 μm) dominate in the range of 1 Pa wall shear stress. This effectively increases the adhesive strength of *S. epidermidis* 12228 to fibrinogen, most likely through an avidity driven strength increase, simply due to an increase in the number of linkages between the cluster and the surface, although it is likely that at some critical cluster size, the increase in the number of adhesive sites is not enough to counteract the increase in viscous drag on the cluster (as the cluster volume scales with L^3, and the number of adhesive sites scales with the surface, or L^2).

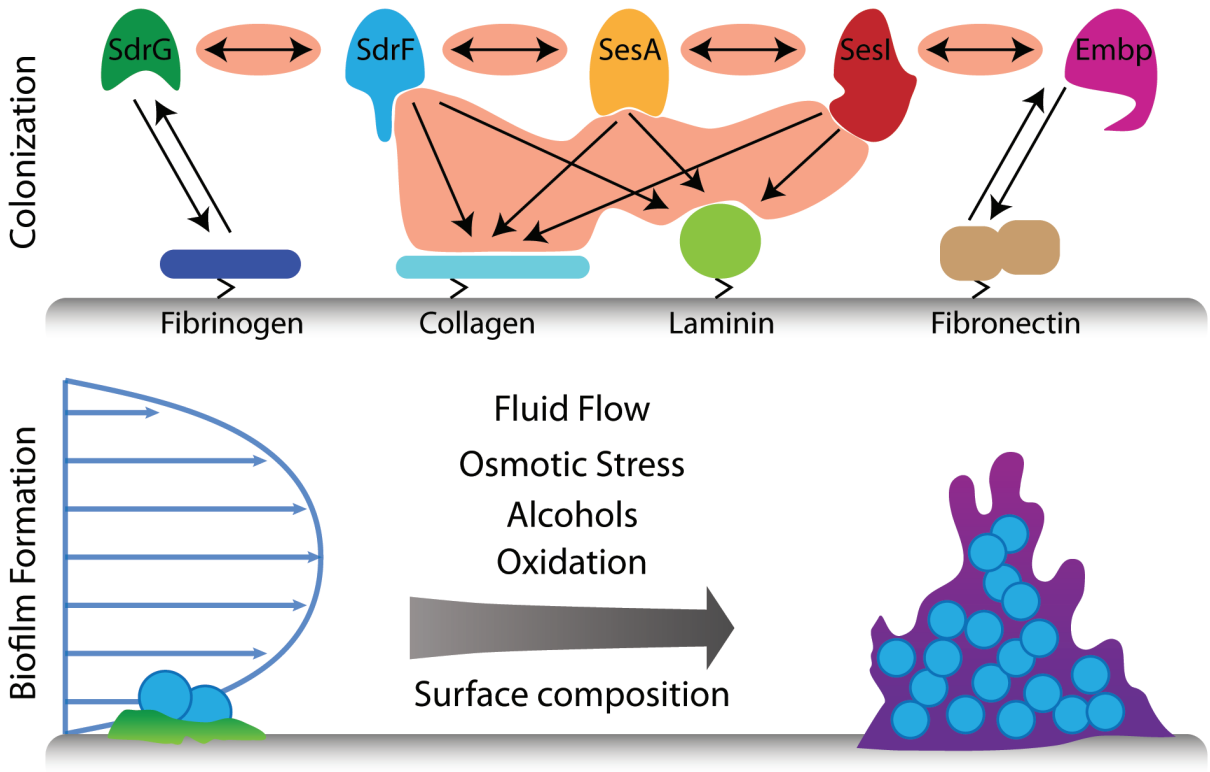

Figure 31: A brief schematic covering known and suspected interactions between Staphylococcal surface proteins and target proteins, as well as environmental factors modulating biofilm phenotypes in Staphylococci.

In some strains of *S. epidermidis*, biofilm formation phenotype can also be modulated with fluid flow, where increasing fluid shear leads to increased biofilm production. This may be either from direct sensing of fluid shear stress (or strain from that stress in surface proteins), or from the disruption of quorum sensing circuits from the convection of fluid away from cells immobilized on the surface. If the ladder were correct, then this mechanisms would fall in a paradigm similar to the one mimicked by the deletion of *agrD* in *S. aureus*, leading to impaired quorum sensing and decreased biofilm formation [33], and if the former were the case then it would fall in line with a mechanism similar to UPEC adhesion to urinary epithelial cells via FimH, which has

been shown to change confirmation under fluid shear and increase its avidity for its target epitope via a ‘catch-bond’ like mechanism [60].

It is clear that the pathogenic cycles of *Stapylococci* are complex, and not well understood. Figure 31 illustrates, albeit briefly, what is known about the adhesive capability of *Staphylococci*, as well as the influences of the environment on biofilm formation. All of this illustrates the need for a well defined, and carefully chosen, set of strains for the initial screens of adhesive landscapes in our platform. To this end, we have chosen a set of laboratory propagated strains of *S. epidermidis* and *S. aureus* with (potentially) different adhesive profiles, as well as a subset of clinical isolates of *S. epidermidis,* representing three distinct phenotypic populations (in regards to environmental regulation of biofilm formation), although they contain all the necessary components (that we are aware of) to form biofilms. The two strains of *S. aureus* used here are both Rosenbach strains (serotype 1), strains 12598 and 55804. Strain 12598 was isolated from a septic arthritis patient with an implantable joint, and has been a regular laboratory standard for a pathogenic *S. aureus* strain since its isolation in 1940 [99]. The second strain, 55804, is a serotype 336 strain, isolated from a urine sample. Two laboratory *S. epidermidis* strains, with fully sequenced genomes will also be used in initial adhesion studies. Both strain 12228 and 35984 contain *embp*, the gene encoding the fibronectin binding protein, as well as *sdrG*, encoding the fibrinogen binding protein. These are of note because they have been extensively studied, both in a-cellular binding studies, as well as using ectopic expression of these genes in *L. lactis* [87]. Other putative surface exposed adhesin genes are harbored in these strains, such as *sdrF,* and *sdrH* which have been implicated in colonization, but the targets for

binding have not been rigorously determined, nor have they been deemed sufficient for colonization of any surface.

In order to determine, functionally, whether these strains are capable of binding any of the target proteins in our assay, a simple well-plate adhesion study was carried out as a pre screen. Thus far, the target proteins that have been characterized in our system, in terms of binding specificity to the streptavidin surface and spot homogeneity, are fibrinogen, fibronectin, collagen I, collagen IV, and laminin. We have covered a wider base in these well plate assays, as they do not require any preliminary conjugations, to include vitronectin and tropoelastin as well. Elastin has been implicated as a binding target for the EbpS surface protein in *S. aureus*. EbpS is unique in that is does not contain the canonical LPXTG motif at the N terminus used to link the protein to the peptidoglycan layer via a sortase-dependent mechanism. Rather, EbpS is a trans-membrane protein containing two trans-membrane domains, with the N terminus extracellular, containing the elastin-binding region [100,101].

Well plate adhesion pre-screens were carried out in glass bottom, black 384 well plates (Greiner Bio-one) as illustrated in figure 32a. Wells were coated with pure protein at a concentration of either 100 μg/ml or 50 μg/ml (vitronectin and laminin) in 1X PBS. Coating was performed at room temperature for 1 hour, followed by extensive washing in 1X PBS (5 aspirations and washes with 100 μl PBS. Proteins conjugated with Cy-5 were adsorbed to plate surfaces, followed by washing and measurement of surface fluorescence in a plate reader to ensure that all proteins were adsorbing to the glass bottom plate surface. Briefly, wells that were either treated with protein or only PBS were then incubated with bacterial cells grown up to mid log phase and washed

three times in 1X PBS. Cells were either added to the wells in their native state, or pre-incubated in a tube with 50μg/ml of soluble protein (the same as the one coated in the well). This was to simulate a titration of the cells from the surface, to determine if the adhesion (if any) to the well surface was specific to the protein on the surface (figure 31a). Cells were allowed to interact with the surface for 1 hour, after a gentle spin down onto the surface at 500xg for 2 min. After the 1-hour incubation at 37^{o}C, the wells were washed and cells fixed with 4% paraformaldehyde, followed by staining with 1μg/ml DAPI. Wells were read in a plate reader, and total well fluorescence reported. Initially, serial dilutions of mid log cells were washed as described, stained with DAPI, and centrifuged down to the well surface at 1500xg for 5 min. Subsequently, the well fluorescence was measured to create a calibration curve and determine the dynamic range of the experiment (figure 31b). The lower limit of detection for this assay is ~10^6 cells on the surface, assuming that all of the cells placed in the well were centrifuged down on the surface. In reality, the number may be lower (typical recovery from centrifugation steps is ~70% at best). Regardless, the order of magnitude approximation of the dynamic range is at least two orders of magnitude, with the lower limit at 10^6cells. It is possible that the upper limit has not been reached in this curve, however this range provides a discernable difference between protein types.

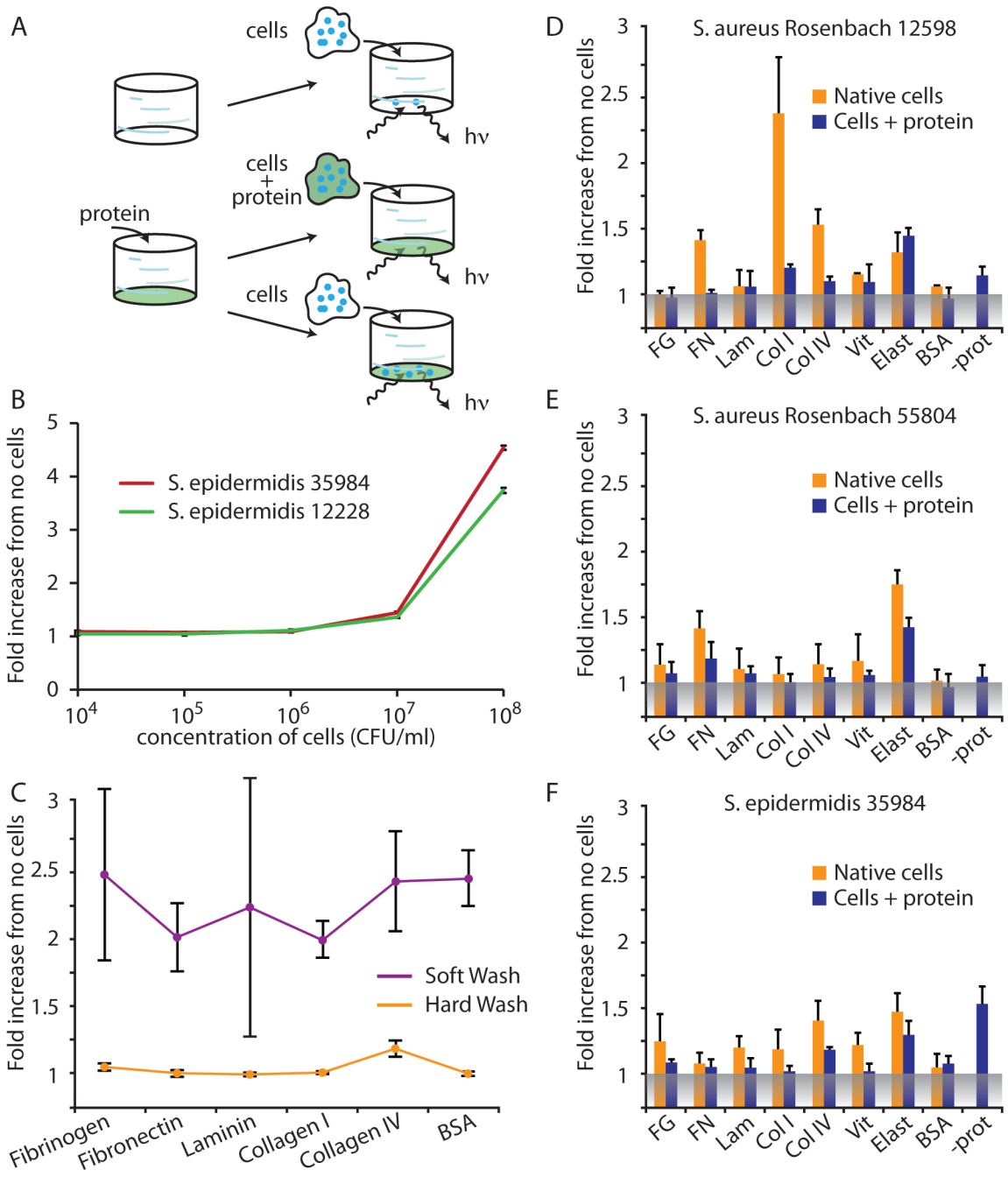

Figure 32: Well plate pre-screen for adhesive phenotypes in both *S. aureus* and *S. epidermidis*. The importance of physical force is illustrated in C, where the wash strength determines output. D-F show the hits resulting from strong interactions between cells and coated surfaces, where *S. epidermidis* has a strong interaction with uncoated wells and *S. aureus* does not.

It is important to realize the limitations of this pre-screen experiment, as although it is simple to perform and relatively quick, the sensitivity of the assay is low, and the dynamic range for adhesive strength is poor. Figure 32c illustrates this point, by comparing experiments with *S. epidermdis* 12228 using different wash methods. The 'soft wash' involves aspiration of 75% of the well volume (from the top of the liquid level), followed by gentle addition of fresh wash solution. A 'hard wash' is simply a full liquid aspiration using a vacuum line, followed by pipetting the full amount of fresh solution back in. Figure 32c indicates that the output metric depends of how well the nuances of the experiment (like well washing) are performed. This makes intuitive sense as the washing step is the point in the experiment at which physical force is applied, separating weak and strong interactions. This step is the crux of the experiment, however, the only way to ensure the experiment is performed in a repeatable fashion is to impart a 'hard wash'. This is due mainly to practical consideration of the experiment like operator error from pipetting and can be alleviated to some degree with liquid handlers. Even with the use of robotics for pipetting, the most reproducible wash is the strongest. This is perfectly fine, and arguably is beneficial in that what we measure in the assay is the strongest interaction, meaning that any detectable signal is due to an interaction in the high end of adhesive strength. Indeed, we see significant differences, not only between proteins, but between strains in this assay. *S. aureus* 12598 adheres strongly and specifically to collagen I, as well as fibronectin and collagen IV (figure 32d), where as *S. aureus* 55804 adheres to elastin and, to a lesser degree, fibronectin (figure 32e). Further, *S. epidermidis* 35984 exhibits significant increases in well florescence on collagen IV, vitronectin, and elastin coated wells. Interestingly, both the fibrinogen and

fibronectin coated wells elicited a very mild (not statistically significant) increase in fluorescence from 35984 (figure 32f), even though this strain contains the adhesins for both targets. Even more striking is the almost completely negative panel observed for *S. epidermidis* 12228 in figure 32c (yellow line). Not only does 12228 contain the genes necessary for adhesion to fibrinogen and fibronectin (verified via cross-referencing genomic data and PCR identification of the presence of the gene), we have performed microfluidic experiments with this exact strain previously and seen significant and specific adhesion to immobilized fibrinogen under flow. These results give both useful first order approximation data regarding adhesive capabilities of the strains, while at the same time indicate the need for a highly tunable system for adhesion.

With these cursory adhesive phenotypes in mind, we have begun to perform adhesion assays without flow using printed microarray substrates. These experiments offer both a small step toward a more controlled binding environment for quantitative adhesion landscapes, as well as assessment of the ability of cells to recognize the epitopes on these proteins after they have been biotinylated, labeled with fluorophore, and spotted onto our surfaces.

As these experiments lend themselves to the generation of large amounts of data quickly, it is beneficial to have an automated system in place for analysis. In the case of our microarrays, the output metrics are surface densities of cells, and colocalization of those signals with protein spots. This information is embedded in the fluorescent images taken of the seeded, washed, and stained substrates, thus an automated image analysis script would be highly desirable for this assay. We have developed an image

analysis suite in Matlab that automatically processes large, stitched images of microarrays.

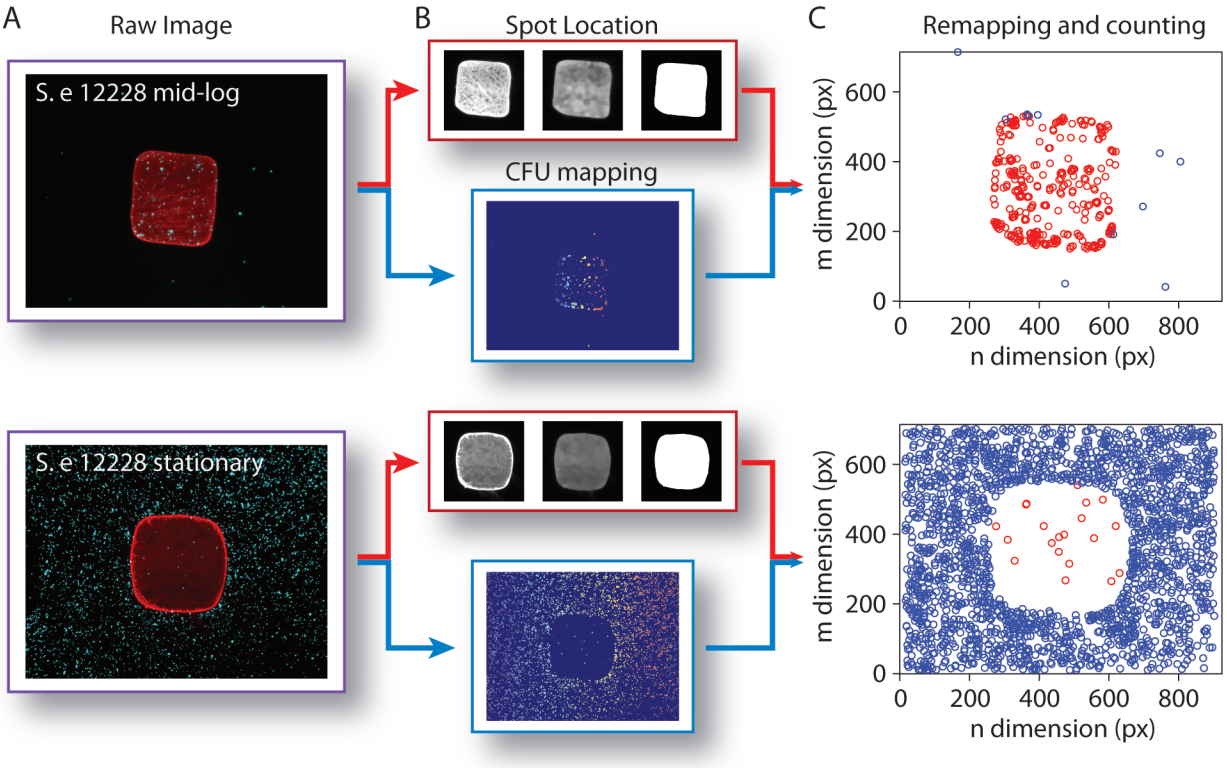

Figure 33: Schematic of automated image analysis script in Matlab. There are three main subroutines run for each filed of view: A: splitting of the raw image data into the fluorescent channels B: analysis of each channel separately to identify spot location and CFU location and C: recombining these data via cross-correlation to determine which CFUs lie within the spot and which do not. Subsequently, *.csv files are written that contain both the raw counts as well as surface density calculations.

The images are multi layered, containing multiple fluorescent channels spatially overlaid (figure 33a) in a multidimensional cell array. Our script first deconstructs that cell array and puts each channel into a 2-dimensional array. These are subsequently handled separately. The protein spot channel is adjusted, and erosion and dilation

filters (in that order) are applied to the image to create smoother gradients within the spot. This image is then converted to a binary black and white image, calculating both the area of the spot, as well as registering each pixel location within the spot for cross reference to bacteria. Simultaneously, the DAPI image of adhered bacteria is normalized to the maximum intensity value, and adjusted. Next, a watershed function is applied to the image, allowing identification of objects of a certain shape to be identified (here we use a kernel of a disk, size 5 pixels). Each CFU is identified and its centroid and area are stored in a separate cell array. Next, the centroid data from each located CFU is cross-correlated to the registry matrix created from the spot array. If the centroid of the CFU lies within the positive values in the matrix, then this CFU is counted as in the spot, and visa versa. Finally, a plot Is generated to visualize the data (figure 33c), and the actual data (both raw numbers and surface densities) are written to a *.csv file for further analysis.

When moving from a bulk experiment like a well plate to a surface patterning technique, one of the main concerns is actually directing the cells to adhere to the pattern on the surface. Non-specific interactions with the areas off-pattern can be a significant challenge to overcome, especially in experiments where cells will be grown on the surface for multiple generations. In our previous experiments using *in situ* linkage and blocking in the microfluidic channel, it was determined that the most effective method of passivation was to create a hydrophobic surface via silanization, then adsorb a PEG block copolymer, pluronic F-127 to the hydrophobic region. Unfortunately the current system, although on a PDMS gasket, does not lend itself to that method, as the streptavidin layer renders the surface hydrophilic. Addition of

pluronic to the surface does reject some adsorption of BSA, however it also appears to remove protein previously printed on the surface, despite the biotin streptavidin linkage. To overcome this challenge, we have investigated two methods to passivation: (i) BSA adsorption after printing and (ii) flooding the surface after printing with a freshly made biotinylated 8-ARM peg star to cover unreacted streptavidin (figure 34a). Both of these methods appear to effectively reject cells from adhering (although not 100%) from off the pattern (figure 34b,c). It should be noted that for data presented henceforth, the blocking mechanism is BSA, as the performance was comparable, and the cost effectiveness of the BSA blocking is far superior to that of the PEG conjugate.

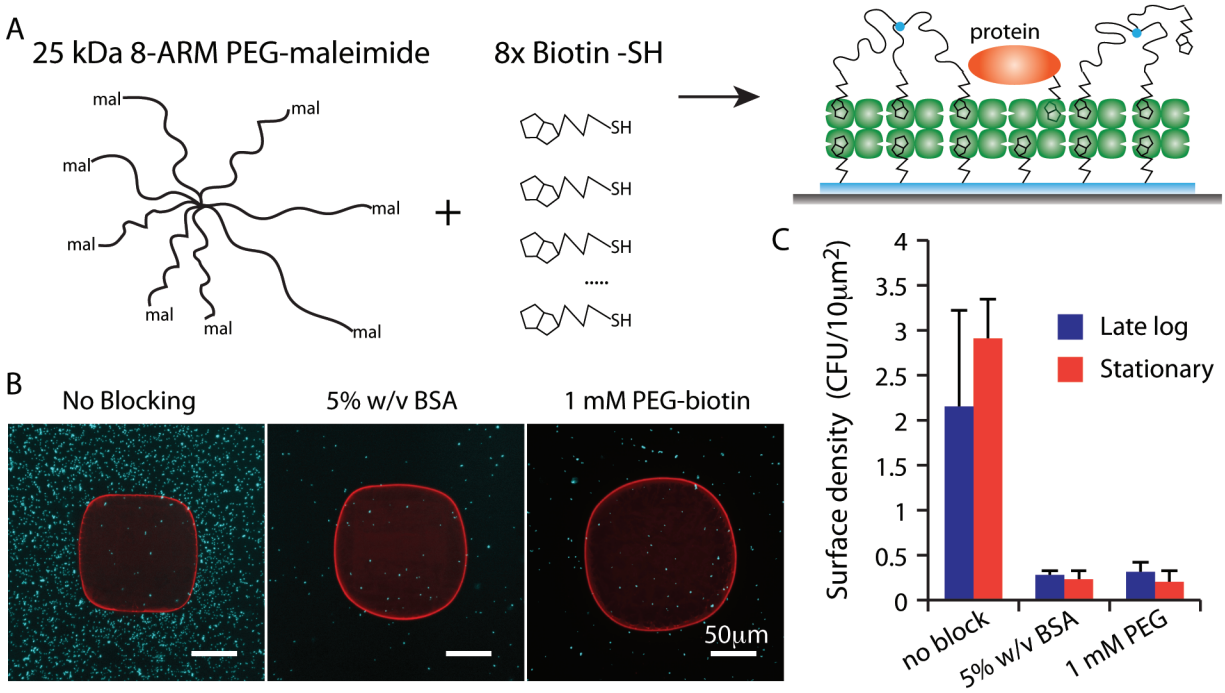

Figure 34: Passivation of the streptavidin surface after printing protein microarrays. Both specific (PEG-biotin) and nonspecific (BSA) methods were employed, and their performance was comparable, however the cost effectiveness of BSA is far superior to that of the expensive PEG conjugate. Here we assume that there is no specific interaction between cells and BSA, given the record of BSA as a general blocking agent.

Secondly, we performed experiments to determine if any conjugation chemistries were altering the binding capacity of the printed proteins. For these experiments we used the model strain *S. epidermidis* 12228. Initially, prints containing the fully conjugated protein, the protein only biotinylated, and also an unconjugated pure protein adsorbed to the streptavidin layer. It should be noted that streptavidin tends to not adsorb proteins as well as a hydrophobic surface, however we have previously shown that there is some non-zero adsorption of non-biotinylated proteins (figure 26d) using protein only conjugated with fluorophore. When comparing conjugated proteins to their native counterparts, it appears that for both collagen I and IV there are no significant changes, however for fibrinogen, the addition of the fluorophore drastically inhibits the binding capacity of the protein. Fibronectin also displays a significant decrease in cell adhesion, although to only about 75% of native protein. This indicates that lysine residues may be especially important in the interaction between *S. epidermidis* and fibrinogen (presumable via SdrG). Although there are no lysines in the 14 aa epitope on the β chain (β6-20) shown to be sufficient to bind recombinant SdrG [24], it is possible that there is some allosteric disruption, or that a neighboring lysine residue is important in increasing binding efficiency, but not necessary to achieve a low level of binding.

For efficient and accurate automation of image analysis of adhesion data, it is necessary to have some way to locate the printed spot. To avoid having the extent of labeling that was shown to decrease binding, but still have a fluorescent spot, we investigated the use of a surrogate fluorescent molecule for printing. A 50 kDa poly-D-lysine molecule was used as a carrier of fluorophore for the spot. Prior to printing, the PDL was both biotinylated and labeled extensively with fluorophore (20:1 molar ratio of

fluorophore to PDL). This was then dialyzed and mixed with target protein prior to printing (figure 35b). When PDL alone is printed (labeled with biotin and fluorophore) a log linear correlation of surface fluorescence to concentration is observed, however when premixed with protein and then spotted, it appears that the interactions between the PDL and the protein are very important for spot homogeneity (figure 35d). For fibrinogen, and both collagen I and IV the spot homogeneity is within the rage of 0.2 CV, however both laminin and fibronectin have very poor spot homogeneity.

It is likely that there are strong electrostatic interactions between the highly charged PDL and the target protein, the nature of which depends on the composition of the target protein itself. For example, fibronectin and laminin are both generally hydrophobic as they are vey large molecules 440kDa and 800kDa respectively, that compose the extracellular matrix and basement membranes. This hydrophobicity may possibly result in an unfavorable interaction with a charged, soluble molecule such as PDL. Further, the addition of PDL to protein spots results in changes in cell adhesion that is not intuitive, given our current understanding of *S. epidermidis* adhesion. In some cases (PDL with fibrinogen and large amounts of PDL with fibronectin) the addition of PDL appears to increase cell adhesion (perhaps through electrostatic interactions), however for collagen IV with PDL there is a decrease in adhesion. Further, the highly irregular dependence of adhesion on the ratio of fibronectin to PDL makes this approach not desirable for generating intuitive and easily interpretable data. In order to effectively interpret the adhesion data, there would have to be an exorbitant amount of control prints, negating the usefulness of the fluorescent spot in the first place.

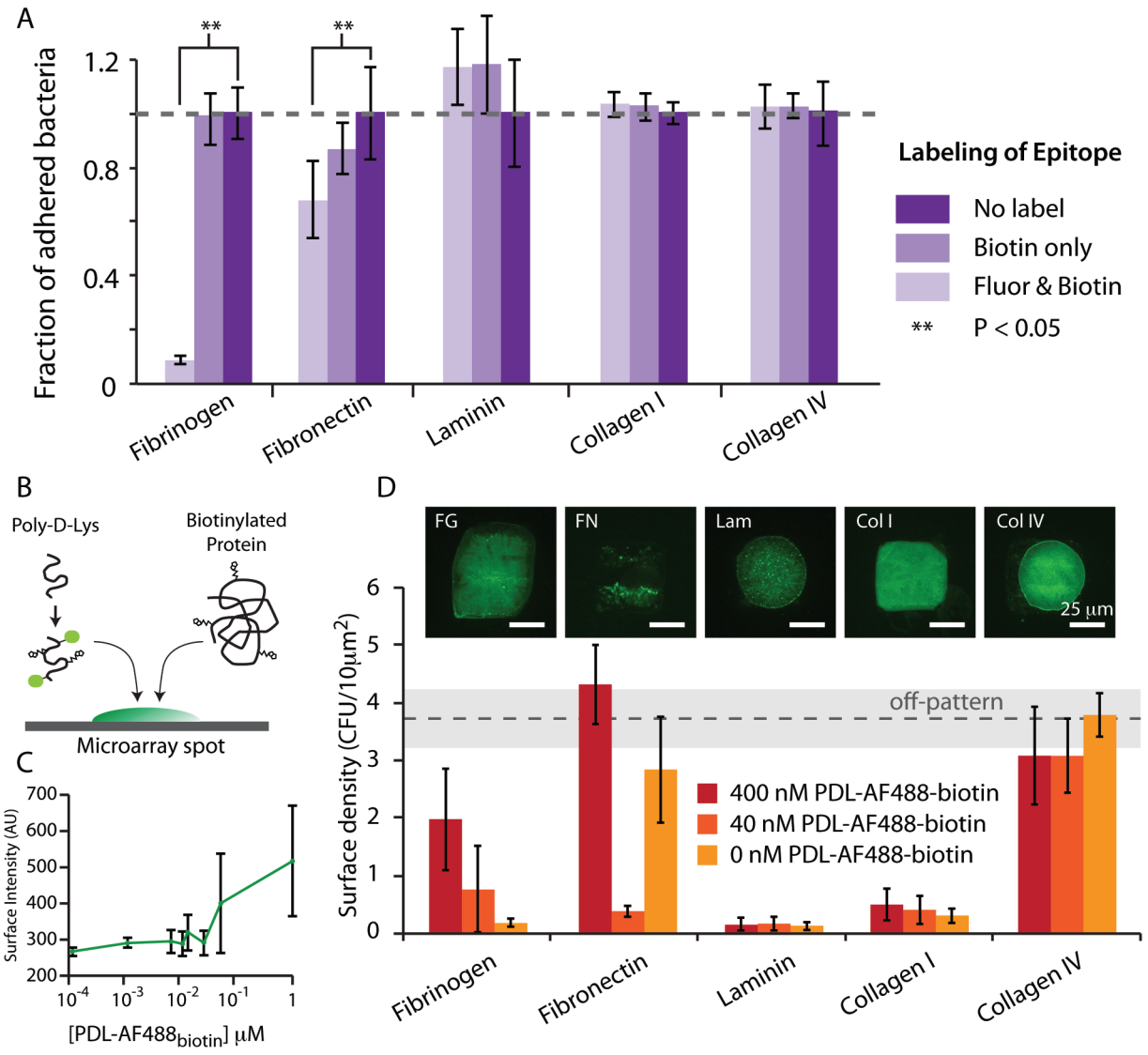

Figure 35: Extent of protein labeling affects the adhesive capacity. A: systematically removing conjugation steps reveals that for fibrinogen, the addition of the fluorophore greatly hinders binding capacity (an order of magnitude decrease). B: An alternative method of co-printing labeled poly-D-lysine as a fluorescent surrogate. C: printing PDL alone gives a long linear relationship between intensity and concentration, however when printed with proteins spot homogeneity decreases. D: Further, addition of PDL to protein spots affects binding differentially for different proteins.

As an alternative method to printing fluorescence on the actual spot where the protein is printed, we investigated the efficacy of using 'registry' spots, to be printed next to each subarray so that then the image analysis script scans through the image, it can locate the centroid of the registry spot, and determine the locations of each spot in the subarray using known distances. Figure 36d illustrates the overall layout and concept, where the register spots are in red. The spots are composed of BSA that has been heavily labeled with fluorophore and biotinylated. The biotinylation is to avoid smearing when the arrays are reconstituted in buffer, as we know from previous blocking experiments that BSA will adhere nonspecifically to the streptavidin surface well. Utilization of BSA as the register spot component allows for integration of another spot, visible to the eye of both human interrogating the substrate, as well as the automated image analysis code, although the spot is 'invisible' to the cells that come in contact with the surface, as the surface will be pre-incubated with BSA for blocking purposes prior to cell adhesion.

Previously, all protein has been printed at a concentration of 300μg/ml for maximum concentrations, however we have found that with our BSA conjugates with results in a poor signal to noise ratio after washing (figure 36). Rather than washing the protein off of the substrate, excess protein that was spotted, but unable to react with the surface in the immediate vicinity of the spot made, smears and reacts with the surrounding surface upon reconstitution in buffer (figure 36a). Titration of the surface with serial dilution of protein reveals that the ideal range for printing concentrations is between 50 and 100 μg/ml. It is important to have good SNR for these register spots as they will be used to calculate the locations of adjacent spots, thus irregularities in

calculated spot shape and location (due to the code improperly assuming that a smear is part of the spot) could lead to incorrect calculations of cell densities on spots.

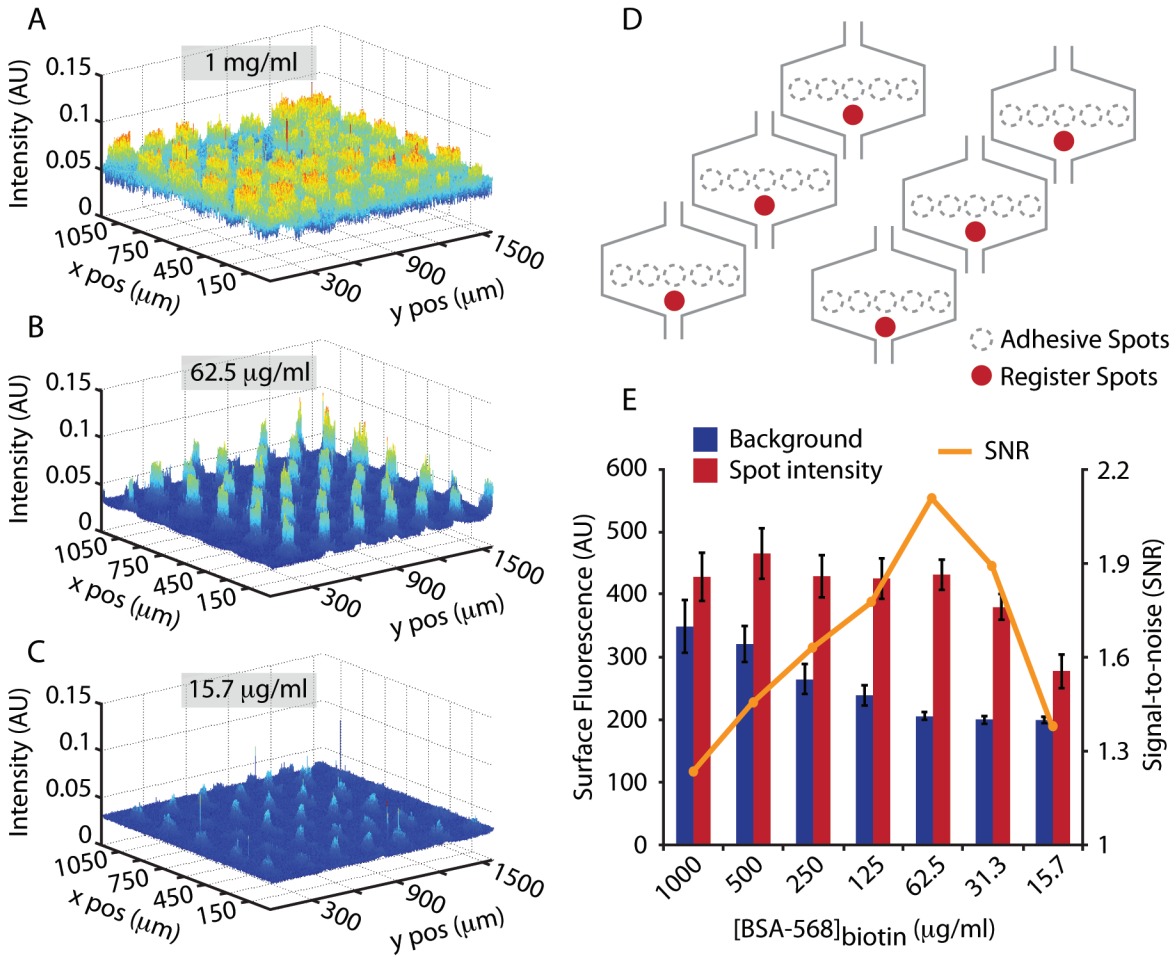

Figure 36: Using register arrays as dummy markers for subarray locations. Biotinylated and fluorescently labeled BSA is printed just under each subarray so that when the image analysis code picks it p and calculates is centroid, the code can then calculate the centers of each subarray spot using known distances.

Finally, it is also important to understand the biological variables present and contribute to adhesive screen efficacy. Specifically, growth phase of bacteria grown *in vitro* has been shown to affect the expression of adhesin genes in some strains of *S. aureus*, indicating a quorum sensing based regulation of these genes. To asses the

growth phase resulting in the greatest adhesive capability, the *S. epidermidis* model strain 12228 was assessed for growth phase depended ashesion. These experiments were performed using static microarray printed substrates (i.e. no flow). For these experiments, cells are grown overnight in BHI medium, then re-inoculated at a ratio of 1:1000 in BHI, and allowed to grow to the appropriate growth phase. For these experiments we assessed mid-log phase, late-log phase, and stationary phase. We hypothesized that, if adhesion is controlled by quorum sensing, then during growth at a lower density (i.e. mid-log) should result in more adhesiveness than at stationary culture. Here the reasoning stems from modulation of life cycle between sessile (i.e. in a biofilm or bacterial community) and free-floating planktonic cells. At high density, the quorum sensing autoregulation should be vey active, due to the high concentration of autoinducer, switching on biofilm formation genes (if the cells contain them) and decreasing expression of adhesins.

Indeed there is a difference in adhesive profiles between growth phases in *S. epidermidis* 12228, however it was not in the manner expected. Our hypothesis was simply that cells would be more adhesive in mid loge phase compared to stationary, and this was partially supported by our findings, however it was not as simple as that. The most striking aspect can be seen in figure 37a, comparing DAPI stained, fixed cells in mid log (left) and stationary phase (right). Upon initial observation, the data would appear to directly refute our hypothesis, as there are more generally cells everywhere at a later growth phase. However, it is important to note that these samples were unblocked prior to the addition of cells. The quantitation can bee seen in figure 37b, illustrating that in mid log, the only adhesive target is fibronectin, however the cells tend

to adhere more generally to all targets at late log and stationary phase (and adhere especially well to collagen IV). The obvious next question is why the cells adhere so much more off the pattern at a later growth phase than at mid log. The concentration of cells was exactly the same in each case, yet the surfaces appear baron at mid log with the exception of fibronectin.

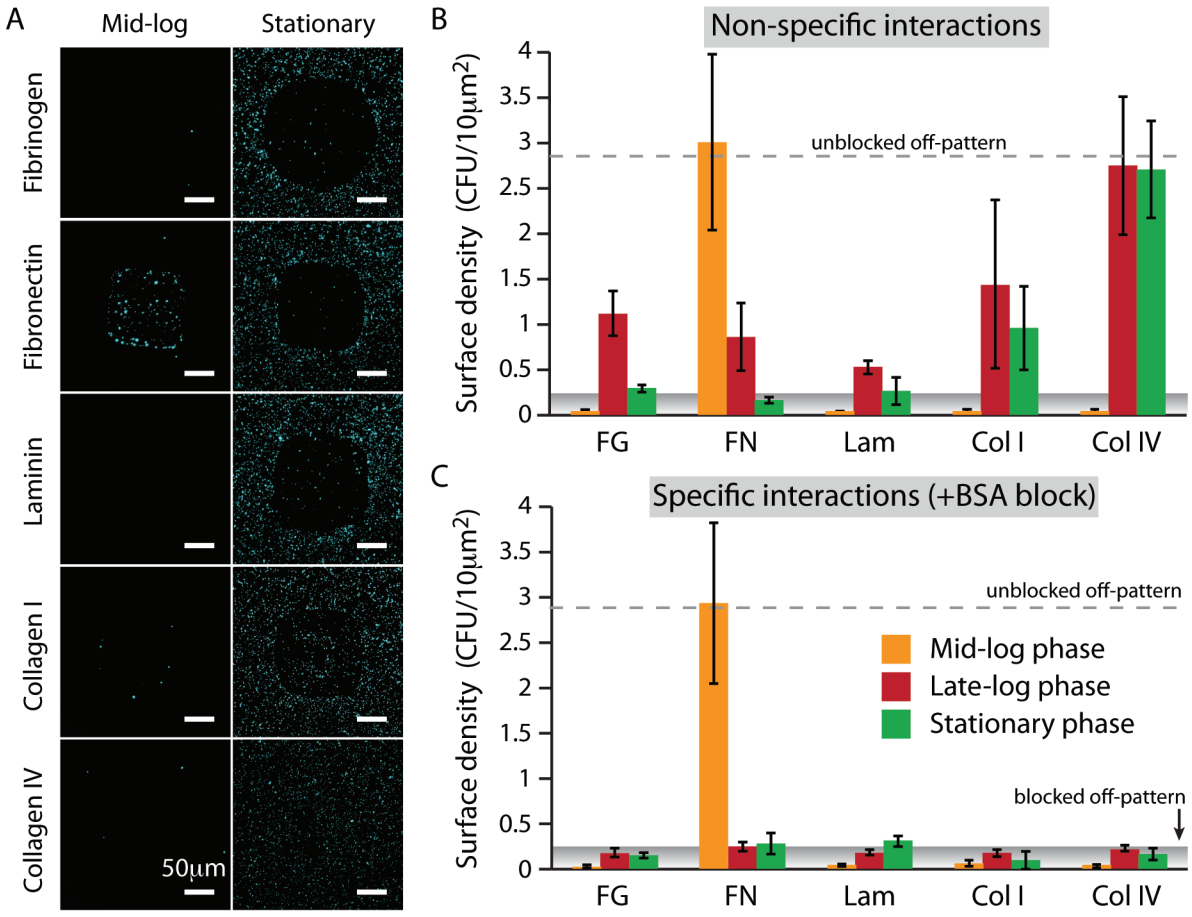

Figure 37: A: Adhesion to host proteins is growth phase dependent in *S. epidermidis* 12228. B: Non specific interactions with surface proteins. C: Blocking using BSA illustrates specific interactions with surface proteins, where only fibronectin at a mid-log phase culture elicits a specific interaction.

The question of off pattern interaction can begin to be answer with the addition of blocking agents to the surface. Figure 37c illustrates that, when the surfaces are pre-incubated with BSA before adhesion, virtually all adhesion is knocked down to background levels at ALL growth phases, with the drastic exception of adhesion to fibronectin at mid-log phase. Very simply, this indicated that the interaction with fibronectin at mid-log phase is both strong and specific, however there are a few questions left unanswered. First, the fact that there is no detectable specific interaction with fibrinogen (a known target for these cells) indicates an unknown is not controlled for here. It should be noted here that this assay was performed with fluorescently labeled proteins, and it is entirely possible that binding is knocked down simply due to over-labeling of the epitope. If the date from the previous experiment is loosely extrapolated and applied here, then the 10 fold change in binding without fluorophore would lead to significant binding here, however these experiments need to be performed outright before a conclusion can be drawn there specifically. Secondly, the fact that these adhesive profiles (even the unblocked ones) in these microarray assays do not overlay with the data collected from the well plate experiments, indicating that the force applied on the substrates during washing is still uncontrolled, further necessitating a highly precise washing step, effectively provided by the microfluidic channels in our screen.

Despite some unanswered questions, we have successfully developed a new platform for assessing binding to immobilized epitopes, and have primed our high throughput adhesive screen experiments with the necessary controls to properly interpret results obtained from our screens of adhesive landscapes.

VI. Conclusions and Future Directions

Healthcare associated infections, especially those arising from the use of implanted devices such as peripherally inserted central catheters, are not only a huge financial burden on hospital systems, but also greatly endanger the patient, leading to increased morbidity and mortality in patients with compromised or underdeveloped immunity; often the patients receiving these catheter devices. Pathogens often cultured from these infections are diverse, including gram negatives and gram positives, however the most frequently isolated bacteria is *Staphylococci*.

Over the past 20 years, a wealth of information regarding the pathogenesis of both *S. aureus* and the increasingly isolated *S. epidermidis* has been gained, however what has resulted is a complex picture of pathogenesis, with many unanswered questions regarding key steps in pathogenesis shared by the seemingly diverse organisms. The current paradigm does not provide a clear path to treatment of infection, however the concept of environmental regulation of virulence factors such as adhesin production, biofilm formation, and toxin production may offer new insight into what aspects we may have control over in the clinic, enabling modulation of virulence and increased efficacy of treatment.

Both adhesion of planktonic cells to implanted device surfaces as well as specific interactions between bacterial proteins and host proteins are thought to contribute to colonization. Subsequently, the ability of those cells to secrete a protective and adhesive matrix allows those cells to grow into stable biofilms. These multicellular structures are thought to allow bacteria to evade host immune defenses, as well as modulate their metabolic profiles to survive antibiotic treatments. Further, the

microenvironment in which these cells reside can drastically modulate the functionality of adhesion and biofilm formation, leading to changes in pathogenic potential.

We have shown that clinically relevant fluid flows exerted in a catheter lumen during normal operation can lead to further modulation of pathogenic potential *in vitro*. We have employed novel microfluidic systems to both create adhesive patterns in channels, and subsequently direct cells to those patterns under a range of fluid shear stresses, assessing adhesive capability and allowing adhered cells to grow and form biofilms under these shear stresses. Our results indicate that shear stress from fluid flow can both increase the overall adhesive capabilities of free flowing *S. epidermidis* cells to immobilized fibrinogen, as well as induce the formation of biofilms in some clinical isolates of *S. epidermidis* that do not normally form biofilm *in vitro*. Effectively, we have further complicated the matter of catheter-related pathogenesis in *Staphylococci*.

In a quest to remedy the lack of clarity in Staphylococcal HAIs, we are developing a next generation *in vitro* assay for a 'top down' engineering approach to pathogenesis. This system incorporates large-scale microfluidic circuits for the interrogation of a wide range of shear stresses simultaneously, functionally integrated with high throughput protein microarrays. The printed microarrays are aligned to the microfluidic circuitry to create a highly defined multidimensional assay for the quantitative development of pathogenicity landscapes for common HAI related bacteria. By systematically controlling all environmental parameters such as fluid shear, protein type, concentration, and combination, we can begin to build intuition about what host factors, as well as environmental pressured imparted from the implanted device itself,

may contribute to pathogenesis *in vivo*. This high throughput, multidimensional assay is an excellent platform for identifying potential therapeutic targets to fight infection by recognizing combinations of host and environmental factors that least to increased adhesion or biofilm formation or, conversely result in significantly less. Given that we have some cursory knowledge regarding the basic molecular connectivity of the bacterial system for adhesion and biofilm formation, by systematically varying the inputs and measuring how the output metrics of adhesion density and total biofilm formation change, we can infer important nuances about the functional connectivity of the whole cell (and even multicellular) systems. This has the potential to shed practical knowledge on the seemingly convoluted mechanisms of pathogenesis in these organisms.

With preliminary fabrication and testing completed on the functional system, the next steps will entail the screening of model organisms with known adhesive phenotypes to ensure that the system is functionally sound. These experiments can also shed light on never before answerable questions about the piecewise contributions of each suspected adhesive target in the overall colonization of a surface by free-floating bacteria. Initial experiments will focus on *Staphylococci*, specifically *S. aureus* and *S. epidermidis*, as we have previously build an adhesive and biofilm formation biological model system by carefully selecting strains from both fully sequenced laboratory strains and phenotypically distinct clinical isolates.

The next steps beyond these experiments involve a divergence down two paths: one being continual usage of this high throughput functional screen to generate massive libraries of adhesive and biofilm formation phenotypes, toward the creation of datasets

that can be used as lookup tables for identification of the critical aspects of adhesion and/or biofilm formation for an unknown bacterial species. Here the goal is to assay as many diverse types of bacteria and fungi as possible, to strengthen the comprehensiveness of our pathogenicity library, perhaps even to be used one day in the clinic as a tool to inform treatment decisions and procedures. The second path is to begin to take pathogenic hits from our first round screens (either scenarios resulting in increased adhesion and/or biofilm formation) and beginning to hone in both physically and molecularly on these, toward the identification of novel therapeutic targets. Here the ultimate goal is to develop a new paradigm of treatment, not relying on the use of antibiotics, but rather treating a specific mechanism by which the pathogen establishes infection.

Although here we focus on bacterial pathogenesis, the system itself lends more quantitative methods for the analysis of cell-surface interactions than any current technology available. This system could be easily applied to developing adhesive profiles for cells harvested from a primary tumor, or secondary metastatic sites, with the aim of developing a functional serotype for the progression of hyperplastic cells to malignant cell types, possibly even shedding new light on the Epithelial to Mesenchymal Transition (EMT), and the highly debated MET (reverse transition) which may be linked to the existence of cancer stem cells [102,103].

In any case, there is no shortage of work to be done in the realm of high throughput quantitative biology. As we, as a scientific community, learn more about the immense complexity of functional biological systems, the more apparent the need for high throughput, quantitative systems. To this end, systems such as this one should be

carefully developed with integration to current high throughput systems in mind, so that the usefulness o the novel technology being developed can be maximized, and scientific discovery can be accelerated, leading to new, more effective treatments actually put into practice.

VI. References

1. Hoshal VL, Jr. (1975) TOtal intravenous nutrition with peripherally inserted silicone elastomer central venous catheters. Arch Surg 110: 644–646. doi:10.1001/archsurg.1975.01360110190032.

2. Levy I, Bendet M, Samra Z, Shalit I, Katz J (2010) Infectious complications of peripherally inserted central venous catheters in children. Pediatr Infect Dis J 29: 426–429. doi:10.1097/INF.0b013e3181c94d9e.

3. Dimick JB, Pelz RK, Consunji R, Swoboda SM, Hendrix CW, et al. (2001) Increased resource use associated with catheter-related bloodstream infection in the surgical intensive care unit. Arch Surg Chic Ill 1960 136: 229–234.

4. Kelly D, Kutney-Lee A, Lake ET, Aiken LH (2013) The critical care work environment and nurse-reported health care-associated infections. Am J Crit Care Off Publ Am Assoc Crit-Care Nurses 22: 482–488. doi:10.4037/ajcc2013298.

5. RELLO J, OCHAGAVIA A, SABANES E, ROQUE M, MARISCAL D, et al. (2000) Evaluation of Outcome of Intravenous Catheter-related Infections in Critically Ill Patients. Am J Respir Crit Care Med 162: 1027–1030.

6. Costerton JW, Stewart PS, Greenberg EP (1999) Bacterial biofilms: a common cause of persistent infections. Science 284: 1318–1322.

7. Uçkay I, Pittet D, Vaudaux P, Sax H, Lew D, et al. (2009) Foreign body infections due to Staphylococcus epidermidis. Ann Med 41: 109–119. doi:10.1080/07853890802337045.

8. Calfee DP (2012) Crisis in hospital-acquired, healthcare-associated infections. Annu Rev Med 63: 359–371. doi:10.1146/annurev-med-081210-144458.

9. Tshamba HM, A Kaut CM, Kyalubile NM, Kakambal AK, Yav GD, et al. (2013) Cost of hospital care for HIV/AIDS infected patients in three general reference hospitals in Lubumbashi, DR Congo: prospective cohort study. Pan Afr Med J 15: 76. doi:10.11604/pamj.2013.15.76.2638.

10. Thom KA, Kleinberg M, Roghmann M-C (2013) Infection prevention in the cancer center. Clin Infect Dis Off Publ Infect Dis Soc Am 57: 579–585. doi:10.1093/cid/cit290.

11. Cheung GYC, Otto M (2010) Understanding the significance of Staphylococcus epidermidis bacteremia in babies and children. Curr Opin Infect Dis 23: 208–216. doi:10.1097/QCO.0b013e328337fecb.

12. Garrod LP (1960) Relative Antibacterial Activity of Three Penicillins. Br Med J 1: 527–529. doi:10.1136/bmj.1.5172.527.

13. Allen HK, Donato J, Wang HH, Cloud-Hansen KA, Davies J, et al. (2010) Call of the wild: antibiotic resistance genes in natural environments. Nat Rev Microbiol 8: 251–259. doi:10.1038/nrmicro2312.

14. Wright GD (2007) The antibiotic resistome: the nexus of chemical and genetic diversity. Nat Rev Microbiol 5: 175–186. doi:10.1038/nrmicro1614.

15. Livermore D (2004) Can better prescribing turn the tide of resistance? Nat Rev Microbiol 2: 73–78. doi:10.1038/nrmicro798.

16. Willemsen I, Bogaers-Hofman D, Winters M, Kluytmans J (2009) Correlation between antibiotic use and resistance in a hospital: Temporary and ward-specific observations. Infection 37: 432–437. doi:10.1007/s15010-009-8325-y.

17. Neuhauser MM, Weinstein RA, Rydman R, Danziger LH, Karam G, et al. (2003) Antibiotic resistance among gram-negative bacilli in us intensive care units: Implications for fluoroquinolone use. JAMA 289: 885–888. doi:10.1001/jama.289.7.885.

18. Tabah A, Koulenti D, Laupland K, Misset B, Valles J, et al. (2012) Characteristics and determinants of outcome of hospital-acquired bloodstream infections in intensive care units: the EUROBACT International Cohort Study. Intensive Care Med 38: 1930–1945. doi:10.1007/s00134-012-2695-9.

19. McCrea KW, Hartford O, Davis S, Eidhin DN, Lina G, et al. (2000) The serine-aspartate repeat (Sdr) protein family in Staphylococcus epidermidis. Microbiol Read Engl 146 (Pt 7): 1535–1546.

20. Fitzgerald JR, Foster TJ, Cox D (2006) The interaction of bacterial pathogens with platelets. Nat Rev Microbiol 4: 445–457. doi:10.1038/nrmicro1425.

21. Josefsson E, Hartford O, O'Brien L, Patti JM, Foster T (2001) Protection against experimental Staphylococcus aureus arthritis by vaccination with clumping factor A, a novel virulence determinant. J Infect Dis 184: 1572–1580. doi:10.1086/324430.

22. Brady RA, Mocca CP, Burns DL (2013) Immunogenicity analysis of Staphylococcus aureus clumping factor A genetic variants. Clin Vaccine Immunol CVI 20: 1338–1340. doi:10.1128/CVI.00275-13.

23. Perkins S, Walsh EJ, Deivanayagam CC, Narayana SV, Foster TJ, et al. (2001) Structural organization of the fibrinogen-binding region of the clumping factor B MSCRAMM of Staphylococcus aureus. J Biol Chem 276: 44721–44728. doi:10.1074/jbc.M106741200.

24. Bowden MG, Heuck AP, Ponnuraj K, Kolosova E, Choe D, et al. (2008) Evidence for the "Dock, Lock, and Latch" Ligand Binding Mechanism of the Staphylococcal Microbial Surface Component Recognizing Adhesive Matrix Molecules (MSCRAMM) SdrG. J Biol Chem 283: 638 –647. doi:10.1074/jbc.M706252200.

25. Chauhan A, Lebeaux D, Decante B, Kriegel I, Escande M-C, et al. (2012) A rat model of central venous catheter to study establishment of long-term bacterial biofilm and related acute and chronic infections. PloS One 7: e37281. doi:10.1371/journal.pone.0037281.

26. Heilmann C, Gerke C, Perdreau-Remington F, Götz F (1996) Characterization of Tn917 insertion mutants of Staphylococcus epidermidis affected in biofilm formation. Infect Immun 64: 277–282.

27. Mack D, Nedelmann M, Krokotsch A, Schwarzkopf A, Heesemann J, et al. (1994) Characterization of transposon mutants of biofilm-producing Staphylococcus epidermidis impaired in the accumulative phase of biofilm production: genetic identification of a hexosamine-containing polysaccharide intercellular adhesin. Infect Immun 62: 3244–3253.

28. Mack D, Rohde H, Dobinsky S, Riedewald J, Nedelmann M, et al. (2000) Identification of three essential regulatory gene loci governing expression of Staphylococcus epidermidis polysaccharide intercellular adhesin and biofilm formation. Infect Immun 68: 3799–3807.

29. Lipowsky HH, S. Kovalcheck, Zweifach BW (1978) The Distribution of Blood Rheological Parameters in the Microvasculature of Cat Mesentery. Circ Res 43: 738–749. doi:10.1161/01.RES.43.5.738.

30. Sun F, Liang H, Kong X, Xie S, Cho H, et al. (2012) Quorum-sensing agr mediates bacterial oxidation response via an intramolecular disulfide redox switch in the response regulator AgrA. Proc Natl Acad Sci U S A 109: 9095–9100. doi:10.1073/pnas.1200603109.

31. Milisavljevic V, Tran LP, Batmalle C, Bootsma HJ (2008) Benzyl alcohol and ethanol can enhance the pathogenic potential of clinical Staphylococcus epidermidis strains. Am J Infect Control 36: 552–558. doi:10.1016/j.ajic.2007.10.025.

32. Knudsen SM, von Muhlen MG, Schauer DB, Manalis SR (2009) Determination of Bacterial Antibiotic Resistance Based on Osmotic Shock Response. Anal Chem 81: 7087–7090. doi:10.1021/ac900968r.

33. Yarwood JM, Bartels DJ, Volper EM, Greenberg EP (2004) Quorum sensing in Staphylococcus aureus biofilms. J Bacteriol 186: 1838–1850.

34. Keller L, Surette MG (2006) Communication in bacteria: an ecological and evolutionary perspective. Nat Rev Microbiol 4: 249–258. doi:10.1038/nrmicro1383.

35. Boedicker JQ, Vincent ME, Ismagilov RF (2009) Microfluidic confinement of single cells of bacteria in small volumes initiates high-density behavior of quorum sensing and growth and reveals its variability. Angew Chem Int Ed Engl 48: 5908–5911. doi:10.1002/anie.200901550.

36. Kastrup CJ, Boedicker JQ, Pomerantsev AP, Moayeri M, Bian Y, et al. (2008) Spatial localization of bacteria controls coagulation of human blood by “quorum acting.” Nat Chem Biol 4: 742–750.

37. O’Loughlin CT, Miller LC, Siryaporn A, Drescher K, Semmelhack MF, et al. (2013) A quorum-sensing inhibitor blocks Pseudomonas aeruginosa virulence and biofilm formation. Proc Natl Acad Sci 110: 17981–17986. doi:10.1073/pnas.1316981110.

38. Otto M (2009) Staphylococcus epidermidis--the “accidental” pathogen. Nat Rev Microbiol 7: 555–567. doi:10.1038/nrmicro2182.

39. Mohamed N, Teeters MA, Patti JM, Hook M, Ross JM (1999) Inhibition of Staphylococcus aureus Adherence to Collagen under Dynamic Conditions. Infect Immun 67: 589–594.

40. Mascari L, Ross JM (2001) Hydrodynamic shear and collagen receptor density determine the adhesion capacity of S. aureus to collagen. Ann Biomed Eng 29: 956–962.

41. Mascari L, Ymele-Leki P, Eggleton CD, Speziale P, Ross JM (2003) Fluid shear contributions to bacteria cell detachment initiated by a monoclonal antibody. Biotechnol Bioeng 83: 65–74. doi:10.1002/bit.10650.

42. Tourovskaia A, Figueroa-Masot X, Folch A (2005) Differentiation-on-a-chip: a microfluidic platform for long-term cell culture studies. Lab Chip 5: 14–19. doi:10.1039/b405719h.

43. Kim L, Vahey MD, Lee H-Y, Voldman J (2006) Microfluidic arrays for logarithmically perfused embryonic stem cell culture. Lab Chip 6: 394–406. doi:10.1039/b511718f.

44. Lu H, Koo LY, Wang WM, Lauffenburger DA, Griffith LG, et al. (2004) Microfluidic shear devices for quantitative analysis of cell adhesion. Anal Chem 76: 5257–5264. doi:10.1021/ac049837t.

45. Rossi M, Lindken R, Hierck BP, Westerweel J (2009) Tapered microfluidic chip for the study of biochemical and mechanical response at subcellular level of endothelial cells to shear flow. Lab Chip 9: 1403–1411. doi:10.1039/b822270n.

46. Akimoto S, Mitsumata M, Sasaguri T, Yoshida Y (2000) Laminar shear stress inhibits vascular endothelial cell proliferation by inducing cyclin-dependent kinase inhibitor p21(Sdi1/Cip1/Waf1). Circ Res 86: 185–190.

47. Mascari LM, Ross JM (2003) Quantification of staphylococcal-collagen binding interactions in whole blood by use of a confocal microscopy shear-adhesion assay. J Infect Dis 188: 98–107. doi:10.1086/375826.

48. Kumar A, Whitesides GM (1993) Features of gold having micrometer to centimeter dimensions can be formed through a combination of stamping with an elastomeric stamp and an alkanethiol "'ink'" followed by chemical etching. Appl Phys Lett 63: 2002. doi:10.1063/1.110628.

49. Rhee SW, Taylor AM, Tu CH, Cribbs DH, Cotman CW, et al. (2005) Patterned cell culture inside microfluidic devices. Lab Chip 5: 102–107. doi:10.1039/b403091e.

50. Kim E, Xia Y, Whitesides GM (1995) Polymer microstructures formed by moulding in capillaries. Nature 376: 581–584. doi:10.1038/376581a0.

51. Rosenthal A, Macdonald A, Voldman J (2007) Cell Patterning Chip for Controlling the Stem Cell Microenvironment. Biomaterials 28: 3208–3216. doi:10.1016/j.biomaterials.2007.03.023.

52. Ren X, Bachman M, Sims C, Li GP, Allbriton N (2001) ref 42 from electrophoresis 2010. J Chromatogr B 762: 117–125.

53. Jang K, Sato K, Tanaka Y, Xu Y, Sato M, et al. (2010) An efficient surface modification using 2-methacryloyloxyethyl phosphorylcholine to control cell attachment via photochemical reaction in a microchannel. Lab Chip 10: 1937–1945. doi:10.1039/c002239j.

54. Fiddes LK, Chan HKC, Lau B, Kumacheva E, Wheeler AR (2010) Durable, region-specific protein patterning in microfluidic channels. Biomaterials 31: 315–320. doi:10.1016/j.biomaterials.2009.09.040.

55. Abate AR, Thiele J, Weinhart M, Weitz DA (2010) Patterning microfluidic device wettability using flow confinement. Lab Chip 10: 1774–1776. doi:10.1039/c004124f.

56. Xia Y, Whitesides GM (1998) Soft Lithography. Annu Rev Mater Sci 28: 153–184.

57. Mascari L, Ross JM (2002) Quantifying the temporal expression of the Staphylococcus aureus collagen adhesin. Microb Pathog 32: 99–103. doi:10.1006/mpat.2001.0481.

58. Hillborg H, Ankner JF, Gedde UW, Smith GD, Yasuda HK, et al. (2000) Crosslinked polydimethylsiloxane exposed to oxygen plasma studied by neutron reflectometry and other surface specific techniques. Polymer 41: 6851–6863. doi:10.1016/S0032-3861(00)00039-2.

59. Fan R, Vermesh O, Srivastava A, Yen BKH, Qin L, et al. (2008) Integrated barcode chips for rapid, multiplexed analysis of proteins in microliter quantities of blood. Nat Biotech 26: 1373–1378. doi:10.1038/nbt.1507.

60. Yakovenko O, Sharma S, Forero M, Tchesnokova V, Aprikian P, et al. (2008) FimH Forms Catch Bonds That Are Enhanced by Mechanical Force Due to Allosteric Regulation. J Biol Chem 283: 11596 –11605. doi:10.1074/jbc.M707815200.

61. Thomas WE, Trintchina E, Forero M, Vogel V, Sokurenko EV (2002) Bacterial adhesion to target cells enhanced by shear force. Cell 109: 913–923.

62. Rosenthal VD, Maki DG, Mehta A, Álvarez-Moreno C, Leblebicioglu H, et al. (2008) International Nosocomial Infection Control Consortium report, data summary for 2002-2007, issued January 2008. Am J Infect Control 36: 627–637. doi:10.1016/j.ajic.2008.03.003.

63. Fey PD, Olson ME (2010) Current concepts in biofilm formation of Staphylococcus epidermidis. Future Microbiol 5: 917–933. doi:10.2217/fmb.10.56.

64. Rupp ME, Ulphani JS, Fey PD, Bartscht K, Mack D (1999) Characterization of the importance of polysaccharide intercellular adhesin/hemagglutinin of Staphylococcus epidermidis in the pathogenesis of biomaterial-based infection in a mouse foreign body infection model. Infect Immun 67: 2627–2632.

65. Rupp ME, Ulphani JS, Fey PD, Mack D (1999) Characterization of Staphylococcus epidermidis polysaccharide intercellular adhesin/hemagglutinin in the pathogenesis of intravascular catheter-associated infection in a rat model. Infect Immun 67: 2656–2659.

66. Mack D, Fischer W, Krokotsch A, Leopold K, Hartmann R, et al. (1996) The intercellular adhesin involved in biofilm accumulation of Staphylococcus epidermidis is a linear beta-1,6-linked glucosaminoglycan: purification and structural analysis. J Bacteriol 178: 175–183.

67. Heilmann C, Schweitzer O, Gerke C, Vanittanakom N, Mack D, et al. (1996) Molecular basis of intercellular adhesion in the biofilm-forming Staphylococcus epidermidis. Mol Microbiol 20: 1083–1091.

68. Conlon KM, Humphreys H, O'Gara JP (2002) icaR encodes a transcriptional repressor involved in environmental regulation of ica operon expression and biofilm formation in Staphylococcus epidermidis. J Bacteriol 184: 4400–4408.

69. Knobloch JK, Bartscht K, Sabottke A, Rohde H, Feucht HH, et al. (2001) Biofilm formation by Staphylococcus epidermidis depends on functional RsbU, an activator of the sigB operon: differential activation mechanisms due to ethanol and salt stress. J Bacteriol 183: 2624–2633. doi:10.1128/JB.183.8.2624-2633.2001.

70. Knobloch JK-M, Horstkotte MA, Rohde H, Kaulfers P-M, Mack D (2002) Alcoholic ingredients in skin disinfectants increase biofilm expression of Staphylococcus epidermidis. J Antimicrob Chemother 49: 683–687.

71. Dice B, Stoodley P, Buchinsky F, Metha N, Ehrlich GD, et al. (2009) Biofilm formation by ica-positive and ica-negative strains of Staphylococcus epidermidis in vitro. Biofouling 25: 367–375. doi:10.1080/08927010902803297.

72. Qin Z, Yang X, Yang L, Jiang J, Ou Y, et al. (2007) Formation and properties of in vitro biofilms of ica-negative Staphylococcus epidermidis clinical isolates. J Med Microbiol 56: 83–93. doi:10.1099/jmm.0.46799-0.

73. Rohde H, Knobloch JK, Horstkotte MA, Mack D (2001) Correlation of biofilm expression types of Staphylococcus epidermidis with polysaccharide intercellular adhesin synthesis: evidence for involvement of icaADBC genotype-independent factors. Med Microbiol Immunol (Berl) 190: 105–112.

74. Rohde H, Burdelski C, Bartscht K, Hussain M, Buck F, et al. (2005) Induction of Staphylococcus epidermidis biofilm formation via proteolytic processing of the accumulation-associated protein by staphylococcal and host proteases. Mol Microbiol 55: 1883–1895. doi:10.1111/j.1365-2958.2005.04515.x.

75. Weaver WM, Dharmaraja S, Milisavljevic V, Di Carlo D (2011) The effects of shear stress on isolated receptor-ligand interactions of Staphylococcus epidermidis and human plasma fibrinogen using molecularly patterned microfluidics. Lab Chip 11: 883–889. doi:10.1039/c0lc00414f.

76. Firrell JC, Lipowsky HH (1989) Leukocyte margination and deformation in mesenteric venules of rat. Am J Physiol 256: H1667–1674.

77. Rusconi R, Lecuyer S, Autrusson N, Guglielmini L, Stone HA (2011) Secondary Flow as a Mechanism for the Formation of Biofilm Streamers. Biophys J 100: 1392–1399. doi:10.1016/j.bpj.2011.01.065.

78. Rusconi R, Lecuyer S, Guglielmini L, Stone HA (2010) Laminar Flow Around Corners Triggers the Formation of Biofilm Streamers. J R Soc Interface 7: 1293–1299. doi:10.1098/rsif.2010.0096.

79. Schaible B, Taylor CT, Schaffer K (2012) Hypoxia Increases Antibiotic Resistance in Pseudomonas Aeruginosa Through Altering the Composition of Multidrug Efflux Pumps. Antimicrob Agents Chemother 56: 2114–2118. doi:10.1128/AAC.05574-11.

80. Walters MC, Roe F, Bugnicourt A, Franklin MJ, Stewart PS (2003) Contributions of Antibiotic Penetration, Oxygen Limitation, and Low Metabolic Activity to Tolerance of Pseudomonas Aeruginosa Biofilms to Ciprofloxacin and Tobramycin. Antimicrob Agents Chemother 47: 317–323. doi:10.1128/AAC.47.1.317-323.2003.

81. Christner M, Heinze C, Busch M, Franke G, Hentschke M, et al. (2012) sarA negatively regulates Staphylococcus epidermidis biofilm formation by modulating expression of 1 MDa extracellular matrix binding protein and autolysis-dependent release of eDNA. Mol Microbiol. doi:10.1111/j.1365-2958.2012.08203.x.

82. Tormo MÁ, Martí M, Valle J, Manna AC, Cheung AL, et al. (2005) SarA Is an Essential Positive Regulator of Staphylococcus epidermidis Biofilm Development. J Bacteriol 187: 2348–2356. doi:10.1128/JB.187.7.2348-2356.2005.

83. Pintens V, Massonet C, Merckx R, Vandecasteele S, Peetermans WE, et al. (2008) The role of σB in persistence of Staphylococcus epidermidis foreign body infection. Microbiology 154: 2827–2836. doi:10.1099/mic.0.2007/015768-0.

84. Bowden MG, Chen W, Singvall J, Xu Y, Peacock SJ, et al. (2005) Identification and preliminary characterization of cell-wall-anchored proteins of Staphylococcus epidermidis. Microbiol Read Engl 151: 1453–1464. doi:10.1099/mic.0.27534-0.

85. Walsh EJ, Miajlovic H, Gorkun OV, Foster TJ (2008) Identification of the Staphylococcus aureus MSCRAMM clumping factor B (ClfB) binding site in the {alpha}C-domain of human fibrinogen. Microbiology 154: 550–558. doi:10.1099/mic.0.2007/010868-0.

86. Pawar P, Shin PK, Mousa SA, Ross JM, Konstantopoulos K (2004) Fluid shear regulates the kinetics and receptor specificity of Staphylococcus aureus binding to activated platelets. J Immunol Baltim Md 1950 173: 1258–1265.

87. Arrecubieta C, Toba FA, von Bayern M, Akashi H, Deng MC, et al. (2009) SdrF, a Staphylococcus epidermidis Surface Protein, Contributes to the Initiation of Ventricular Assist Device Driveline–Related Infections. PLoS Pathog 5: e1000411. doi:10.1371/journal.ppat.1000411.

88. Arrecubieta C, Lee M-H, Macey A, Foster TJ, Lowy FD (2007) SdrF, a Staphylococcus epidermidis surface protein, binds type I collagen. J Biol Chem 282: 18767–18776. doi:10.1074/jbc.M610940200.

89. Fordyce PM, Gerber D, Tran D, Zheng J, Li H, et al. (2010) De novo identification and biophysical characterization of transcription-factor binding sites with microfluidic affinity analysis. Nat Biotechnol 28: 970–975. doi:10.1038/nbt.1675.

90. Fordyce PM, Pincus D, Kimmig P, Nelson CS, El-Samad H, et al. (2012) Basic leucine zipper transcription factor Hac1 binds DNA in two distinct modes as revealed by microfluidic analyses. Proc Natl Acad Sci U S A 109: E3084–3093. doi:10.1073/pnas.1212457109.

91. Sollier E, Murray C, Maoddi P, Di Carlo D (2011) Rapid prototyping polymers for microfluidic devices and high pressure injections. Lab Chip 11: 3752. doi:10.1039/c1lc20514e.

92. Vuong C, Gerke C, Somerville GA, Fischer ER, Otto M (2003) Quorum-sensing control of biofilm factors in Staphylococcus epidermidis. J Infect Dis 188: 706–718. doi:10.1086/377239.

93. Huebner J, Goldmann DA (1999) Coagulase-negative staphylococci: role as pathogens. Annu Rev Med 50: 223–236. doi:10.1146/annurev.med.50.1.223.

94. Chatterjee SS, Joo H-S, Duong AC, Dieringer TD, Tan VY, et al. (2013) Essential Staphylococcus aureus toxin export system. Nat Med 19: 364–367. doi:10.1038/nm.3047.

95. Malachowa N, Kobayashi SD, Freedman B, Dorward DW, Deleo FR (2013) Staphylococcus aureus Leukotoxin GH Promotes Formation of Neutrophil Extracellular Traps. J Immunol Baltim Md 1950. doi:10.4049/jimmunol.1301821.

96. Sina H, Ahoyo TA, Moussaoui W, Keller D, Bankolé HS, et al. (2013) Variability of antibiotic susceptibility and toxin production of Staphylococcus aureus strains

isolated from skin, soft tissue, and bone related infections. BMC Microbiol 13: 188. doi:10.1186/1471-2180-13-188.

97. Chambers HF, DeLeo FR (2009) Waves of resistance: Staphylococcus aureus in the antibiotic era. Nat Rev Microbiol 7: 629–641. doi:10.1038/nrmicro2200.

98. Arya R, Princy SA (2013) An insight into pleiotropic regulators Agr and Sar: molecular probes paving the new way for antivirulent therapy. Future Microbiol 8: 1339–1353. doi:10.2217/fmb.13.92.

99. Ankerst J, Christensen P, Kjellén L, Kronvall G (1974) A rountine diagnostic test for IgA and IgM antibodies to rubella virus: absorption of IgG with Staphylococcus aureus. J Infect Dis 130: 268–273.

100. Downer R, Roche F, Park PW, Mecham RP, Foster TJ (2002) The Elastin-binding Protein of Staphylococcus aureus(EbpS) Is Expressed at the Cell Surface as an Integral Membrane Protein and Not as a Cell Wall-associated Protein. J Biol Chem 277: 243–250. doi:10.1074/jbc.M107621200.

101. Park PW, Rosenbloom J, Abrams WR, Rosenbloom J, Mecham RP (1996) Molecular Cloning and Expression of the Gene for Elastin-binding Protein (ebpS) in Staphylococcus aureus. J Biol Chem 271: 15803–15809. doi:10.1074/jbc.271.26.15803.

102. Brabletz T (2012) EMT and MET in Metastasis: Where Are the Cancer Stem Cells? Cancer Cell 22: 699–701. doi:10.1016/j.ccr.2012.11.009.

103. Dalerba P, Cho RW, Clarke MF (2007) Cancer Stem Cells: Models and Concepts. Annu Rev Med 58: 267–284. doi:10.1146/annurev.med.58.062105.204854.